A PERFORMANCE MODEL OF A SPARK IGNITION WANKEL ENGINE: INCLUDING THE EFFECTS OF CREVICE VOLUMES, GAS LEAKAGE, AND HEAT TRANSFER

by

TIMOTHY JOHN NORMAN

B.S.M.E. University of Massachusetts, Amherst
(1981)

Submitted to the Department of
Mechanical Engineering
in Partial Fulfillment of the
Requirments of the Degree of

MASTER OF SCIENCE IN MECHANICAL ENGINEERING

at the

MASSACHUSETTS INSTITUTE OF TECHNOLOGY

June 1983

Signature of Author: _____
Department of Mechanical Engineering, 1 March 1983

Certified by: _____
Jack Ekchian
Thesis Supervisor

Accepted by: _____
Warren M. Rohsenow
Chairman, Mechanical Engineering Department Committee

A PERFORMANCE MODEL OF A SPARK IGNITION WANKEL ENGINE: INCLUDING THE EFFECTS OF CREVICE VOLUMES, GAS LEAKAGE, AND HEAT TRANSFER

by

TIMOTHY JOHN NORMAN

Submitted to the Department of Mechanical Engineering on March 1, 1983 in partial fulfillment of the requirements for the Degree of Master of Science in Mechanical Engineering

ABSTRACT

Recent aviation gasoline price and supply problems have created a need for general aviation airplane engines that burn kerosene. N.A.S.A. researchers have determined that a stratified charge Wankel engine is a likely engine choice for this purpose. This paper describes the initial work towards modelling such an engine.

A zero-dimensional (or thermodynamic) model of a spark ignition engine has been constructed. Three engine performance loss submodels have been included; they are heat transfer, gas leakage, and crevice volumes. Previous models of the Wankel engine have not included a model of performance loss resulting from crevice volumes.

Preliminary rotary engine performance testing is being conducted by N.A.S.A. on a gasoline, spark ignition Wankel engine. Motoring data from this engine was used to calibrate the computer model. A shortage of firing engine data has made the calibration incomplete but the reported values of crevice volume and leakage area are 0.875 cm^3/apex and 1.0 mm^2/apex respectively. A parametric study on the effects of reducing leakage, heat transfer, and crevice volumes was performed for light load and motoring. As was predicted, gas leakage is the predominant effect in these operating regimes. Crevice volumes and heat transfer have little effect on engine performance at very light load but can be expected to become more significant at higher loads and speeds.

Thesis Supervisor: Professor John B. Heywood

Title: Professor of Mechanical Engineering

Director Sloan Automotive Laboratory

Thesis Supervisor: Dr. Jack A. Ekchian

Title: Manager Sloan Automotive Laboratory.

ACKNOWLEDGEMENTS

This is the bittersweet part of any research thesis. Sweet because my work is complete but bittersweet because it means I must say goodbye to my good friends and family at M.I.T. and in the Boston area.

I want to first thank Professor John Heywood for all his expert help with the research and my career at M.I.T. It has been a privilege to work with such an outstanding engineer and person. I would also like to thank Jack Ekchian, my surrogate advisor these last few months, for his help in finishing the research and thesis. Thanks also to Professor Gyftopoulos for getting me started at M.I.T. Steve Poulos and Hossein Mansouri were both helpful in explaining their work from which this research started.

I would also like to thank my wife (and starter motor) Moni for her typing, love, and devotion . Pat Condon and Karla Stryker deserve recognition for all the help they have provided me. Thanks also to Bruce Marcham (drafting and late nights), Rick Babikian, Yi-Chung Doo, Pepper White, Harry Katz, Chris Shea and Craig Noble (and all the others that I'm forgetting) for all of your friendship. Special thanks to my parents Les and Janet for Sunday dinners and being there, Mona and Tom Widmer for their love and balanced perspective (no more horse-hair sweaters?), and Stanley Cath for his guidance, objectivity, and friendship.

This research has been sponsored by N.A.S.A. and all their help is greatly appreciated.

I would like to dedicate this thesis to my brother Anthony and his children Luke, and Zoe. Peace.

TABLE OF CONTENTS

CONTENTS OF SECOND VOLUME

LIST OF TABLES

LIST OF FIGURES

1.0 INTRODUCTION

This chapter outlines the structure of the computer simulation developed in this project and the steps necessary for completion of the simulation. Background material is presented to acquaint the reader with the goals and some of the peculiarities of the engine under study. The second chapter discusses the specifics of the simulation and derives the differential equations for a closed system. Chapter Three investigates, in detail, the crevice and leakage model and then presents the derivation of the differential equations for an open system. The validation and calibration of the model through the use of engine data supplied by N.A.S.A. is discussed in Chapter Four. The fifth chapter presents the results from a parametric study on the effects of varying heat transfer, crevice volumes, and leakage areas. Chapter Six summarizes the results and presents a set of conclusions and recommendations.

1.1 BACKGROUND

1.1.1 OVERALL N.A.S.A. GOAL

N.A.S.A. has begun a development process that will by the end of this decade produce an engine for lightweight general aviation airplanes that will not require aviation gasoline. Distributors of high octane aviation gasoline have determined that continued supply to remote locations is no longer profitable. Uncertainty over fuel availability and price have worked to limit the commuter aircraft market (1).

The general aviation community has proposed that any new powerplant should burn the same fuel that powers commercial aircraft (aviation kerosene or jet fuel). This will reduce the uncertainty over fuel

availability and minimize the inevitable dislocations within the fuel distribution network.

N.A.S.A. has begun a preliminary engineering program to determine the best engine for this application. Powerplants that have been considered include gas turbines, diesel engines, spark ignition reciprocating engines, and Wankel engines (2&3). Since the engine is to be used in light aircraft beginning in the 1990's, each powerplant choice has been rated for various operating characteristics, using assumed advanced technologies, and engine/airplane system requirements such as range and load capability (Tables 1 and 2).

1.1.2 ENGINES UNDER CONSIDERATION BY N.A.S.A.

Each design characteristic of the various engines being considered was weighted according to importance and a total score was assigned to each type of engine. From these studies N.A.S.A. has decided to concentrate on two choices:

1) a light-weight, turbo-charged, turbo compound, two-stroke diesel engine.
2) a turbo-charged, turbo-compound, stratified charge Wankel engine.

A primary design factor in an aircraft engine is the power density (power to weight ratio). Turbo-charging increases power density and will also allow the engines to operate at higher elevations. Reduction of engine weight, for the same power output, will increase the power density. Consequently, the two stroke engine, which has twice the power density of an equivalent four stroke engine is more desirable for this application. Some early studies of the two engines (no turbo-compounding) predict a

power density of 1.25 hp/lb for the rotary engine and 0.98 hp/lb for the diesel. This advantage for the Wankel engine is somewhat offset by a slightly higher brake specific fuel consumption.

Both engines will use turbo-compounding which recovers more of the exhaust gas enthalpy, by driving a heat engine coupled to the engine shaft, which increases power output. This results in a higher thermal efficiency for the engine/compound cycle system. With the use of ceramic materials to reduce heat transfer losses within the engines, turbo-compounding could become more effective as the thermodynamic availability of the exhaust gases from the cylinder will be increased. Since, approximately one third of the fuel energy is converted to work, another one third is lost by heat transfer to the cooling system (in a conventional engine), and the remaining one third is exhausted; a turbo-compounding system that recovers 50% of the exhaust enthalpy of a truly adiabatic engine would double the power output or alternatively halve the engine size for the identical power.

In order for the Wankel engine to burn aviation kerosene the engine will have to be of a stratified charge design. In this engine, fuel is injected directly into the combustion chamber and ignition is insured through the use of one or more spark plugs. Past work by Curtiss-Wright has demonstrated the feasibility and advantages of a rotary stratified charge engine (4). The most significant advantages over a spark ignition rotary engine are:

improved fuel tolerance

higher thermal efficiency, η_{th} (higher compression ratio)

lower emissions (except at light load)

reduced throttling losses

1.2 THE WANKEL ENGINE

1.2.1 WANKEL ENGINE DESCRIPTION

In the Wankel engine a three-sided rotor is mounted on an eccentric shaft that is centered at the geometric center of the rotor housing (figs. 1 & 2). The rotor and housing assembly simultaneously form three isolated chambers. As the crank rotates, an internal gear on the rotor face mates with an external gear on the side plate (1:3 ratio), and forces the rotor to revolve at one third of the crank's angular velocity. This means that one chamber requires three crank shaft revolutions to complete the four strokes of an equivalent reciprocating engine cycle. However, because there are three chambers per rotor there is one induction process and one power "stroke" per crank revolution. Thus a single rotor Wankel engine is equivalent to one, two-cylinder, 4-stroke reciprocating engine. The rotary engine does not require mechanically complex valve trains but instead relies on intake and exhaust ports that are opened and closed by the action of the rotor. The intake ports are typically located on the side plate (known as side intake ports), and there are usually two intake ports per rotor. An exhaust port is located in the rotor housing (a peripheral exhaust port).

There are gas seals at each corner of the rotor (apex seals), along the edges of the rotor (side seals), and at the junctions between the apex and side seals (corner seals) (fig.3) . Oil is introduced into the intake system in order to lubricate these gas seals. The rotor is oil cooled and a set of oil seals prevent the flow of oil from the rotor to the chambers. The spark plugs and fuel injectors (for a stratified charge engine) are located near the top dead center position. The basic geometric design

parameters are the rotor radius, which is the distance from the center of the rotor to the apex, the eccentricity of the shaft, and the depth or height of the rotor housing. With these dimensions and the volume of the cutout in the rotor, the theoretical compression ratio can be calculated as can the displacement per rotor.

1.2.2 ADVANTAGES AND DISADVANTAGES OF THE WANKEL ENGINE

The Wankel engine has been considered a dead issue by much of the technical community since the end of Wankel engine development programs at major automobile manufacturers such as General Motors, Toyota, and Ford. In order to determine if the present interest in the engine is justified, it is instructive to look at the reasons for termination of these developmental programs and what if any improvements have been made.

By far the most important reason for discontinuing Wankel engine research was the poor fuel economy of the engine, which became unacceptable after the OPEC oil embargo of 1973 and the subsequent gasoline price increases. This poor fuel economy is generally believed to be caused by unburned fuel/air mixture leaking past the apex seals during compression and combustion to adjacent chambers. This leakage is also thought to be the prime contributor to the high hydrocarbon emissions of the Wankel (5). Other major concerns were the projected high production and tooling costs for an engine which was of such radically different geometry from the conventional automotive engine. Engine reliability was also a consideration as early production models had serious apex seal wear problems. Although most Wankel engine programs were terminated in the mid 1970's a few projects have continued, most notably at Toyo Kogyo (Mazda) and at Curtiss-Wright. These projects have resulted in production tooling

and engines with improved fuel economy and proven reliability. The RX-7, Mazda's production sports car model that employs a two rotor Wankel engine, is now rated at 25 mpg by the EPA, and meets all emissions standards (6). Curtiss-Wright's stratified charge rotary engine is not currently in production, but test results have given very promising emissions and fuel economy data (7). These continued efforts have shown that in certain applications such as general aviation airplanes the Wankel may be a good power plant choice.

For light aircraft duty the stratfied charge Wankel has some specific advantages over its diesel engine competitor:

higher power density

better fuel tolerance

smaller package volume

- lower frontal area
- easier maintenance access

better low temperature starting

lower noise levels

shorter lift-off

faster climb

reliability (fewer moving parts)

1.3 PROGRAM

The research proposal calls for three phases of activity that are to be completed in series. During the first phase a reciprocating engine cycle simulation was converted to a Wankel engine simulation. A stratified charge combustion model will be added during the second phase, so that more

detailed design questions can be considered. In the third phase turbo-charge and turbo-compound models will be incorporated into the cycle simulation.

The author's task has been to complete the first phase, in order for preliminary engine performance and sizing calculations to be made. A secondary research aim, during this phase of the project, was to develop a crevice volume model for the Wankel engine to assess the importance of crevices on engine performance. Experimental data from a Mazda spark ignition engine has been collected by N.A.S.A. to allow a calibration of the computer model developed in this research effort.

1.4 DESCRIPTION OF PROJECT TASKS

1.4.1 DEFINITION OF TASKS

An extant quasi-dimensional model of a reciprocating engine was used as a starting point for the Wankel engine simulation (8). Figure 4 is a flow chart that illustrates the deletions and additions necessary for the conversion. There were five major steps necessary for the conversion process:

a) change in geometry

b) removal of turbulent combustion model

c) addition of leakage model

d) addition of crevice volume model

e) change in heat transfer model

1.4.2 OUTLINE OF CODE

The four engine processes, intake, compression, combustion-expansion, and exhaust are separated into different subroutines (Fig. 5). The Main

program controls, through ODERT (a numerical integrator) the program flow. That is, Main decides when each engine process begins and ends or what, if any, numerical data should be outputted.

The program begins by supplying Main the required input data. A calculation is then performed to initialize the thermodynamic state of the chamber gas at the beginning of the intake process, which is defined as the point where the intake port begins to open. The intake routine is then called by ODERT. Intake calls other subroutines where, for a given crank angle the working fluid thermodynamic properties are evaluated, and the direction, composition, and magnitude of mass flow rates through the intake and exhaust ports or valves are computed. The heat transfer rate is then calculated as is the rate of change of chamber volume. Next, leakage and crevice volume mass flow rates are calculated. Finally, Intake has enough information to evaluate the rates of change of pressure, temperature, work, heat transfer, and mass flow. The program control returns to ODERT which integrates the differential variables through time (crank angles) until program flow returns to Main. This interaction between Main and ODERT is repeated until each engine process is finished and the cycle is completed. The final values of chamber pressure, temperature, and mass are compared to the initialized values and if each property is within the error criteria. the calculation ends. However, if these criteria are not met, the program begins again with the final property values used as the initial quantities for the second iteration. Convergence occurs quickly, usually requiring three, or at most four iterations.

This segmented style of programming along with good documentation of the code is vital for any lengthy program such as this. This particular code allows end users to quickly find necessary information, and also great

flexibility for logic changes similar to those described already.

1.4.3 CHANGE IN GEOMETRY

A major program alteration was the change in the simulation code required to reflect the different engine geometry. Most of these changes were in the geometry subroutine CSAVDV where chamber surface area, volume, and rate of change of volume expressions are evaluated. Other changes were required in the subroutines that evaluate valve open areas and discharge coefficients to reflect the use of ports rather than valves. The Main program also needed to be modified to account for the extra crankshaft revolution per chamber cycle. The geometric equations developed in the texts by Ansdale and Yamamoto were used to define the engine geometry (10&11).

1.4.4 COMBUSTION ROUTINE CHANGES

In order to run a firing case for the rotary engine the combustion subroutine required some minor modifications. A turbulent entrainment combustion model was included in the reciprocating engine simulation that was specific to that geometry. A specified burn rate combustion model was also included as an option. The turbulent entrainment model was removed and therefore the combustion routine required a specified burn rate input in order to operate. In the resulting program the combustion chamber is modeled with two zones; one each for the cool unburned charge and hot burned products (Fig. 6). The NO formation model was also removed.

1.4.5 ADDITION OF GAS LEAKAGE MODEL

The importance of gas leakage as a performance and emissions mechanism in the Wankel is well known. It is crucial, then, to model this mass transfer between adjacent chambers in order to quantify its effect on performance and measure its relative effect vis-a-vis heat transfer and crevice volumes. The leakage and crevice volume models were combined to reduce complications. The implementation and physical justification of this assumption are described in the next section.

1.4.6 ADDITION OF CREVICE VOLUME MODEL

It has been hypothesized that crevice volume effects could be significant not only as a source of hydrocarbon emissions, but also as a mechanism for performance loss. Engine crevices are small volumes associated with gas seals and spark plugs that are connected to the chamber. As chamber pressure rises, working fluid is forced into these crevices which then re-enters the chamber as this pressure falls. Since crevice volumes have a high surface-to-volume ratio, the gas entering the crevice is cooled and the combustion reactions are quenched in these regions.

A subroutine which calculates the leakage and crevice mass flow rates was added to the program. Since the addition of the model makes the chamber an open thermodynamic system throughout the cycle, rather than just during intake and exhaust, the final differential equations governing chamber pressure, temperature, and composition were changed and evaluated within this subroutine. Also in order to evaluate the composition, direction, and magnitude of the crevice and leakage mass flow rates, a

history of adjacent chamber pressures and crevice compositions versus crank angle was required. As this cycle pressure history does not exist during the first cycle iteration, the crevice and leakage models are not activated until the second iteration.

1.4.7 CHANGES TO HEAT TRANSFER MODEL

An important concern regarding the Wankel rotary engine has been its high rate of heat transfer. During the combustion process the surface-to-volume ratio of the combustion chamber is higher than in equivalent reciprocating engines (Fig. 7). The charge is also swept along, by the rotor motion, at high velocities which naturally increases the heat transfer to the walls. Obviously a heat transfer model is required to predict engine performance and evaluate the effect of insulating ceramic materials.

2.0 COMPUTER MODEL

2.1 BACKGROUND

Computer models of internal combustion engines can be grouped into three general classifications: zero-dimensional models, quasi-dimensional models, and multidimensional models. Zero-dimensional models use the First Law of Thermodynamics and a specified combustion rate to predict engine operating characteristics. Quasi-dimensional models add a turbulent combustion submodel to predict the burning rate which requires an assumption about flame front shape. Multidimensional models use the conservation equations for mass, energy, momentum and species to predict the flame propagation through the combustion chamber (12).

The research work presented here has used a zero-dimensional model for several reasons. Multi-dimensional models are currently restricted by available computing power to only two dimensional analyses. They are consequently not yet suitable for this application. Also, it was felt that although the initial test data would be from a spark ignition engine, the final goal of the simulation program was the study of a stratified charge plant. Thus, the implementation of a pre-mixed turbulent combustion model, such as the model present in the reciprocating engine simulation was not considered worthwhile.

The model will be able to predict the engine size required for a given task. Parametric studies can then be performed in order to judge the relative merits of different research efforts. For example, questions concerning the importance of reducing heat loss, crevice volumes, and leakage can be addressed.

2.2 CALCULATION OF THERMODYNAMIC PROPERTIES

2.2.1 SIMULATION FRAMEWORK AND BASIC ASSUMPTIONS

The simulation is separated into four distinct but sequential processes: intake, compression, combustion (and expansion), and exhaust. Intake starts as the intake ports begin to open (IPO) and continues until they are completely closed (IPC). The compression process begins at IPC and ends at the spark ignition point (TSPARK). The combustion process is initiated with the occurrence of the spark and continues through expansion until the exhaust port begins to open (EPO). The exhaust process occurs from this point until the intake ports start to open once again (not EVC). The cycle lasts exactly 1080 crank angle degrees.

To solve the differential form of the First Law equation for the chamber contents some basic assumptions must be made. Except during combustion, the chamber contents are assumed to be an homogeneous mixture of non-reacting ideal gases. Therefore the contents have a single mean temperature. During intake and compression chamber contents are characterized as a mixture of fresh charge (air and fuel vapor) and residual burned gas. The intake and exhaust manifolds are assumed to have constant temperatures and pressures. During exhaust only burned product is assumed to be present in the chamber. Unburned gas that leaks into the exhaust chamber is treated as burned product and the amount of fuel energy lost is accounted for. During combustion two zones are created, one each for the unburned gas and the burned product. Each zone is assumed to be homogeneous i.e. of uniform temperature and composition. It is assumed that there are no pressure waves within the chamber so gas pressure is constant throughout the chamber.

2.2.2 SOLUTION OF THERMODYNAMIC EQUATIONS WITHOUT CREVICE VOLUME

In this section the method for generating differential equations to find the thermodynamic state of the chamber's contents is briefly outlined. To be useful the final equation must evaluate the rate of temperature change independently of the rate of change of chamber pressure.

The First Law of Thermodynamics for an open system, in differential form, is:

$$\dot{E} = \sum(\dot{m}_j h_j) - \dot{Q} - \dot{W} \qquad (2.1)$$

Note that heat loss from the system is positive. From the definition of internal energy:

$$\dot{E} = \frac{d(mh - pV)}{dt} = \dot{m}h + m\dot{h} - \dot{p}V - p\dot{V} \qquad (2.2)$$

where;

m : mass

h : enthalpy

p : pressure

v : volume

The First Law equation can be rewritten as:

$$m\dot{h} = \dot{Q}_w - h\Sigma(\dot{m}_j) + \Sigma(\dot{m}_j h_j) + V\dot{p} \qquad (2.3)$$

During intake, chamber composition changes as fresh charge is added to the fresh charge/residual gas mixture already present. If fresh charge and residual gas are taken to be the two ideal gas components making up the

mixture the change in enthalpy can be expressed as:

$$\dot{h} = \frac{d(x_1 h_1 + x_2 h_2)}{dt} = \dot{x}_1 h_1 + x_1 \dot{h}_1 + \dot{x}_2 h_2 + x_2 \dot{h}_2 \qquad (2.4)$$

Where:

x_i : mass fraction of component i

i = 1 : refers to fresh charge

i = 2 : refers to residual gas

$$x_1 + x_2 = 1 \qquad (2.5)$$

Differentiating equation 2.5 yields:

$$\dot{x}_1 = - \dot{x}_2 \qquad (2.6)$$

Substituting this last relationship into equation 2.4 gives:

$$\dot{h} = \dot{x}_1 (h_1 - h_2) + x_1 \dot{h}_1 + x_2 \dot{h}_2 \qquad (2.7)$$

The change in enthalpy for each component can be expressed as changes in the system temperature and pressure:

$$\dot{h}_i = c_{p_i} \dot{T} + c_{T_i} \dot{p} \qquad (2.8)$$

Where:

$$c_p \equiv (\partial h / \partial T)_p \qquad (2.9)$$

$$c_T \equiv (\partial h / \partial p)_T \qquad (2.10)$$

From the ideal gas law :

$$\rho = \frac{p}{R\,T} \tag{2.11}$$

So, differentiating both sides gives:

$$\frac{d\rho}{dt} = \dot{\rho} = (\partial\rho/\partial p)\dot{p} + (\partial\rho/\partial R)\dot{R} + (\partial\rho/\partial T)\dot{T} \tag{2.12}$$

Rearranging equation 2.12 provides a differential equation for pressure in terms of rates of change of density, temperature, and the gas constant:

$$\dot{p} = \frac{\rho}{(\partial\rho/\partial p)} = \left[\frac{\dot{\rho}}{\rho} - \frac{\dot{R}}{\rho}(\partial\rho/\partial R) - \frac{\dot{T}}{\rho}(\partial\rho/\partial T) \right] \tag{2.13}$$

Referring to equation 2.11 it can be shown that:

$$(\partial\rho/\partial R) = -\frac{\rho}{R} \tag{2.14}$$

From the definition of density:

$$\rho = \frac{m}{V} \tag{2.15}$$

it is apparent that:

$$\frac{\dot{\rho}}{\rho} = \frac{\dot{m}}{m} + \frac{\dot{V}}{V} \tag{2.16}$$

The rate of change of the gas constant is:

$$\dot{R} = \frac{d(x_1R_1 + x_2R_2)}{dt} = \dot{x}_1R_1 + \dot{x}_2R_2 = \dot{x}_1(R_1 - R_2) \tag{2.17}$$

Combining equations 2.13 through 2.17 results in:

$$\dot{p} = \frac{\rho}{(\partial\rho/\partial p)} \left[\left(\frac{R_1 - R_2}{R} \right) \dot{x}_1 + \frac{\dot{m}}{m} - \frac{\dot{V}}{V} - \frac{\partial\rho}{\partial T} \frac{\dot{T}}{\rho} \right] \qquad (2.18)$$

Finally substitution of equations (2.2), (2.4), (2.7), (2.8) and(2.18) into the energy equation (2.1) gives an equation for temperature independent of the unknown rate of change of pressure:

$$\dot{T} = \frac{B}{A} \left[\dot{x}_1 \left(\frac{R_1 - R_2}{R} + \frac{h_2 - h_1}{B} \right) + \frac{\dot{m}}{m} \left(1 - \frac{h}{B}\right) - \frac{\dot{V}}{V} + \frac{1}{mB} \left(\sum m_j h_j - \dot{Q} \right) \right] \qquad (2.19)$$

Where:

$$A = C_p + \frac{(\partial\rho/\partial T)_p}{(\partial\rho/\partial p)_T} \left(\frac{1}{\rho} - C_T \right) \qquad (2.20)$$

$$B = \frac{(1 - \rho C_T)}{(\partial\rho/\partial p)_T} \qquad (2.21)$$

$$C_p = x_1 C_{p_1} + x_2 C_{p_2} \qquad (2.22a)$$

$$C_T = x_1 C_{T_2} + x_2 C_{T_2} \qquad (2.22b)$$

However, equation 2.18 assumes that the rate of mass flow into or out of the chamber is independent of the rate of change of pressure. This is not a valid assumption if a crevice volume is present within the chamber. The thermodynamic implications of the crevice volume model are discussed in Chapter 3.

2.3 ENGINE PROCESS MODELS

2.3.1 INTAKE AND EXHAUST FLOW PROCESSES

A quasi-steady compressible flow model is used to evaluate the mass exchange between the chamber and intake or exhaust manifolds. The manifolds are considered to be infinite plenums with specified pressure, i.e. manifold pipe dynamics are not modeled. The intake gas is a mixture of fresh charge (fuel-air mixture) and recirculated exhaust gas (EGR). If back flow occurs chamber contents are sent back to the intake manifold but are not mixed with the intake charge (a plug flow assumption). Instead, if flow reverses again, all the back mass is assumed to return to the chamber before any additional intake charge enters the chamber. However, at IPO, only intake charge is present in the manifold. Gas in the exhaust manifold is assumed to be completely burned products of combustion at the instantaneous chamber temperature.

The port open areas are determined by assuming that the ports open linearly with crank angle. The discharge coefficients are assumed constant as a function of pressure ratio and equal to 0.75. This value was based on data from two-stroke diesel engines (13). With open area, coefficient of discharge, and the pressure ratio across the port known, the mass flow rate can be calculated from:

$$\dot{m} = C_d A \frac{P_o}{RT_o} \sqrt{\gamma R T_o} \left\{ \frac{2}{\gamma - 1} \left[\left(\frac{P_s}{P_o} \right)^{2/\gamma} - \left(\frac{P_s}{P_o} \right)^{(\gamma+1)/\gamma} \right] \right\} \quad (2.23)$$

where:

C_d : coefficient of discharge

A : port open area

p_o : upstream stagnation pressure

p_s : static pressure at restriction

T_o : upstream stagnation temperature

γ : ratio of specific heats

R : gas constant

For choked flow the equation is:

$$\dot{m} = C_d A \frac{p_o}{RT_o} A \sqrt{\gamma R T_o} \left(\frac{2}{\gamma + 1} \right)^{(\gamma+1)/2(\gamma-1)} \qquad (2.24)$$

The sign convention adhered to in the model is as follows: intake flow into the chamber is positive and exhaust flow out of the chamber is also positive.

2.3.2 COMBUSTION

During combustion the chamber is divided into two zones. The first containing unburned mixture, the second composed of combustion products. Mass is transferred from the unburned zone to the burned zone according to a specified equation for the mass fraction burned. The equation is of the form proposed by Wiebe (14).

$$x_b = 1 - e^{-a\left[(\theta - \theta_o)/\Delta\theta_b \right]^{m+1}} \qquad (2.25)$$

where:

x = mass fraction burned in chamber

a = efficiency parameter

m = form factor

θ = crank angle

θ_o = start of combustion (not spark timing)

$\Delta\theta_b$ = burn duration

The form factor and efficiency parameter in equation (2.25) are inputs to the program. These constants generally fall between:

$$1 < m < 3 \tag{2.26a}$$

$$3 < a < 10 \tag{2.26b}$$

for real engines (15). For a closed system differentiation of Eq. 2.25 would define the rate of combustion. However, with the presence of leakage and crevice volume mass flows, the system is open during combustion and the combustion rate should reflect this change. The combustion rate equation is derived in Chapter 3.

2.3.3 HEAT TRANSFER

Heat transfer in the Wankel rotary engine is a major source of concern. Most heat transfer in an internal combustion engine occurs during the combustion and the expansion stroke. The shape of this engine's combustion chamber, which has a high surface area to volume ratio, leads one to expect high heat transfer rates near the top dead center position. Also since the charge is pushed at high velocities past the housing walls even higher heat transfer rates can be expected. The general area of heat transfer from internal combustion engines is lacking in quantitative equations to describe the phenomenon, and experimental data is necessary to

calibrate the model. This is especially difficult for the Wankel engine where little heat transfer data has been published.

The analysis starts with the general forced convective heat transfer equation:

$$Nu = \alpha\, Re^{a}\, Pr^{b} \qquad (2.27)$$

where;

$Nu \equiv hL/k$: Nusselt number

$Re \equiv VL/\nu$: Reynolds number

$Pr \equiv \mu C_p/k$: Prandtl number

α : constant

a : constant

b : constant

h : heat transfer coefficient

L : characteristic length

k : thermal conductivity of fluid

V : characteristic velocity

ν : kinematic viscosity

μ : dynamic viscosity

C_p: specific heat at constant pressure

The Prandtl number is assumed to be unity. The flow pattern is assumed to be similar to that of forced convection over a flat plate. This provides values for the constants in Eq. 2.27 of (16).

$\alpha = 0.037$

$a = 0.8$

In reciprocating engines the cylinder bore is used as the characteristic dimension. In the Wankel an equivalent dimension to the

bore is the housing depth. These dimensions are similar in that both are constant throughout the cycle and perpendicular to the primary component of the flow. The last piece of information needed to solve Eq. 2.27 for the heat transfer coefficient is the characteristic gas velocity.

The model uses the approach originally suggested by Woshni, i.e. a velocity composed of two parts (17). The first component velocity is proportional to the mean rotor velocity in the Wankel engine, which turns at one third the crank shaft speed:

$$V_{non-firing} = \left(\frac{2\pi}{60}\right)\left(\frac{RPM}{3}\right) R \qquad (2.28)$$

The second velocity component is proportional to the combustion intensity. Woschni believed that the rapid expansion of the burning charge caused large velocities within the chamber. The combustion intensity is characterized by the difference in chamber pressure between a firing case and a non-firing case at the same crank angle. A term is added to account for the amount of fuel inducted which affects the pressure trace.

$$V_{fire} = C_1 V_{non-fire} + C_2 V_s \left(\frac{T}{pV}\right)_{IPC} (p - p_{non-fire}) \qquad (2.29)$$

Where:

V_s : chamber volume

T_{IPC} : chamber temperature at intake port close

p_{IPC} : chamber pressure at intake port close

V_{IPC} : chamber volume at intake port close

Woschni found that for diesel engines a value for C_2 of .00324 (m / sec K) correctly accounted for the increased heat transfer during combustion. Danieli used a value of unity for the non-firing velocity constant (18). These data were used as starting points for the calibration of the heat transfer model.

In order to evaluate the heat transfer the chamber surface area must be calculated:

$$\dot{Q} = h\,A\,(T - T_{wall}) \tag{2.30}$$

During combustion heat is transferred from both zones so chamber surface areas for each zone need to be defined.

$$Q = h\,A_u\,(T_u - T_{wall}) + h\,A_b\,(T_b - T_{wall}) \tag{2.31}$$

The rotor surface area is constant throughout the cycle and is approximated by a circular arc :

$$A_{rotor} = 2\,R_x\,\beta\,b \tag{2.32}$$

Where:

$$R_x = \frac{R^2 - 2eR + 4e^2}{R - 4e} \quad : \text{Radius of circular arc approximation}$$

$$\beta = \arctan\left[\frac{\sqrt{3R}}{\left(\frac{6eR}{R-4e}\right) + R + 2e}\right] \quad : \text{One half the angle subtended by the approximate circular arc}$$

It is assumed that the rotor cutout adds negligible surface area. The side plate surface is calculated during the volume calculation and is :

$$A_{side} = 2V / depth \tag{2.33}$$

To find the exact housing surface area would require a double integration. It was decided instead to follow Danieli's approach by devising a rectangular box of the same volume as the chamber (Fig. 8). From this the housing area is approximated as:

$$A_{housing} = A - A_{rotor} - 2 A_{side}$$

$$= 2 \frac{V}{2} + bL + C \tag{2.34}$$

Where :

$A = 2\left(\frac{V}{b} + \frac{V}{L} + bL\right) + C$: Total surface area

$L = 2 R_x \beta$: Arc length of rotor face

C : A correction factor

During combustion the following approximation is used to divide the individual surface areas between the burned and unburned zones :

$$\frac{A_b}{A_u} = \left(\frac{V_b}{V_u}\right)^{2/3} \tag{2.35}$$

2.3.4 LEAKAGE

Leakage past the apex and side seals is a major problem for the Wankel engine. It has been estimated that side seal leakage accounts for one quarter to as much as one third of the total leakage mass flow (19). Previous computer models have neglected side seal leakage and modeled apex seal leakage only (20&21). These models have assumed that leakage during combustion is composed of unburned gas alone, while at the end of

combustion only burned product is leaked. This results from the assumption of a linearly propagating flame front, which implies that the apices do not "see" burned gas until combustion is complete (Fig. 9). These models have also used the overall chamber or zone (during combustion) temperature as the upstream temperature.

It was felt that some effort should be made to model the significant leakage past the side seals. The gas that passes the side seals enters the volume between the oil seals, rotor side, side plate, and side seals (Fig. 10). This mass then enters the side intake ports as the rotor passes over them and so indirectly enters the intake chamber.

By using bulk gas temperatures, previous models may have overestimated the size of the leakage areas . Gas leaking past the apex seals comes from areas with high surface to volume ratios where large gas velocities are believed to exist due to: rotor rotation, vortices set up by the apex seals, and the "squish" of the rotor against the housing. This large surface area and high gas velocity indicates that the leakage mass is likely to be relatively cool and could even approach the wall temperature. Mass that leaks past the side seal must reside in the small clearance volume formed by the rotor side, side seal, and side plate prior to passing the side seal. Again, because of a high surface-to-volume ratio the leakage gas should be relatively cool.

2.3.5 CREVICE VOLUME

Much previous work has concentrated on the effect of crevice volumes on hydrocarbon emissions from spark ignition engines (22). It is now becoming apparent that crevices could also be an important source of performance loss in internal combustion engines. This performance loss is

caused by the heat lost from hot combustion products as they enter the crevices and the removal of charge during the useful portion of the cycle.

A brief description of the crevice volume model along with major implications for the cycle simulation program is provided in this section. A more thorough investigation of crevice volumes is given in Chapter 3 .

The leakage and crevice volume models were linked together for two major reasons. First the belief that leakage gas is cooled prior to its transmission from one chamber to the next suggests the use of the crevice temperature as the upstream temperature to reduce the number of independent parameters. Secondly in the Wankel, major crevice volumes and leakage sites occur at the same locations. That is, significant crevice volumes are found in the Wankel adjacent to the side and apex seals .

3.0 CREVICE AND LEAKAGE MODEL

This chapter presents the assumptions made in the model for the analysis of the effects of leakage and crevice volume on engine performance. Engine geometric data is analyzed that suggests crevice volumes in the Wankel are possibly significant factors in performance degradation. The model is then presented and the thermodynamic equations for the open system are derived. Finally, some of the programming considerations for implementing the submodel are discussed.

3.1 CREVICE LOCATIONS AND LEAKAGE POINTS

The author investigated the locations and relative sizes of crevice volumes by taking measurements from a Mazda model (12B) RX-4 engine. The engine was, of course, cold at the time so the absolute magnitude of the crevice volumes should not be considered as final values during operation, as thermal expansion will affect clearances. The major crevices were around the apex seals and side seals; other smaller volumes were associated with spark plugs and transducers (Fig. 11). In typical reciprocating engines the total crevice volume is 3% of the clearance volume and as much as 10% of the cylinder mass is pushed into the crevice at peak pressure. The total measured crevice volume on the Wankel engine was 5% of the clearance volume so a proportionately larger effect should be expected. Table 3 presents the measured and estimated sizes of all the crevices in the rotary engine. It should be noted that the volume associated with the side seal lands and side seals is approximately one half that of the volume behind the apex seals and below the corner seals. This is precisely the same ratio as between apex seal leakage and side seal leakage in the Wankel previously reported.

By ignoring side seal leakage and heat transfer from the leakage gas, leakage areas may have been overestimated in previous models and some effort should be expended to model these effects. After all, one third of the total leakage is significant. The primary difference between the apex and side seal leakage paths is that the side seal will "see" burned gas during combustion in proportion to the surface area "wetted" by the burned gas volume. A secondary difference is the indirect leakage path from the side seal to the rotor side, to the side intake port, and finally to the intake chamber. Therefore, most of the side seal leakage ends up in the intake chamber and not distributed evenly between the leading and trailing chambers as is the case for apex leakage.

3.2 OPTIONS

Figure 12 shows a schematic of a model that includes each leakage path and crevice volume explicitly. This model would be far too complex for the purpose at hand. Separate temperatures, areas, volumes, and compositions leave a virtually unlimited combination of crevice volumes and leakage paths. Most of these combinations are too complex to successfully calibrate with available data (Fig. 13).

The chosen model uses two crevices and two leakage areas per chamber located at each apex seal (Fig. 14). To account for the effect of burned gas entering the side seal crevices, the composition of gas entering the modeled crevices is related to the mass fraction burned, not the volume fraction burned, to grossly account for the relative size of the side crevices.

To account for side seal leakage, the mass composition of the leaked gas is taken to be equal to the crevice composition. In effect, the model implies that leakage occurs directly from the crevice, to the adjacent

chamber, which is probably not true at the apex seal. This is not a large error until the end of combustion when too much unburned gas may start to leak out. However, complete combustion is characterized by a falling chamber pressure and hence a return of crevice mass into the chamber adjacent to the apex seal. It can be reasonably expected, therefore, that the crevice gas which returns, leaves the chamber immediately, via the direct leakage path (Fig.15). Leakage occuring from the crevices allows for the transmission of burned product as well as unburned mixture throughout the cycle.

The performance loss caused by crevice volumes is due to the large amount of heat transfered to the engine components and the removal of charge from the combustion chamber. Leakage reduces power by decreasing volumetric efficiency (real and effective), and by allowing unburned fuel energy and sensible enthalpy to escape. Real volumetric efficiency is decreased by burned product entering the induction chamber from the adjacent combustion and exhaust chambers. Effective volumetric efficiency is decreased as charge escapes from the compression chamber to the exhaust and intake chambers prior to combustion. The assumptions made by the leakage and crevice volume model are listed below.

a) Constant leakage area at apex seals. Side leakage effects are modelled implicitly.

b) Quasi one-dimensional isentropic leakage flow.

c) Leakage composition and temperature is equal to the crevice composition and temperature.

d) Crevices modeled at apex seals only. Side crevice effects are lumped into apex crevice volumes.

e) A crevice has constant volume and gas temperature.

f) Crevice gas pressure is equal to chamber pressure.

g) Only one crevice exists per apex seal. The crevice is associated with the chamber at higher pressure and assumes that pressure.

h) The composition of gas entering the crevice is assumed to equal the mass fraction burned in order to account for burned gas that enters side crevices.

i) For computational simplicity burned and unburned gas are perfectly mixed in the crevice but return to their respective zones when they re-enter the chamber.

As there is only one crevice per apex seal the program must be capable of deciding which of the two adjacent chambers contains the crevice. In this model, it is postulated that the crevice is located behind the apex seal and that the crevice is associated with the chamber at higher pressure. If the pressure difference across the apex seal reverses, the seal moves across its seat and the crevice is again associated with the chamber at higher pressure (Fig. 16). A table of chamber pressure versus crank angle is stored within the program, enabling evaluation of the pressure difference across each apex seal to determine crevice location and leakage direction. Since the pressure history is not constructed until the first cycle is completed the leakage and crevice volume models are not activated until the second iteration begins.

At crank angles where pressure is low gas, leaks into the system from the leading and trailing chambers. To determine the composition of this flow the crevice composition is stored in the same manner as chamber pressure, and is used to assign composition to the leakage flows entering

the system in the next iteration. Over the first cycle iteration this information is not available so initial values are assumed at the start of the second iteration.

It should be noted that the program sets the leakage composition equal to the mass fraction unburned , which allows the program to operate if the crevice volume is set equal to zero. A variable was added to account for the fuel energy that escapes unburned to the exhausting chamber.

3.3 THERMODYNAMIC EQUATIONS OF CREVICE VOLUME AND LEAKAGE MODEL

The final thermodynamic equations of Chapter 2 (Eqs. 2.18 and 2.19) assumed that all mass flows are independent of changes in system pressure. This is clearly not the case when crevice volumes are present. The driving force for mass flow into or out of the crevice is a change in chamber pressure. Figure 17 shows the thermodynamic system boundary superimposed on the crevice and leakage model schematic. It should be noted that the system only contains the chamber and not the crevice volumes themselves. Positive direction flows are as shown for each mass flux. The perfect gas equation applied to a crevice volume holds that:

$$m_{crevice} = \left(\frac{pV}{RT}\right)_{crevice} = p\left(\frac{V}{RT}\right)_{crevice} \qquad (3.1)$$

Since crevice volume and temperature are constant, differentiating both sides of equation 3.1 yields:

$$\left(\frac{\dot{m}}{m}\right) = \frac{\dot{p}}{p} - \left(\frac{\dot{R}}{R}\right)_{crevice} \qquad (3.2)$$

If the rate of change of the gas constant is assumed to be negligible Eq. 3.2 reduces to:

$$\dot{m}_{crevice} = \frac{\dot{p}}{p} m_{crevice} \tag{3.3}$$

The total mass flow into the chamber is then defined as:

$$\dot{m} = \sum \dot{m}_j = \dot{m}_{intake} - \dot{m}_{exhaust} - (\dot{m}^{lead} + \dot{m}^{lag})_{leakage} - (\dot{m}^{lead} + \dot{m}^{lag})_{crevice} \tag{3.4}$$

Substituting equation 3.3 in for the crevice flow terms of the last equation yield:

$$\dot{m} = \dot{m}_{in} - \dot{m}_{ex} - (\dot{m}^{lead} + \dot{m}^{lag})_{leak} - \frac{\dot{p}}{p}(m^{lead} + m^{lag})_{crev} \tag{3.5}$$

An equivalent expression for the mass flow is:

$$\dot{m} = d^* - c^* \dot{p} \tag{3.6}$$

Where:

$$d^* = \dot{m}_{in} - \dot{m}_{ex} - (\dot{m}^{lead} + \dot{m}^{lag})_{leak} \tag{3.7a}$$

$$c^* = \frac{1}{p}(m^{lead} + m^{lag})_{crev} \tag{3.7b}$$

The mass fraction of fresh charge is defined as:

$$x_1 \equiv \frac{m_1}{m} \tag{3.8}$$

Differentiating both sides gives:

$$\frac{\dot{x}_1}{x_1} = \frac{\dot{m}_1}{m_1} - \frac{\dot{m}}{m} = \frac{\dot{m}_1 - \dot{m}x_1}{mx_1} \tag{3.9}$$

Therefore:

$$\dot{x}_1 = \frac{\dot{m}_1 - \dot{m}x_1}{m} \tag{3.10}$$

The mass flow of fresh charge entering the system is :

$$\dot{m}_1 = \Sigma\, \dot{m}_j x_{1_j} \tag{3.11}$$

where :

x_{1j} = Mass fraction of fresh charge in the j^{th} flow.

$$m_1 = (mx_1)_{in} - (mx_1)_{ex} - [\,(m_{leak} + m_{crev})\, x_1^{lead}\,] - [\,(\dot{m}_{leak} + \dot{m}_{crev})\, x_1^{lead}\,] \tag{3.12}$$

Recalling that exhaust manifold flow is assumed to be fully burned, the rate of change of mass fraction fresh charge can be expressed as :

$$\dot{x}_1 = \frac{1}{m}\Big[\, \dot{m}_{in}(x_1^{in} - x_1) - \dot{m}_{leak}^{lead}(x_1^{lead} - x_1) - \dot{m}_{leak}^{lag}(x_1^{lag} - x_1) - \frac{\dot{p}}{p} m_{crev}^{lead}(x_1^{lead} - x_1) - \frac{\dot{p}}{p} m_{crev}^{lag}(x_1^{lag} - x_1) \tag{3.13}$$

Alternatively :

$$\dot{x}_1 = a^* - b^*\dot{p} \tag{3.14}$$

where :

$$a^* = \frac{1}{m}\left[\dot{m}_{in}(x_1^{in} - x_1) - \dot{m}_{leak}^{lead}(x_1^{lead} - x_1) - \dot{m}_{leak}^{lag}(x_1^{lag} - x_1)\right] \quad (3.15a)$$

$$b^* = \frac{1}{pm}\left[\dot{m}_{crev}^{lead}(x_1^{lead} - x_1) + \dot{m}_{crev}^{lag}(x_1^{lag} - x_1) \right] \quad (3.15b)$$

Eq. 2.18 is rewritten here in order to make the changes due to crevice volumes clear.

$$\dot{P} = \frac{\rho}{(\partial\rho/\partial p)}\left[\left(\frac{R_1 - R_2}{R}\right)\dot{x}_1 + \frac{\dot{m}}{m} - \frac{\dot{V}}{V} - \left(\frac{\partial\rho}{\partial T}\right)_\rho \dot{T} \right] \quad (3.16)$$

We have seen that $\dot{x}_1$ and $\dot{m}$ are dependent on $\dot{p}$, so:

$$\dot{p} = \frac{\rho}{(\partial\rho/\partial p)}\left[\left(\frac{R_1 - R_2}{R}\right)(a^* - b^*\dot{p}) + \left(\frac{d^* - c^*\dot{p}}{m}\right) - \frac{\dot{V}}{V} - \frac{\dot{T}}{\rho}\frac{\partial\rho}{\partial T} \right] \quad (3.17)$$

Factoring all the p terms to the left hand side gives:

$$p = \left[\frac{1}{\frac{(\partial\rho/\partial\rho)}{\rho} + b^*\frac{R_1 - R_2}{R} + \frac{c^*}{m}} \right] \left[\left(\frac{R_1 - R_2}{R}\right)a^* - \frac{\dot{V}}{V} - \frac{\dot{T}}{\rho}\frac{\partial\rho}{\partial T} + \frac{d^*}{m} \right] \quad (3.18)$$

Giving the first term a separate variable name shortens the equation:

$$\dot{p} = c^*\left[\left(\frac{R_1 - R_2}{R}\right)a^* - \frac{\dot{V}}{V} - \frac{T}{\rho}\frac{\partial\rho}{\partial T} + \frac{d^*}{m} \right] \quad (3.19)$$

where:

$$z^* = \left[\frac{1}{\frac{(\partial\rho/\partial p)}{\rho} + b^*\left(\frac{R_1 - R_2}{R}\right) + \frac{c^*}{m}} \right] \tag{3.20}$$

The enthalpy flux into the chamber can be written as:

$$\sum \dot{m}_j h_j = (\dot{m}h)_{in} - (\dot{m}h)_{ex} - (\dot{m}_{leak}h)^{lead} - (\dot{m}_{leak}h)^{lag} - (\dot{m}_{crev}h)^{lead} - (\dot{m}_{crev}h)^{lag} \tag{3.21a}$$

$$= (\dot{m}h)_{in} - (\dot{m}h)_{ex} - (\dot{m}_{leak}h)^{lead} - (\dot{m}_{leak}h)^{lag} - \frac{\dot{p}}{p}\left[(m_{crev}h)^{lead} + (m_{crev}h)^{lag} \right] \tag{3.21b}$$

$$= e^* - f^*\dot{p} \tag{3.21c}$$

where:

$$e^* = (\dot{m}h)_{in} - (\dot{m}h)_{ex} - (\dot{m}_{leak}h)^{lead} - (\dot{m}_{leak}h)^{lag} \tag{3.22a}$$

$$f^* = \frac{1}{p}\left[(m_{crev}h)^{lead} + (m_{crev}h)^{lag} \right]$$

Recalling the First Law expression of Eq. 2.3 rewritten here:

$$m\dot{h} = -\dot{Q}_w - h\sum\dot{m}_j + \sum\dot{m}_j h_j + V\dot{p} \tag{3.23}$$

Using the definitions of the dummy variables defined in Eqs. (3.15a), (3.15b), (3.20), (3.22a), and (3.22b) the energy balance is:

$$m\{ (h_1 - h_2)a^* + [c_p - b^*(h_1 - h_2)]\dot{p} + c_p\dot{T} \} =$$

$$-Q_w - h(d^* - c^*p) + e^* - f^*p + Vp \tag{3.24}$$

An expression for the rate of change of temperature is found to be:

$$\dot{T} = \frac{1}{mc_p}\{ \dot{p} [V - f^* + hc^* + mb^*(h_1 - h_2) - c_T m] -$$

$$ma^*(h_1 - h_2) - hd^* + e^* - \dot{Q}_w \qquad (3.25)$$

Substituting Eq. 3.19, derived from the perfect gas equation of state, into the last equation yields:

$$T = \frac{1}{mc_p}\{ z^* [(\frac{R_1 - R_2}{R})a^* - \frac{\dot{V}}{V} - \frac{\dot{T}}{\rho}\frac{\partial \rho}{\partial T} + \frac{d^*}{m}] [V - f^* + hc^*$$

$$+ mb^*(h_1 - h_2) - cT_m] - ma^*(h_1 - h_2) - hd^* + e^* - \dot{Q}_w \} \qquad (3.26a)$$

$$T = [\frac{1}{mc_p + (\frac{w^* z^*}{\rho})(\partial \rho / \partial T)}] \{ w^* z^* [(\frac{R_1 - R_2}{R})a^* - \frac{\dot{V}}{V} + \frac{d^*}{m}] -$$

$$ma^*(h_1 - h_2) - hd^* + e^* - \dot{Q}_w \} \qquad (3.26b)$$

where:

$$w^* = V - f^* + hc^* + mb^*(h_1 - h_2) - c_T m \qquad (3.27)$$

Equation 3.26b is valid for intake, compression and exhaust. During the combustion-expansion phase two separate zones are hypothesized and each has an individual gas temperature. The First Law for a system with no compositional variation shows:

$$m\dot{h} = mc_p\dot{T} + mc_T\dot{p} = -\dot{Q}_w - h_j\dot{m}_j + \sum(\dot{m}_j h_j) + V\dot{p} \qquad (3.28)$$

Since only ideal gases are considered, the specific heat at constant temperature term is zero. The unburned and burned zone temperatures may be

written as:

$$\dot{T}_u = \frac{1}{m_u c_{p_u}} \left[\sum(\dot{m}_j h_j)_u - h_u \sum(\dot{m}_j)_u + V_u \dot{p} - \dot{Q}_u \right] \tag{3.29a}$$

$$\dot{T}_b = \frac{1}{m_b c_{p_b}} \left[\sum(\dot{m}_j h_j)_b - h_b \sum(\dot{m}_j)_b + V_b \dot{p} - \dot{Q}_b \right] \tag{3.29b}$$

From the definition of density:

$$V = \frac{m}{\rho} \tag{3.30}$$

We have:

$$\frac{\dot{V}}{V} = \frac{\dot{m}}{m} - \frac{\dot{\rho}}{\rho} = \frac{\dot{m}}{m} - \frac{1}{\rho} \left[\left(\frac{\partial \rho}{\partial T}\right) \dot{T} + \left(\frac{\partial \rho}{\partial p}\right) \dot{p} \right] \tag{3.31}$$

So for each zone we have:

$$\frac{\dot{V}_u}{V_u} = \frac{\dot{m}_u}{m_u} - \frac{1}{\rho} \left[\left(\frac{\partial \rho}{\partial T}\right)_u \dot{T}_u + \left(\frac{\partial \rho}{\partial p}\right)_u \dot{p} \right] \tag{3.32a}$$

$$\frac{\dot{V}_b}{V_b} = \frac{\dot{m}_b}{m_b} - \frac{1}{\rho} \left[\left(\frac{\partial \rho}{\partial T}\right)_b \dot{T}_b + \left(\frac{\partial \rho}{\partial p}\right)_b \dot{p} \right] \tag{3.32b}$$

Also, since the rate of change of chamber volume is known:

$$\frac{\dot{V}_b}{V_b} = \frac{\dot{V} - \dot{V}_u}{V_b} = \frac{\dot{V}}{V_b} - \frac{\dot{V}_u}{V_u} \frac{V_u}{V_b} \tag{3.33}$$

Combining Eqs. 3.32 and 3.33 and solving for the rate of change of unburned volume yields:

$$\frac{\dot{V}_u}{V_u} = \frac{V_b}{V_u}\left\{\frac{1}{\rho_b}\left[(\partial\rho/\partial T)_b\dot{T}_b + (\partial\rho/\partial p)_b\dot{p}\right] - \frac{\dot{m}_b}{m_b} + \frac{\dot{V}}{V_b}\right\} \quad (3.34)$$

Equating Eqs. 3.34 and 3.32a and using the expressions for temperature from Eqs. 3.29a and 3.29b provides:

$$\frac{\dot{m}_u}{m_u} - \frac{1}{\rho_u}\left\{\left(\frac{\partial\rho}{\partial T}\right)_u \frac{1}{m_u c_{p_u}}\left[\sum(\dot{m}_j h_j)_u - h_u\sum(\dot{m}_j)_u + V_u\dot{p} - \dot{Q}_u\right] + \left(\frac{\partial\rho}{\partial p}\right)_u\dot{p}\right\}$$

$$= \frac{V_b}{V_u}\left\{\frac{\dot{V}}{V_b} - \frac{\dot{m}}{m_b} + \frac{1}{\rho_b}\left[\left(\frac{\partial\rho}{\partial T}\right)_b \frac{1}{m_b c_{p_b}}\left[\sum(\dot{m}_j h_j)_b - h_b\sum(\dot{m}_j)_b + V_b\dot{p} - \dot{Q}_b\right] + \left(\frac{\partial\rho}{\partial p}\right)_b\dot{p}\right\} \quad (3.35)$$

Again, the mass flows and enthalpy fluxes are pressure change dependent so let:

$$\sum(\dot{m}_j h_j)_u = \left(-\dot{m}^{.lead}_{leak} - \dot{m}^{.lag}_{leak} - \frac{m^{lead}_{crev}}{p}\dot{p} - \frac{m^{lag}_{crev}}{p}\dot{p}\right)_u - \dot{m}_{comb} \quad (3.36a)$$

$$= d^*_u - c^*_u\dot{p} \quad (3.36b)$$

$$\sum(\dot{m}_j h_j)_b = \left(-\dot{m}^{.lead}_{leak} - \dot{m}^{.lag}_{leak} - \frac{m^{lead}_{crev}}{p}\dot{p} - \frac{m^{lag}_{crev}}{p}\dot{p}\right)_b + \dot{m}_{comb} \quad (3.36c)$$

$$= d^*_b - c^*_b\dot{p} \quad (3.36d)$$

$$\sum(\dot{m}_j h_j)_u = \{ - (\dot{m}_{leak}h)^{lead} - (\dot{m}_{leak}h)^{lag} - \frac{\dot{p}}{p}[(m_{crev}h)^{lead} + m_{crev}h)^{lag}]_u - \dot{m}_{comb}h_u \} \quad (3.36e)$$

$$= e^*_u - f^*_u\dot{p} \quad (3.36f)$$

$$\sum(\dot{m}_j h_j)_b = \{ - (\dot{m}_{leak}h)^{lead} - (\dot{m}_{leak}h)^{lag} - \frac{\dot{p}}{p}[(m_{crev}h)^{lead} + (m_{crev}h)^{lag}]_b + \dot{m}_{comb}h_b \} \quad (3.36g)$$

$$= e^*_b - f^*_b\dot{p} \quad (3.36h)$$

Substituting Eqs. 3.36 into Eq. 3.35 and solving for the rate of pressure change gives:

$$\dot{p} = \frac{\frac{d^*_u}{m_u} + \frac{(\partial\rho/\partial T)_u}{(\rho m c_p)_u}(d^*_u h_u + \dot{Q}_u - e^*_u) + \frac{d^*_b V_b}{m_b V_u}(d^*_b h_b - e^*_b + \dot{Q}_b)\frac{V_b}{V} - \frac{\dot{V}}{V_u}}{\frac{c^*_u}{m_u} + \frac{(\partial\rho/\partial T)_u}{(\rho m c_p)_u}(c^*_u h_u + V_u - f^*_u) + \frac{(\partial\rho/\partial p)_u}{\rho_u} + \frac{V_b}{V_u}\left[\frac{(\partial\rho/\partial p)_b}{\rho_b} + \frac{c^*_b}{m_b} + \frac{(\partial\rho/\partial T)_b}{(\rho m c_p)_b}(c^*_b h_b + V_b - f^*_b)\right]} \quad (3.37)$$

Once the rate of change of pressure is known the rates of change for temperature and volume of each zone can be found from previous equations; they are rewritten here using the dummy variables of Eq. 3.36:

$$\dot{T}_u = \frac{e^*_u - d^*_u h_u - \dot{Q}_u + (c^*_u h_u - f^*_u + V_u)\dot{p}}{(mc_p)_u} \quad (3.38)$$

$$\dot{T}_b = \frac{e^*_b - d^*_b h_b - \dot{Q}_b + (c^*_b h_b - f^*_b + V_b)\dot{p}}{(mc_p)_b} \qquad (3.39)$$

$$\dot{V}_u = V_u \left\{ \frac{d^*_u}{m_u} - \frac{(\partial\rho/\partial T)_u}{\rho_u} \dot{T}_u - \left[\frac{(\partial\rho/\partial p)_u}{\rho_u} + \frac{c^*_u}{m_u} \right] \dot{p} \right\} \qquad (3.40)$$

$$\dot{V}_b = \dot{V} - \dot{V}_u \qquad (3.41)$$

3.4 PROGRAMMING CONSIDERATIONS

In order to evaluate the differential equations of Chapter 3, enthalpies must be assigned to each flow. Since the rate of pressure change is not known until later in the calculation it is not possible to determine which direction the combined crevice and leakage flow goes at both the leading and trailing apices. This is resolved by assuming a net direction and checking the assumption when the pressure change has been calculated.

During combustion it is necessary to split the combined crevice and leakage mass flow rates between the burned and unburned zones. When net flow is out of the chamber the fraction of burned gas leaving is equal to the mass fraction burned. For return flow back into the chamber the unburned zone receives only unburned mixture and the burned zone receives only burned products.

$$\alpha = \begin{cases} 1 - x_b & : \text{ flow out of chamber} \\ \dfrac{1}{1 - x_{fresh}} x_{1_c} & : \text{ flow into chamber} \end{cases} \qquad (3.42)$$

where:

x ≡ Mass fraction unburned in flow

x_{l_c} ≡ Mass fraction fresh charge in crevice

x_{fresh} ≡ Mass fraction fresh charge in unburned zone (a constant)

It also should be noted that the rate of combustion in an open system is not equal to the rate of increase of burned products characterized by the Wiebe function. The combustion rate also depends on the mass flows to and from the chamber:

$$\dot{m}_b = \dot{x}_b m + x_b \dot{m} = \dot{m}_{comb} - (\dot{m}^{lead}_{leak})_b - (\dot{m}^{lag}_{leak})_b - (\dot{m}^{lead}_{crev})_b - (\dot{m}^{lag}_{crev})_b \quad (3.43)$$

so that:

$$\dot{m}_{comb} = \dot{x}_b m + x_b \dot{m} + (\dot{m}^{lead}_{leak})_b + (\dot{m}^{lag}_{leak})_b + (\dot{m}^{lead}_{crev})_b + (\dot{m}^{lag}_{crev})_b \quad (3.44)$$

Again the crevice mass flow rates are not known until the rate of change of pressure is calculated. However, the combustion rate is needed to evaluate the pressure change. This dilemma is circumvented by approximating the crevice flows by using the last known value.

4.0 MODEL VALIDATION AND CALIBRATION

4.1 INTRODUCTION

To ensure that program output is logical and correct each major change to the program, described in Chapter 1, was separately validated. For this checking process it was often helpful to have the similar reciprocating engine program in order to compare results. This chapter presents the methods used to validate the programming changes and the submodels. A discussion of the procedure used to calibrate the submodels once validation was complete follows.

4.2 GEOMETRY VALIDATION

The alteration of the geometry subroutine and the geometry effects embedded in the rest of the code was the first change made to the program; thus no leakage, crevice volume, or heat transfer models were, as yet, included. The first checks were made by comparing volume and rate of change of volume graphs. A graphical analysis of the slopes and areas under the curve showed that the two variables were consistent. The calculation of compression ratio made by the program was also found to be correct proving that the chamber volume equations were behaving as expected. After the geometry switch had been accomplished a motoring run was made to allow comparison of this pressure trace to the pressure trace of a motoring run on a reciprocating engine with no heat transfer. The traces were similar enough for engines with somewhat different compression ratios and no obvious errors were apparent. The constant for a polytropic compression in the Wankel engine simulation was found to be 1.33 which is within the expected range of :

$1.3 < \gamma < 1.35$

The program itself has several built in error checks that are useful for the end user. The fact that the program converges to a solution is a good indication , in itself, that the program is running smoothly. Calculations made at the end of each cycle also provide consistency checks. For instance, a motoring run with no heat transfer, leakage, or crevice volume energy loss models activated should have a gross indicated mean effective pressure (gross IMEP) of exactly zero. The program also performs a global energy balance and prints out the net energy gain over a complete cycle divided by the enthalpy of the charge inducted. Errors of less than one percent can be expected for motoring runs.

Specified burn rate firing runs were made on both the reciprocating and rotating engine simulations, and the outputs checked against each other. Again, the pressure traces were similar and no obvious discontinuities existed. Cycle outputs such as volumetric efficiency, indicated mean effective pressure, and exhaust energy were also cross-checked and found to be comparable. For the firing case the code again provides a useful check on the program operation. The global energy gain as a percentage of the fuel energy inducted should be on the order of one percent for a converged cycle.

4.3 CREVICE AND LEAKAGE MODEL VALIDATION

To gain more detailed information about the crevice and leakage model behaviour a separate output file was created for this subprogram. In order to check this model a crevice volume of 2 cm^3 per apex seal and a leakage area of 1 mm^2 per apex seal were used. These values were taken from experimental data and previous computer simulations of the Wankel engine.

One good quantitative check of the model is that over the entire cycle the algebraic addition of leakage mass past each apex seal is zero (by mass conservation). A second quantitative check is that the crevice mass, and composition should be the same for both chambers at the crank angle where a crevice transfers from one chamber to the other. It must be remembered that the lead crevice which transfers out of the chamber at approximately +500° is, as far as the program is concerned, the same as the lag crevice that switches into the chamber at -220°. Also, at any crank angle that a crevice transfers into or out of the chamber the pressure difference across the appropriate apex seal and the leakage flow rate are zero. Qualitatively the crevice volumes flatten out (vertically compress) the pressure trace and leakage reduces peak pressure and advances the crank angle for peak pressure.

4.4 HEAT TRANSFER VALIDATION

The total heat loss from a spark ignition engine is about one third of the fuel energy input. Once the heat transfer subroutine had been debugged the model predicted roughly this amount of heat loss. An additional check was made by comparing output from the original reciprocating engine simulation to ensure that heat transfer rates were correct at least to an order of magnitude.

4.5 MODEL CALIBRATION

Once all the program code had been debugged and each new subprogram validated the submodel parameters required calibration so that the model would accurately predict the engine operating characteristics at different loads and speeds. These parameters requiring calibration were leakage

area, crevice volume, and heat transfer velocity. Finding appropriate values for each of these input variables required matching computer output with data supplied by N.A.S.A. .

N.A.S.A. has provided us with sufficient motoring engine data useful for a preliminary calibration. However, a lack of data from a firing engine makes the results discussed in the next chapter limited in scope.

Motoring data allows the matching of three engine operating characteristics :

volumetric efficiency	(m_{in})
peak pressure	(p_{max})
crank angle at peak pressure	(Θ_{peak})

The calibration strategy was to select nine motoring runs made at three engine speeds (1000, 2000, and 3,000 RPM) and three throttle settings (33%, 66% , and 100% open) and construct a test matrix, (Table 4). The model was then calibrated to match as closely as possible the data from the median engine speed and throttle position. Computer runs were then made at different speeds or throttle settings (four separate points) while the model calibration parameters were held constant to check that the model adequately matched engine data. A first attempt to match the data provided good agreement with peak pressure, and volumetric efficiency at parameter values of :

$V_{crevice}$ = 1.0 cm^3 per apex

A_{leak} = 0.004 cm^3 per apex

$Vel_{non-fire}$ = 0.5 V_{rotor}

However, the pressure at the end of intake was appreciably in error and an effort was made to correct this problem.

4.5.1 INTAKE PORT OPEN AREA

Table 5 shows the basic engine geometric information supplied by N.A.S.A. for the Mazda test engine . The N.A.S.A. engine has been modified by enlarging one of the two side ports. By comparing engine data and model output that uses the intake port timings supplied, it can be seen that the modelled port opens approximately 10 degrees later in the model, than in the engine, as shown by the shift in the pressure drop that occurs as the port opens (Fig. 18). Also the port closing time appears to be significantly late. The intake port timings were advanced 10 crank angle degrees in the model to match the port opening pressure trace but intake port close pressure was still significantly low.

All attempts to match the intake port closing pressure while also matching the other operating characteristics by varying the submodel parameters failed. The only method that allowed a good match for all four characteristics was by variation of the intake port closing profile. Initially the intake port was assumed to open and close at a constant rate. Once the experimental modification to the intake port became known the closing profile was adjusted (Fig 19). To match p_{IPC} a set of exponential profiles were used to close the extended portion of the port. The profile which gave the best data fit is shown on the last figure. There appears to be a discrepency between the intake port timing data provided, and the input data that matches the pressure trace. This is a problem which should be fairly easy to resolve by accurately measuring the intake port open area profile on the engine. By using the exponential port closing profile the intake port is effectively closed at -210°, some 40° advanced from the reported value.

Because the port area was reduced during the last stages of induction,

the reverse flow out of the chamber was minimized and the volumetric efficiency increased to a level significantly higher than measured. To decrease the volumetric efficiency the intake manifold pressure was decreased by 2% and the leakage area and heat transfer velocity were increased (Fig. 20).

4.5.2 FINAL MOTORING CALIBRATION

Because heat transfer and leakage had been increased from the values reported above, in order to decrease volumetric efficiency, the crevice volume was reduced in order to match peak chamber pressure.

$V_{crevice}$ = 0.875 cm^3 per apex seal

A_{leak} = 0.010 cm^2 per apex seal

$Vel_{non-fire}$ = 0.75

Table 6 shows the computer output for the variables matched and the relative error between predicted and measured values. No attempt was made to match the crank angle at peak pressure for two reasons. First, at low speeds the measured θ_{peak} was consistently after top dead center (TDC). This is not reasonable since it would require a net energy influx. The second reason for not attempting to match θ_{peak} was the trend of the measured values with RPM. For motored conditions θ_{peak} is strongly affected by leakage and heat transfer, which are both time dependent energy loss mechanisms. The time dependence of both of these phenomena suggests that at slower speeds θ_{peak} becomes further advanced as more energy is lost due to leakage and/or heat transfer.

This predicted trend is opposite from the observed trend of lower energy loss (even a net gain) with reduced engine speed. The reason for this behaviour of the data is not immediately obvious, although it could be

explained by a speed dependent leakage area or experimental errors. The fact that θ_{peak} occured at + 0.5° and + 1.5° consistently for engine speeds of 1000 and 1500 RPM respectively, is an indication of at least some experimental error. The variable leakage area problem is currently being evaluated by the N.A.S.A. researchers in a dynamic study of apex seal motion. Leakage area may be increased at points in the cycle where the apex seal possibly lifts off from the housing surface due to dynamic forces. In the future, a variable leakage area may be included in the model.

A comparison between predicted and measured pressure traces during compression and expansion is shown in Fig. 21. Agreement is good except through top dead center. During expansion, predicted pressures are significantly below measured values. To check compression and expansion pressures a normalized logarithmic plot of chamber pressure versus volume was made (Fig. 22). The graph clearly shows that for all three engine speeds the polytropic expansion exponent is not constant for the engine data; in fact the measured chamber pressures at +180° are greater than or equal to the chamber pressures at -180° (nominal intake port close). During compression the measured polytropic constant also appears to change appreciably. This behaviour may be due to pressure transducer calibration problems, phasing difficulties with the angle indicator, or possibly very high heat transfer or leakage rates in the engine.

To check the calibrated model four other motoring runs were made, selecting a different speed or throttle position than the run used for calibration. The model was in good agreement with experimental data for each of these runs except the low speed case. Two other runs were made at 1000 RPM to see if the model problems were speed dependent only. For each

run at 1000 RPM the volumetric efficiency agreement was good to excellent, however, the predicted maximum pressure was significantly higher than the measured value. This leads one to expect that the crevice volumes may be somewhat larger than the calibrated value as this would decrease peak pressure without significantly affecting the volumetric efficiency or θ_{peak}.

4.5.3 FIRING CASE CALIBRATION

Only one cycle of firing data was available from N.A.S.A., which made firing case calibration preliminary. The engine operating condition was extremely throttled (11% open) at 2000 RPM. The equivalence ratio was assumed to be 1.2 which is typical of throttled conditions for reciprocating engines . While the calibration was necessarily limited by the lack of engine data, matching the light load engine data may provide some useful insights into an operating regime where the Wankel engine has been criticized for poor fuel economy and high HC emissions. A parametric study on the effects of reducing either crevice volume, heat transfer, or leakage will identify the major causes of poor engine performance at light load.

By varying the mass fraction burned equation (Eq. 2.25) variables, a fair agreement between predicted and measured pressure traces was found (Fig 23). There was no need to alter the leakage area for firing conditions which both Danieli, and Eberle & Klomp had reported. This is possibly a result of using a constant gas temperature for the leakage gas. The pressures during expansion were somewhat low presumably the consequence of the transducer calibration error discussed above. The timing of peak pressure was again advanced compared to the engine data, similar to the motored pressure traces.

4.5.4 COMMENTS ON CALIBRATION

Calibration of the model indicates the importance of various aspects of the test engine geometry and experimental data. These are:

a) Intake port timing and open area profile.

b) Chamber pressure rise above intake manifold pressure before bottom center of the intake stroke

c) Timing of peak pressure.

Once further information is available it will be possible to recalibrate the model parameters.

5.0 MODEL RESULTS

Once the simulation had been calibrated by using the experimental data a parametric study was conducted on the effects of changes in heat transfer rates, crevice volume, or leakage area on engine performance. Motoring computer runs for this parametric study were all made at a baseline operating point used to calibrate the model (2000 RPM, and 66% open throttle setting). The firing case runs were made at the light load setting available from N.A.S.A.. Since this firing case is extremely throttled, the chamber pressures and temperatures are low, so crevice volume effects can be expected to be minimal in comparison to the performance effects due to leakage and heat transfer. The results of this study are presented in this chapter.

5.1 MOTORING

Motored engine data is used in research activities to determine, approximately, the friction power of a given engine. Indicated power losses are generally not included in the calculation. However, for motored Wankel engines gas leakage between adjacent chambers is an appreciable power sink. The program's calculations may, therefore, be useful for experimental research into the actual friction power loss of the engine.

5.1.1 MOTORING VOLUMETRIC EFFICIENCY

Figure 24 shows the effect of changing the submodel parameters on the motored engine's volumetric efficiency. It can be seen that both heat transfer and crevice volumes have little effect on volumetric efficiency; in fact the calibrated values for these parameters are near the point where

they have the largest negative effect upon the engine's breathing. Increasing heat transfer rates or crevice volumes to values larger than calibrated, results in compression and expansion pressures being somewhat lowered. Consequently, a net reduction in leakage results in increased volumetric efficiency. Decreasing heat transfer causes the residual gases at the end of the cycle to be hotter, and therefore less dense. Therefore, during intake the smaller mass of residual gas is cooled to a lower temperature by the incoming charge. This results in a somewhat higher volumetric efficiency and a lower residual fraction. The leakage area has the greatest influence on volumetric efficiency.

5.1.2 MOTORING GROSS INDICATED MEAN EFFECTIVE PRESSURE

The significant effect of leakage on motoring engine power is shown in Fig. 25 where the effect on motoring gross IMEP by varying the three simulation parameters is shown. A reduction of 50% of motoring indicated power is predicted by the model if leakage could be eliminated. Reducing heat transfer would also have a significant effect on the motored engine's power consumption. The crevice volume effect is negligible because the working gas pressures and temperatures are too low for significant amounts of heat transfer to occur within the crevice.

5.1.3 MAXIMUM PRESSURE AND θ_{PEAK}

The compression expansion pressure traces for each variation in a parameter value are shown in figures 26-28. The effects of the submodel variables on maximum pressure and the angle where maximum chamber pressure is attained are shown in figures 29 and 30. Changing the crevice volume size does not affect θ_{peak} but does have a significant effect on maximum

pressure without altering gross IMEP. During motoring the crevice volume effect is quite symmetrical about top dead center. It appears that for the parameter values chosen crevice volumes have a greater effect on peak pressure than heat transfer, because energy is lost during compression while gas is pushed into the small volume; whereas convection heat transfer to the chamber walls is concentrated over the period before and after top dead center when gas temperatures are highest. Again, leakage is shown to be the dominant loss mechanism during motoring. Leakage out of the chamber occurs during compression and expansion so it has a large effect upon peak pressure and advances it significantly.

5.2 FIRING

The parametric study for a firing engine was made at the throttled operating condition for which experimental data was available. The chamber pressures and temperatures for this load point are low so heat transfer and, especially crevice volume losses are expected to be lower than for a high load operating condition. Also, at faster engine speeds the crevice volume losses will become a greater fraction of the total loss because of the time dependence of heat transfer and leakage. Additionally, the calibrated size of the crevice volume may be conservative as noted in Chapter 4.

5.2.1 FIRING VOLUMETRIC EFFICIENCY

The effects of parametric variation on volumetric efficiency show the same trends as for the motored engine with the exception of the zero heat transfer case (Fig. 31). This result may be amplified as wall temperature increases for high load conditions. In a fired adiabatic engine the

residual gases at the end of exhaust are hotter than in a conventional engine (Fig. 32) . The incoming fresh charge is heated by the residual gases and the intake chamber walls provide no cooling so less fresh charge is inducted. Crevice volumes have a negligible effect on volumetric efficiency for this case.

5.2.2 FIRING GROSS INDICATED MEAN EFFECTIVE PRESSURE

Figure 33 shows the dominance of leakage as the primary performance loss mechanism at light load. While power output is not a critical issue at light load it is instructive to note that a 36% gain in gross indicated power could be realized by eliminating leakage from the engine. Reducing the heat transfer coefficient has little effect on gross IMEP because any gain due to reduced energy losses is offset by a reduction in volumetric efficiency. The crevice volumes have negligible effect on engine power at such light load because of the low peak pressures and gas temperatures.

5.2.3 UNBURNED FUEL ENERGY EXHAUSTED

The model predicts that at the light load condition tested, 3.75% of the inducted fuel escapes to the exhaust chamber (Fig. 34). By reducing the leakage area to zero the escaping fuel energy can be reduced as no leakage path would exist for mass transfer between the high pressure expansion chamber and the exhaust chamber. Some fuel is left unburned because the crevice volumes withhold a significant amount of charge from the combustion process. The figure shows the effect of reducing leakage area or crevice volume on the fraction of charge that escapes. A 30% reduction is predicted by the model if the crevice volumes are eliminated.

While complete elimination of leakage or crevice volume is impossible an effort to reduce the size of the engine's crevice volumes should result in large decreases of fuel energy loss and quite possibly a significant reduction in HC emissions.

As the crevice volume model is designed to predict performance loss only, its predictions cannot be strictly used to infer HC emissions data. This is because unburned fuel that returns to the expansion or exhaust chamber will partially burn in the engine. This burn up phenomenon and the other variables that influence HC emissions are not included in the simulation. However, the predicted data does provide insight into the reduction of HC emission possible by reducing crevice volumes.

The model also predicts that reduced heat transfer will result in an increased percentage of fuel energy leaving through the exhaust port. There are two major causes for this, both relating to the induction phase. First, the residual gas fraction is lower, so the charge that enters the crevice volumes before escaping from the chamber is less dilute. Secondly, the volumetric efficiency is lower but chamber pressures during compression and early combustion are equivalent to the baseline case because of an increased thermal efficiency . Therefore, comparable amounts of gas escape but a larger fraction of the trapped mass leaves the chamber. Since the exhaust gases are hotter in an adiabatic engine, more partially burned charge will oxidize in the exhaust chamber and manifold. A turbocharger or compound device would recover this 'lost' energy.

5.2.4 RESIDUAL FRACTION

The effect of varying the submodel parameters on residual fraction is shown in Figure 35. It can be seen that leakage area strongly affects the

light load residual fraction. Burned product leaks past the apex seal from the exhaust chamber to the intake chamber and also flows past the side seals during combustion which reaches the intake chamber as previously explained. Reducing residual fraction in the Wankel could therefore result in increased combustion stability which has been a problem for the engine at light load (23).

Reduced heat transfer also affects the residual fraction, due to the lower density of the chamber contents at the end of exhaust. So less mass remains in the chamber at the beginning of the induction phase. Conversely, reduced crevice volume lowers the exhaust chamber temperatures allowing more mass to reside in the clearance volume.

5.3 DISCUSSION

As was predicted, the major energy loss mechanism for motoring and light load is the gas leakage problem which confirms the results of previous work (5,19,20). Heat transfer was also found to have significant influence on the engine's thermal and volumetric efficiency. These two effects offset each other in an adiabatic engine (at light load) and no change in gross IMEP is predicted. Crevice volumes have little effect on engine performance or efficiency for motoring and light load conditions. However, at higher speed and higher load conditions, crevice effects may become important.

6.0 SUMMARY AND CONCLUSIONS

6.1 SUMMARY

The purpose of this modelling study has been to construct a computer simulation of a spark ignited, pre-mixed charge Wankel rotary engine. Since the model is to be used for preliminary studies on engine performance characteristics and size requirements a zero-dimensional model using a specified combustion rate was used. The model can also be used to predict the performance changes brought about by advances in engine design and technology, such as the use of improved seal materials and/or insulative ceramic components. An evaluation of crevice volumes in the Wankel engine was undertaken which determined that their size and location are a possible source of performance loss. A crevice volume model was included in the simulation, for the first time in a model of the Wankel , to evaluate the relative importance of the crevice volumes on the engine's performance.

Previous research has shown that Wankel engine performance and efficiency is severely degraded by gas leakage between adjacent chambers. Most earlier models have ignored side seal leakage as a mode of mass loss, although side seal leakage has been documented to be one third of the total leakage of gas from the engine. The program implicitly includes the effect of side seal leakage by using the crevice gas compositions as the leakage gas composition. This enables the model to leak burned and unburned gas throughout the engine cycle as occurs in the real engine.

Engine motoring data collected by N.A.S.A. researchers from a Mazda two rotor Wankel engine was used to calibrate the submodel parameters. At the present time only one, low load, data point for a firing cycle is

available. Comparison of engine data and model predictions have shown some significant discrepencies, especially during intake and expansion. Some of these differences were reduced by changing the intake port timing and open area profile. It is believed that the calibration of the expansion chamber pressure transducer may be the cause of the discrepencies in the expansion chamber pressure between engine data and model calculations. It should be realized that running experimental and theoretical programs concurrently, commonly results in a more thorough understanding of the results from both efforts.

A clear need exists to resolve questions concerning the intake port timing. The possible errors in engine pressure data have made the parameter calibration values somewhat suspect and new data should be used to recalibrate the model. A lack of firing data at high load and speed points make any predictions about these operating regimes impossible at the present time. A light load engine data point was used to study the effects of crevice volumes, heat transfer, and leakage on engine performance at this operating condition.

The calibration of the model for motoring data produced simulation parameter values of:

$$A_{leak} = 1.0 \text{ mm}^2 \text{ per apex}$$

$$V_{crevice} = 0.875 \text{ cm}^3 \text{ per apex}$$

$$Vel_{non\text{-}fire} = 0.75\ (V_{rotor})$$

There was generally good agreement between model and engine data at various engine speeds and throttle settings. There was, however, a significant error in the predicted value of peak pressure at low engine speeds (1000 RPM). It is believed that this last problem is due to a conservative estimate of crevice volume.

A sensitivity study of the effects of changing leakage areas, crevice volumes, and heat transfer rates was done for motoring. At the mid speed and throttle setting tested the leakage area has the strongest effect on volumetric efficiency, gross indicated mean effective pressure, and maximum pressure. The crevice volumes had negligible effect on engine performance but strongly affected maximum chamber pressure. Reducing heat transfer had a negligible effect on volumetric efficiency but increased the mean effective pressure by virtue of an increased thermal efficiency.

The same parametric study was performed on the light load firing case. At light load the relative (to leakage) performance effects of heat transfer and crevice volume are small. The model shows that gas leakage is the primary source of performance loss at very light load, low volumetric efficiency and a large amount of unburned fuel energy that escapes to the exhaust results in a low IMEP. Burned product leaking into the induction chamber results in a higher residual fraction that could possibly cause combustion stability problems.

Crevice volume effects had little impact on engine performance at this light load. However, the crevice did strongly influence the amount of unburned fuel energy that escapes to the exhaust. This is due to the crevices storing unburned charge that eventually leaks out of the chamber.

The model's predictions for an adiabatic engine at light load are a reduced volumetric efficiency, a reduced residual fraction, an increase in thermal efficiency, an increase in the fuel energy that escapes to the exhaust, and a large increase in the temperature of the exhaust gases.

6.2 CONCLUSIONS

It may be concluded that:

a) The cycle simulation is behaving well and although some discrepancies exist between predicted and measured data, the problems can be resolved quickly.

b) The calibration, although preliminary, yielded some useful information relative to the experimental data.

c) The sensitivity study on the performance effects of the heat transfer crevice volume and leakage models, showed that at light loads and motoring conditions leakage has the greatest effect upon engine performance.

REFERENCES

1. Willis, E.A. , "Development Potential of Intermittent Combustion (I.C.) Aircraft Engines For Commuter Transport Applications, " N.A.S.A. T.M.-82869, 1982.

2. Zmroczek, L.A. , "Advanced General Aviation Comparative Engine/Airframe Integration Study, " N.A.S.A. C.R.-165565, 1982.

3. Huggins, J.L. and Ellis, D.R. , "Advanced General Aviation Comparative Engine/ Airframe Integration Study, " N.A.S.A. C.R.- 165564, 1981.

4. Jones, C. , "An Update of Applicable Automotive Engine Rotary Stratified Charge Developments, " SAE paper 820347, 1982.

5. Burley, H.A., Melogeny, M.R., and Stark, T.L. , "Sources of Hydrocarbon Emissions in Rotary Engines, " SAE paper 780419, 1978.

6. Yamamoto, K., Muroki, T. , "Development on Exhaust Emissions and Fuel Economy of the Rotary Engine at Toyo Kogyo, " SAE paper 780417,1978.

7. Jones, C., Lamping, H.D., Myers,D.M., and Loyd, R.W. , "An Update of the Direct Injected Stratified Charge Rotary Combustion Engine Developments at Curtiss-Wright, " SAE paper 770044, 1977.

8. Poulos, S.G. , "The Effect of Combustion Chamber Geometry On S.I. Engine Combustion Rates- A Modeling Study, " M.I.T. Department of Mechanical Engineering, SM Thesis, 1982.

9. Shampine, L.F., and Gordon, M.K. , "Computer Solutions of Ordinary Differential Equations: The Initial Value Problem, " Freeman, 1974.

10. Ansdale, R.F. , The Wankel RC Engine, Iliffe Books Ltd., London, 1968.

11. Yamamoto, K. , Rotary Engine, Toyo Kogyo Co. Ltd, Hiroshima, 1969.

12. Heywood, J.B. , "Engine Combustion Modeling - An Overview, " From Combustion Modeling Reciprocating Engines. Ed. by Mattavi and Amann, Plenum Corp., New York, 1980.

13. Annand, W.J.D. and Roe, G.E. , Gas Flow in the Internal Combustion Engine, Haessner Publishing, Inc. , 1974.

14. Wiebe, J.J. , "Das Wiebe - Brenngesitz ein Fortschnitt in der Kreigspozesse von Verbrennungsmotoren, " Trans. by Prof A. Joute and T.H. Dresen, Kraftadrzeugtechnik, Vol. 9 (1960).

15. Heywood, J.B., Higgins, J.M., Watts, P.A., and Tabaczynski, R.J. , "Devlopment and Use of a Cycle Simulation to Predict SI Engine Efficiency and NO_x Emissions, " SAE paper, 1979.

16. Rohsenow, W.M., and Choi, H.Y. , Heat Mass and Momentum Transfer, Prentice-Hall, New Jersey, 1961.

17. Woshni, G. , "A Universally Applicable Equation for the Instantaneous Heat Transfer Coefficient in the Internal Combustion Engine, " SAE Transactions, Vol. 76, paper 670931, (1968).

18. Danieli, G.A., Ferguson, C.R., Heywood, J.B. and Keck, J.C. , "Predicting the Emissions and Performance Characteristics of a Wankel Engine, " SAE Transactions, Vol. 83, paper 740186, (1974)

19. Eberle, M.K., and Klomp, E.D. , "An Evaluation of the Potential Performance Gain From Leakage Reduction in Rotary Engines, " SAE paper 730117, 1973.

20. Danielli, G.A., Keck, J.C., and Heywood, J.B. , "Experimental and Theoretical Analysis of Wankel Engine Performance, " SAE paper 780416, 1978.

21. McCuiston, F.D. , "Analytical Evaluation of the Effect of Leakage on no Emissions From a Rotary Engine, " SAE paper 750023, 1975.

22. Namazian, M. and Heywood, J.B. , "Flow in the Piston-Cylinder-Ring Crevices of a Spark Ignition Engine: Effect of Hydrocarbon Emissions, Efficiency and Power, " SAE paper 820088, 1982.

23. Kohno, T., Ito, R., Morita, M., and Mizuno, N. , "Analysis of Light-Load Performance in Rotary Engines, " SAE paper 790435, 1979.

Solid-State Ignition Trigger Vs Mechanical Trigger

Plasma Jet Ignition System

Eliminating Pilot Injector

High Temperature Aluminum Castings

Turbocharger

Thin Wall (Iron) Rotor

Exhaust Port Thermal Liner (Metallic)

Improved Lubricants

Multiple Power Source for Ignition

Induction Air Intercooler

Variable Displacement Pressure Oil Pump

Provision for Counter-Rotating Propellers

Total Diagnostics

Electronic Ignition Schedule

Computer Vs Mechanical Timing

Fiber Optics Data Bus

Low Pressure Drop Heat Exchangers

NASVYTIS Traction Speed Reducer (Prop)

Alternate Cooling Fluid

Composite Rotor Housing (Wear Resistant Liner)

Wing Leading Edge with Integral Coolant Cooler

Alternate Materials Seals

Retracting Apex Seals

Thermostatically Controlled Rotor Oil Cooling

Turbocharger with Variable Area Turbine

Spark Ignition Start/Auto-Ignition Run

Aluminum Rotor (Reinforced Lands)

Insulated Rotor - Thermal Barrier Coating

Independent Dual Ignition

Variable Compression Ratio

Insulated Rotor - Inserts on Metallic Pad Insulator

Adiabatic Engine Ceramic End Walls

Composite Rotor (Reinforced Apex Seal Land)

Electronic Injection (Fuel)

Adiabatic Engine Ceramic Rotor Inserts

Turbocompound

Adiabatic Engine - Ceramic Rotor Housing Liner

Pilot Nozzle Trigger for Ignition System

High Speed Propeller (No Reduction Gear)

NASVYTIS Traction Speed Reducer (Turbocompound Drive - If Used)

Adiabatic Engine - Ceramic Rolling Element Bearings

Table 1. Advanced rotary engine technologies.

ENGINE	RN SINGLE	RN TWIN	RN TOTAL
BASELINE	100	100	200
ADVANCED TECHNOLOGY SPARK IGNITION	121	126	247
HIGHLY ADVANCED TECHNOLOGY SPARK IGNITION	139	143	282
HIGHLY ADVANCED TECHNOLOGY DIESEL	140	145	285
ADVANCED ROTARY	137	141	278
HIGHLY ADVANCED ROTARY	144	149	293
GATE TURBINE (REVISED)	124 (131)	131 (138)	255 (269)

Table 2. Final engine/airframe rankings for different engine concepts relative to a base general aviation engine.

LOCATION	SIZE
behind apex seal	0.746 cm^3
beneath corner seal	0.093 cm^3
side seal land	0.285 cm^3
beneath side seal	0.225 cm^3
spark plug recesses	0.142 cm^3
spark plug threads	?

Table 3 location and size of crevice volumes in a model 12B Mazda Wankel engine.

Throttle Setting	1029 RPM	2052 RPM	2925 RPM
30-33%	m_{in} = 0.393 g P_{max} = 14.02 atm θ_{peak} = +0.5°	m_{in} = 0.406 P_{max} = 14.91 atm θ_{peak} = -1.1°	m_{in} = 0.353 g P_{max} = 13.27 atm θ_{peak} = -3.2°
60-66%	m_{in} = 0.448 g P_{max} = 14.44 atm θ_{peak} = +0.5°	m_{in} = 0.469 g P_{max} = 16.37 atm θ_{peak} = -1.1°	m_{in} = 0.460 g P_{max} = 16.38 atm θ_{peak} = -2.6°
100%	m_{in} = 0.436 g P_{max} = 13.75 atm θ_{peak} = +0.5°	m_{in} = 0.476 g P_{max} = 16.56 atm θ_{peak} = -1.1°	m_{in} = 0.475 g P_{max} = 16.59 atm θ_{peak} = -2.6°

Table 4. Motored engine test matrix with experimental data.

ENGINE GEOMETRY

Rotor radius	10.5 cm
Eccentricity	1.5 cm
Housing depth	7.0 cm
Compression ratio	9.4 : 1
Displacement	573 cm^3 x 2 rotors

INTAKE PORT DATA

Number of intake ports	2 per rotor
Total area	13.8 cm^2 per rotor
Ports open at	- 520 (deg ATDC)
Larger port closes at	- 170 (deg ATDC)
smaller port closes at	- 230 (deg ATDC)

Table 5. Basic engine geometry as supplied by N.A.S.A. .

Throttle Setting	1029 RPM	2052 RPM	2925 RPM
30-33%	m_{in} = 0.412 g relative error = +4.8% P_{max} = 14.94 atm relative error = +6.5% θ_{peak} = -4.5°	m_{in} = 0.419 g relative error = +3.2% P_{max} = 15.10 atm relative error = +1.3% θ_{peak} = -2.7°	
60-66%	m_{in} = 0.445 g relative error = -0.7% P_{max} = 15.36 atm relative error = +9.3% θ_{peak} = -4.5°	m_{in} = 0.476 g relative error = +1.4% P_{max} = 16.54 atm relative error = +1.0% θ_{peak} = -2.7°	m_{in} = 0.480 g relative error = +4.3% P_{max} = 16.50 atm relative error = +0.7% θ_{peak} = -2.1°
100%	m_{in} = 0.434 g relative error = -0.4% P_{max} = 15.26 atm relative error = +10.9% θ_{peak} = -4.5°	m_{in} = 0.488 g relative error = +2.5% P_{max} = 16.64 atm relative error = +0.5% θ_{peak} = -2.7°	

Table 6. Motored engine test matrix with computer results and, relative to measured engine data, error.

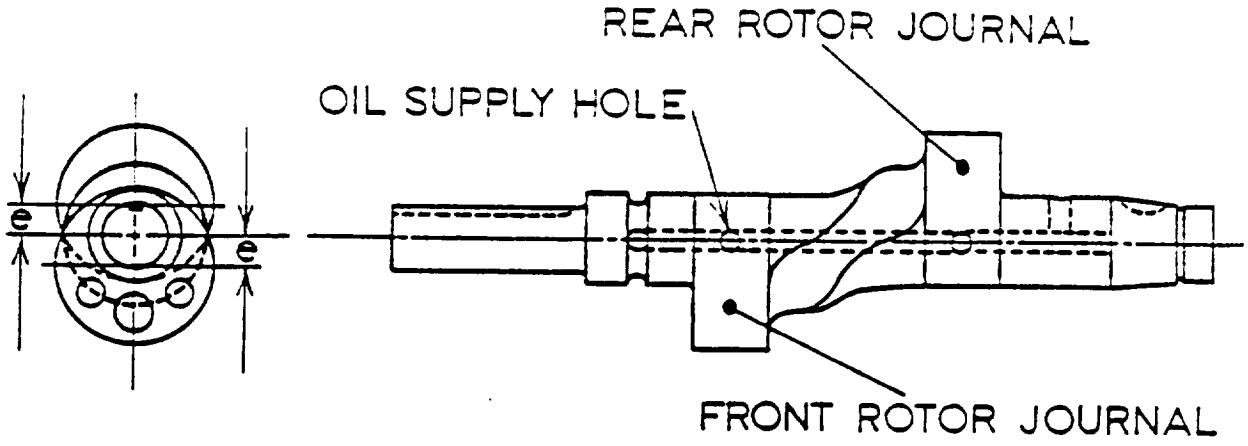

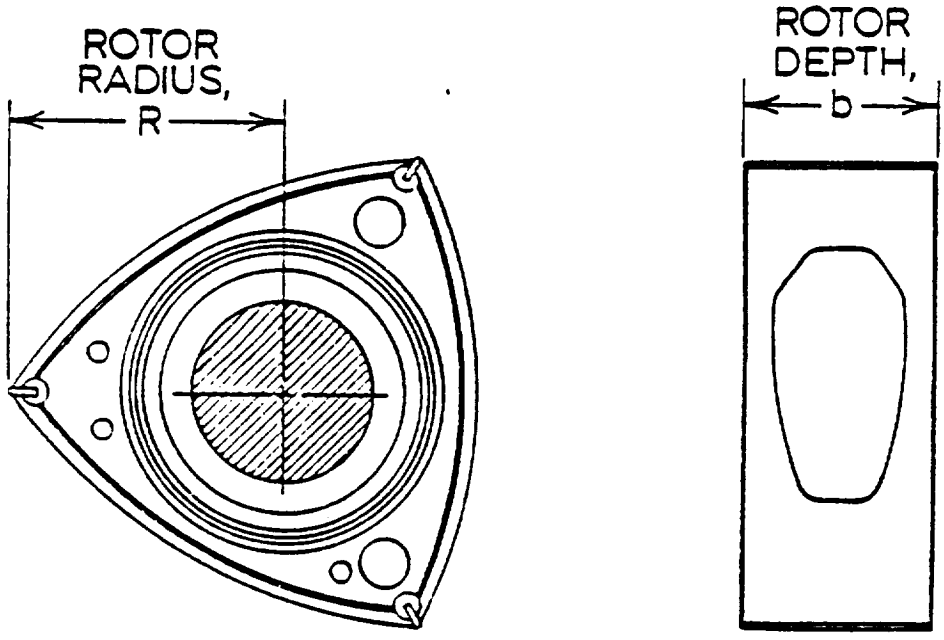

Figure 1. Side and end views of shaft and rotor showing basic engine dimensions.

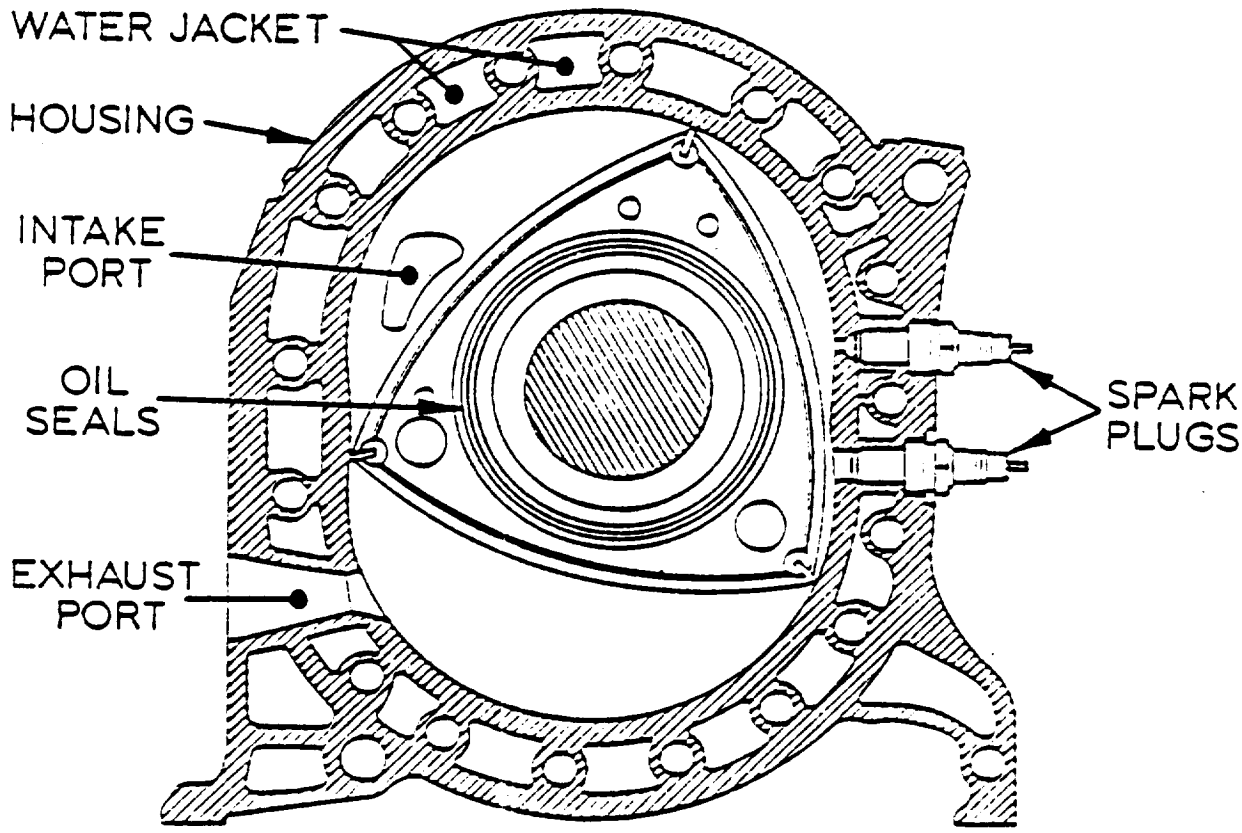

Figure 2. Side view of rotor and housing detailing engine geometry.

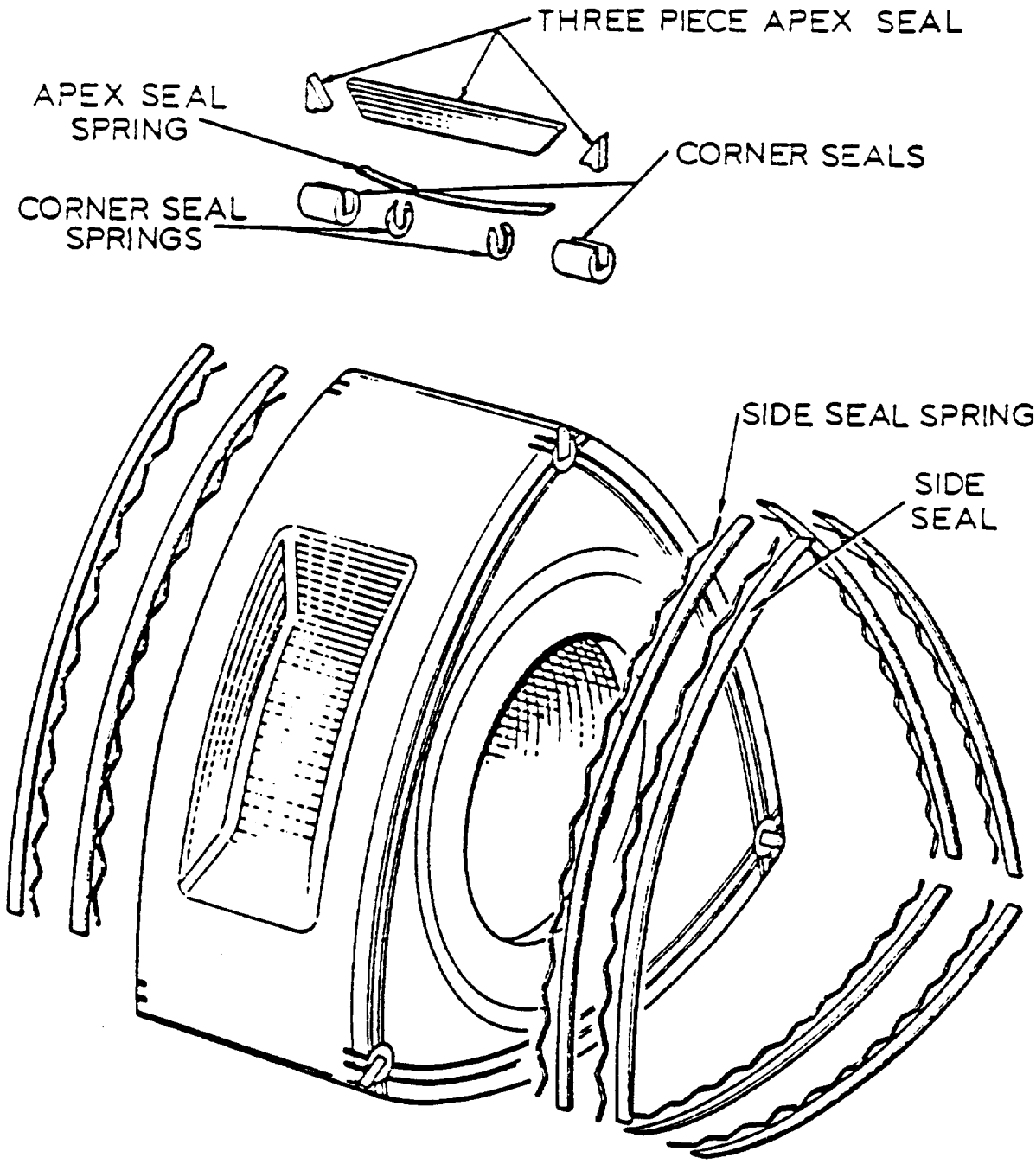

Figure 3. Exploded view of typical engine gas seals.

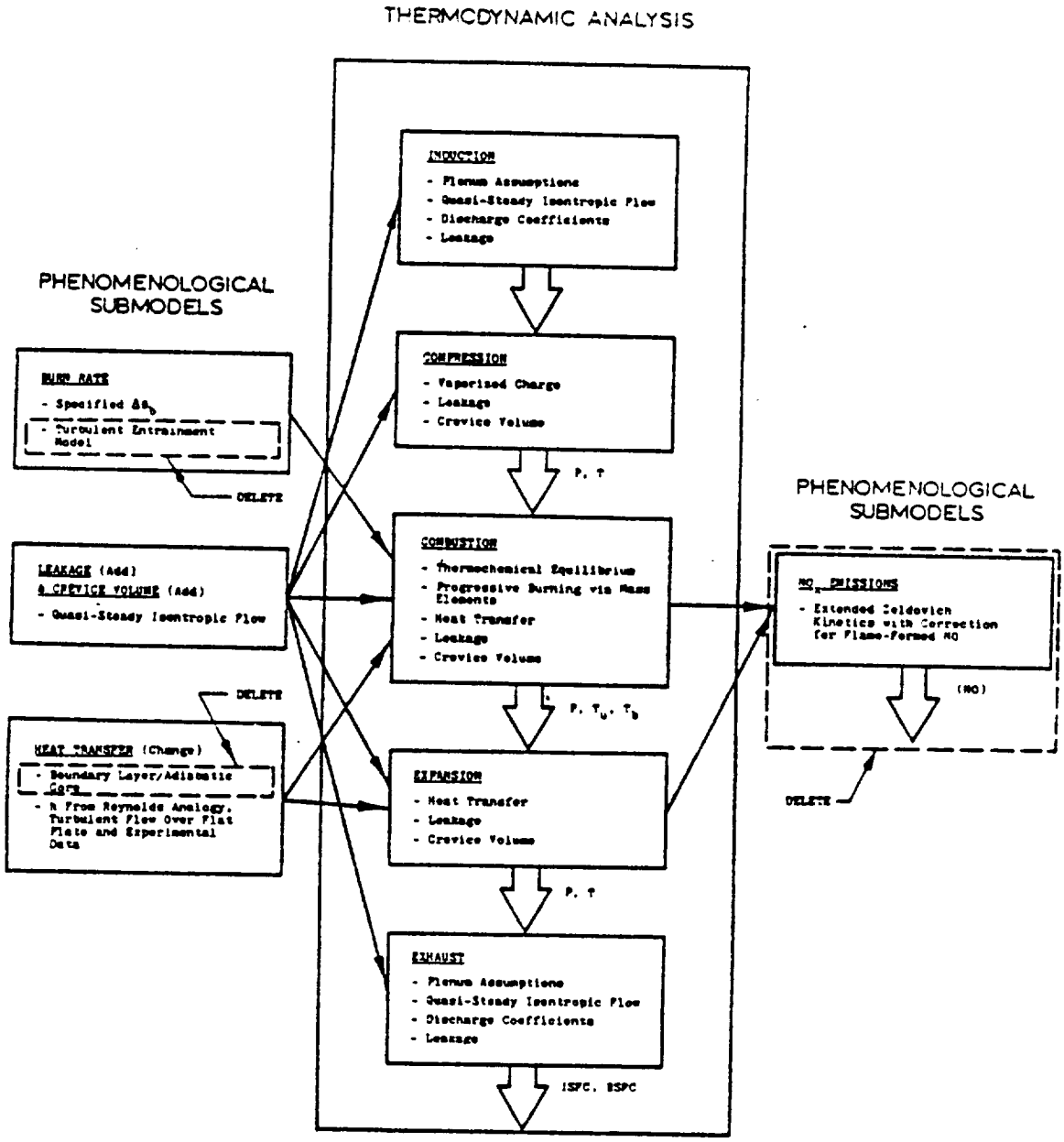

Figure 4. Flow chart of reciprocating engine program indicating deletions, additions, and alterations required for transformation to a Wankel engine simulation.

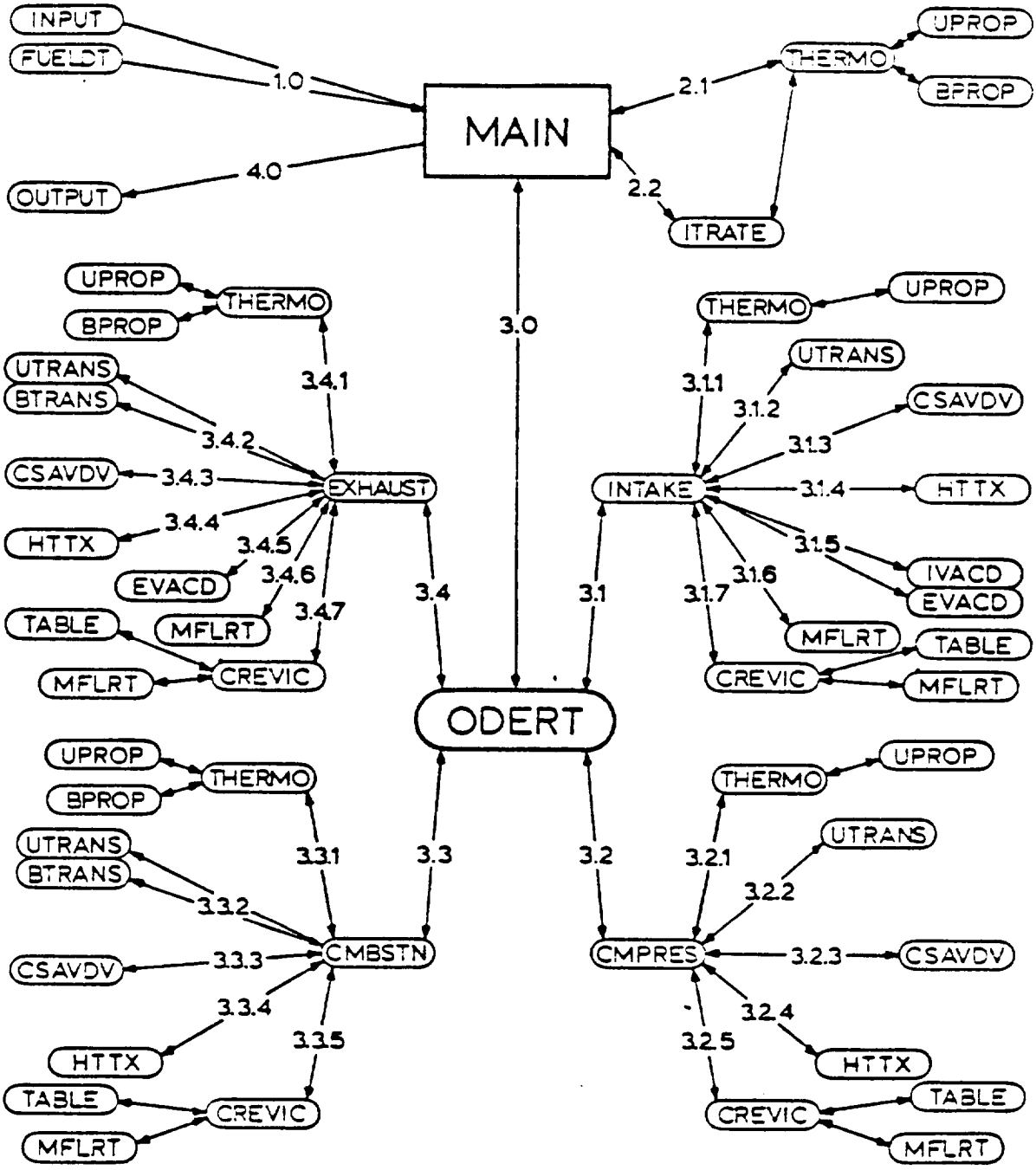

Figure 5. Detailed flow chart of Wankel simulation showing the order of subroutine calls.

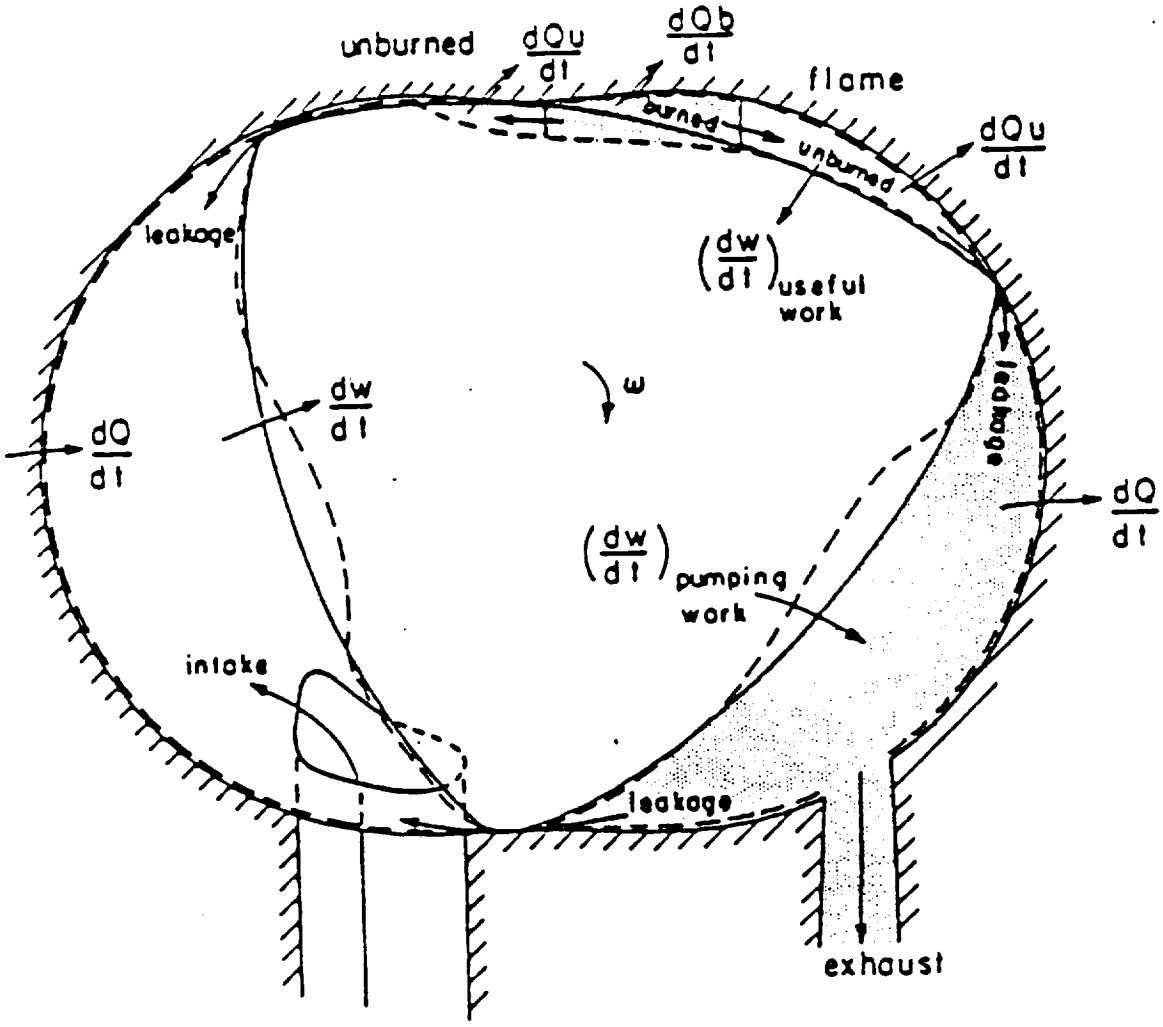

Figure 6. Schematic diagram depicting the coupling of three engine chambers by leakage past the apex seals and the two zone combustion model.

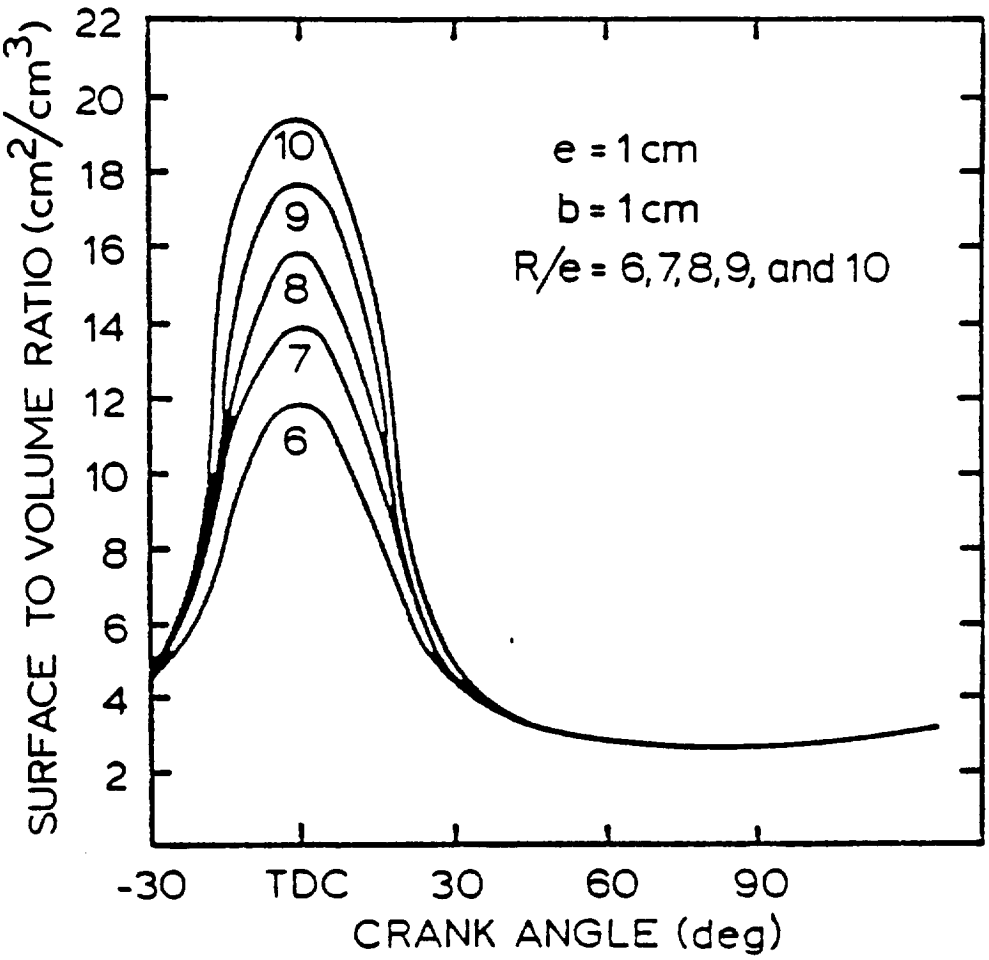

Figure 7. Wankel engine surface to volume ratio versus crank angle for several engine geometries.

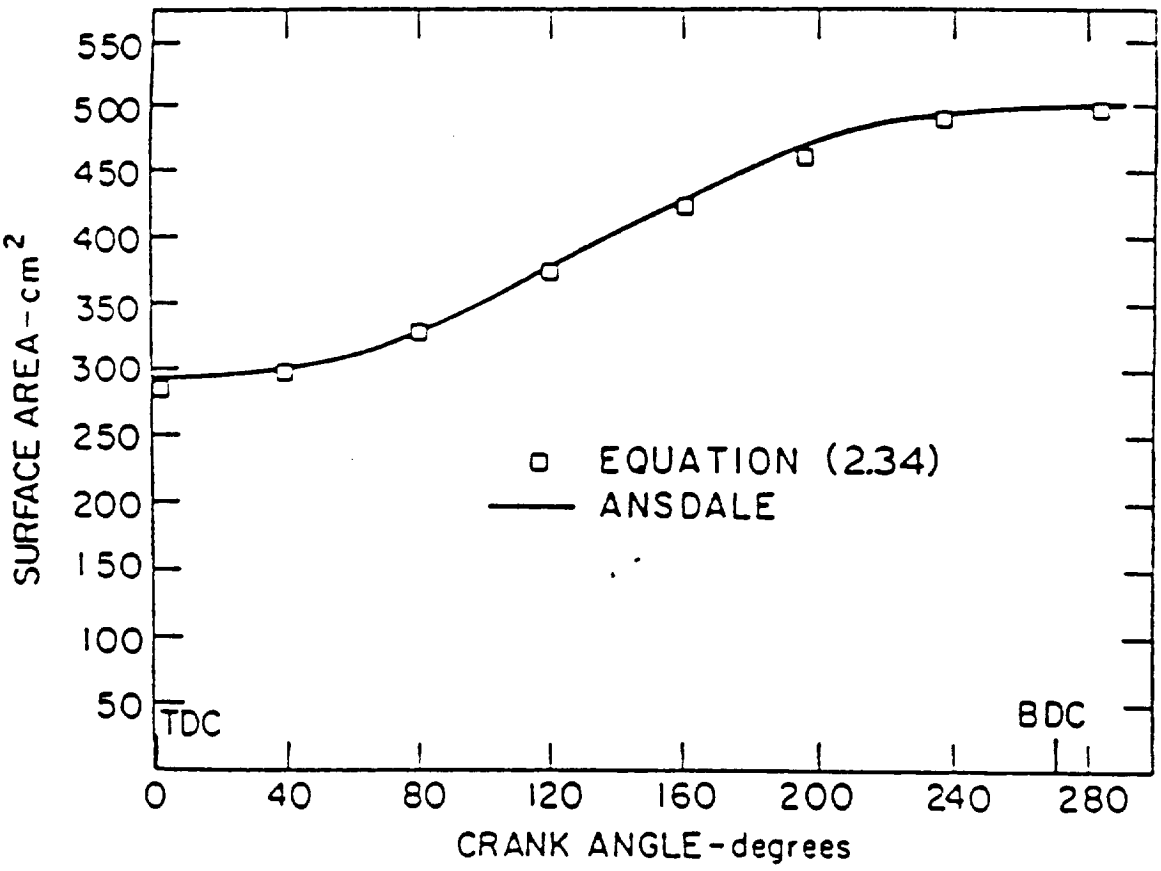

Figure 8. Comparison of true and approximate Wankel engine surface area calculations.

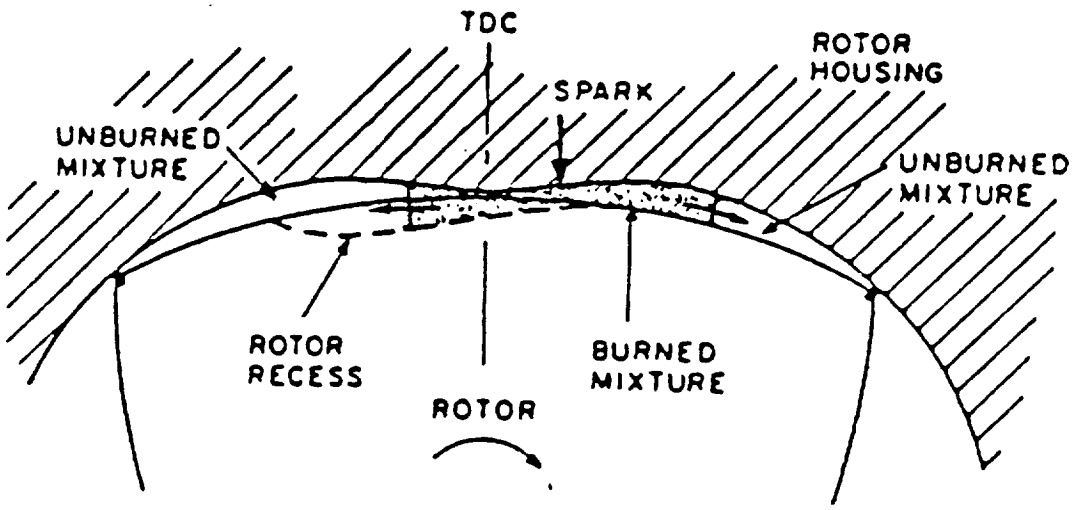

Figure 9. Diagram of the assumed flame front propagation.

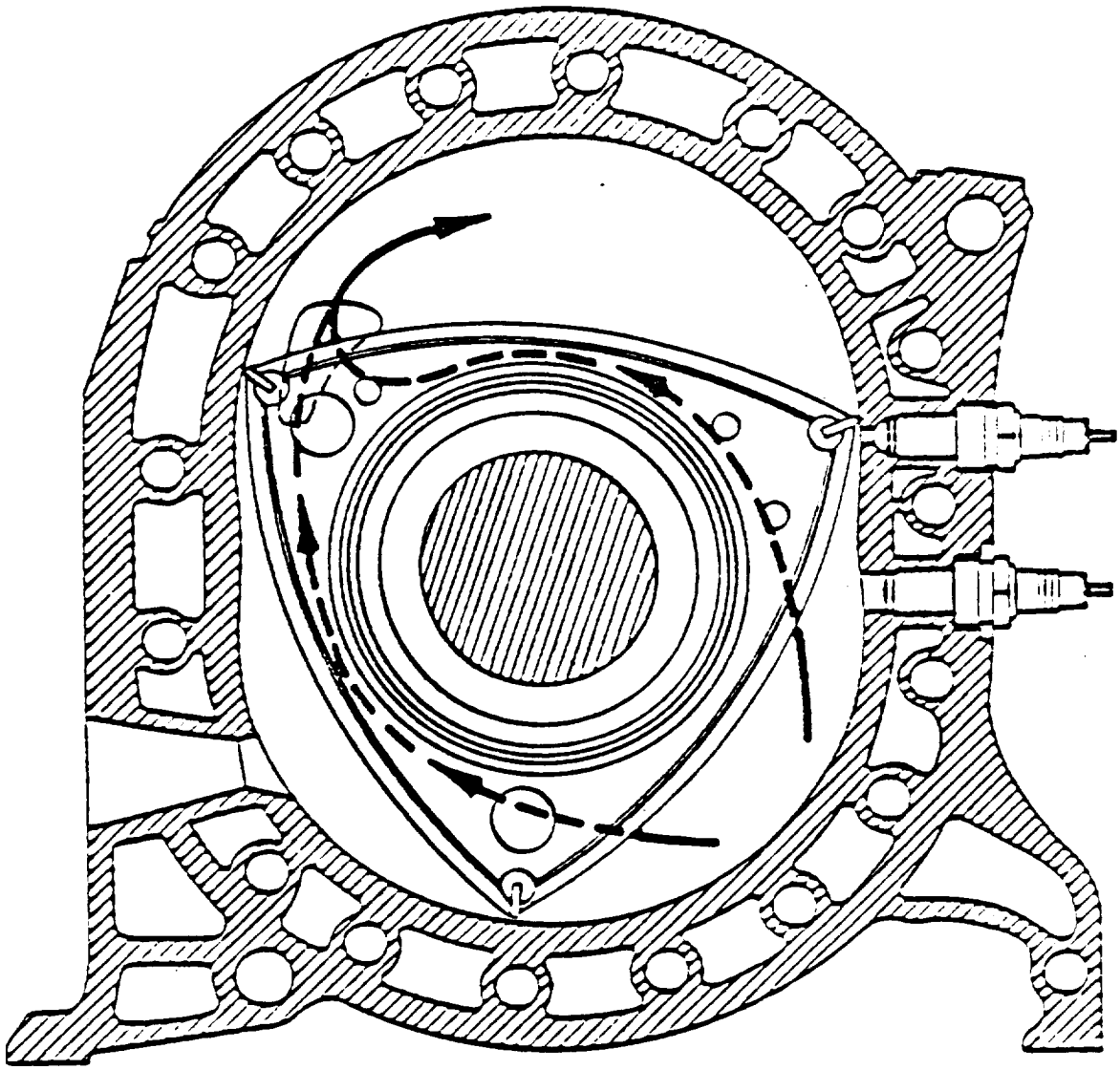

Figure 10. Schematic diagram of side seal leakage path.

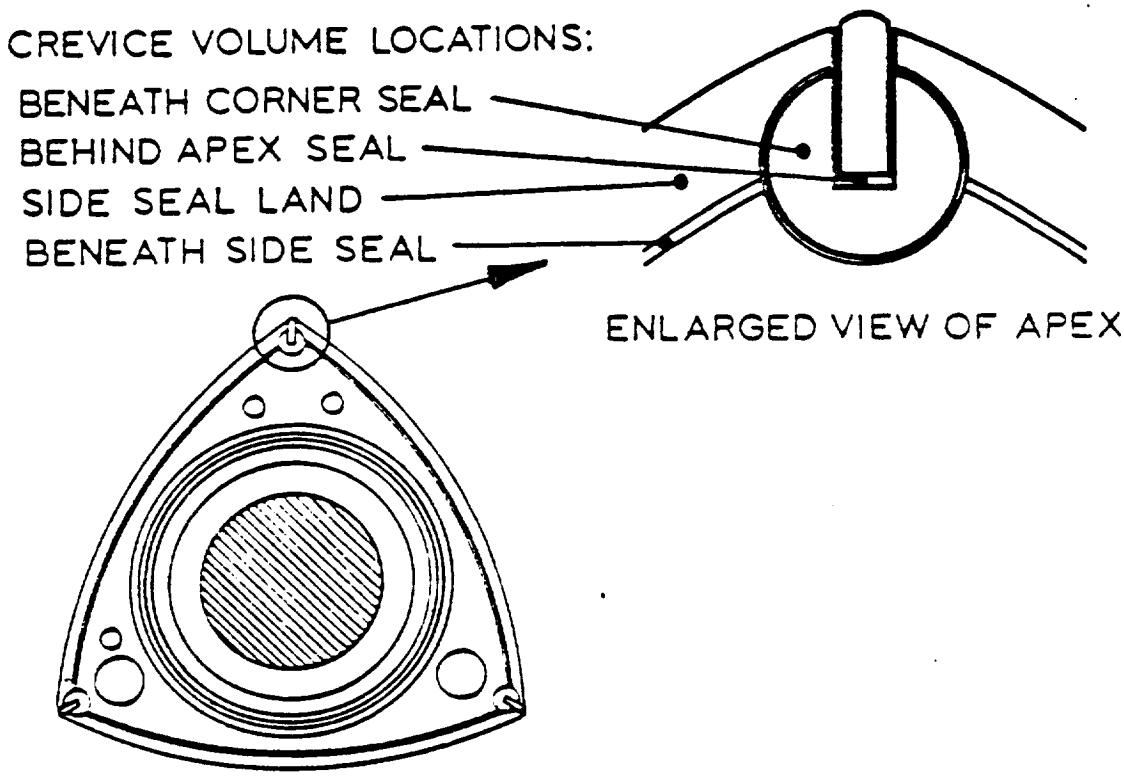

Figure 11. Diagram of crevice volume locations in the Wankel engine.

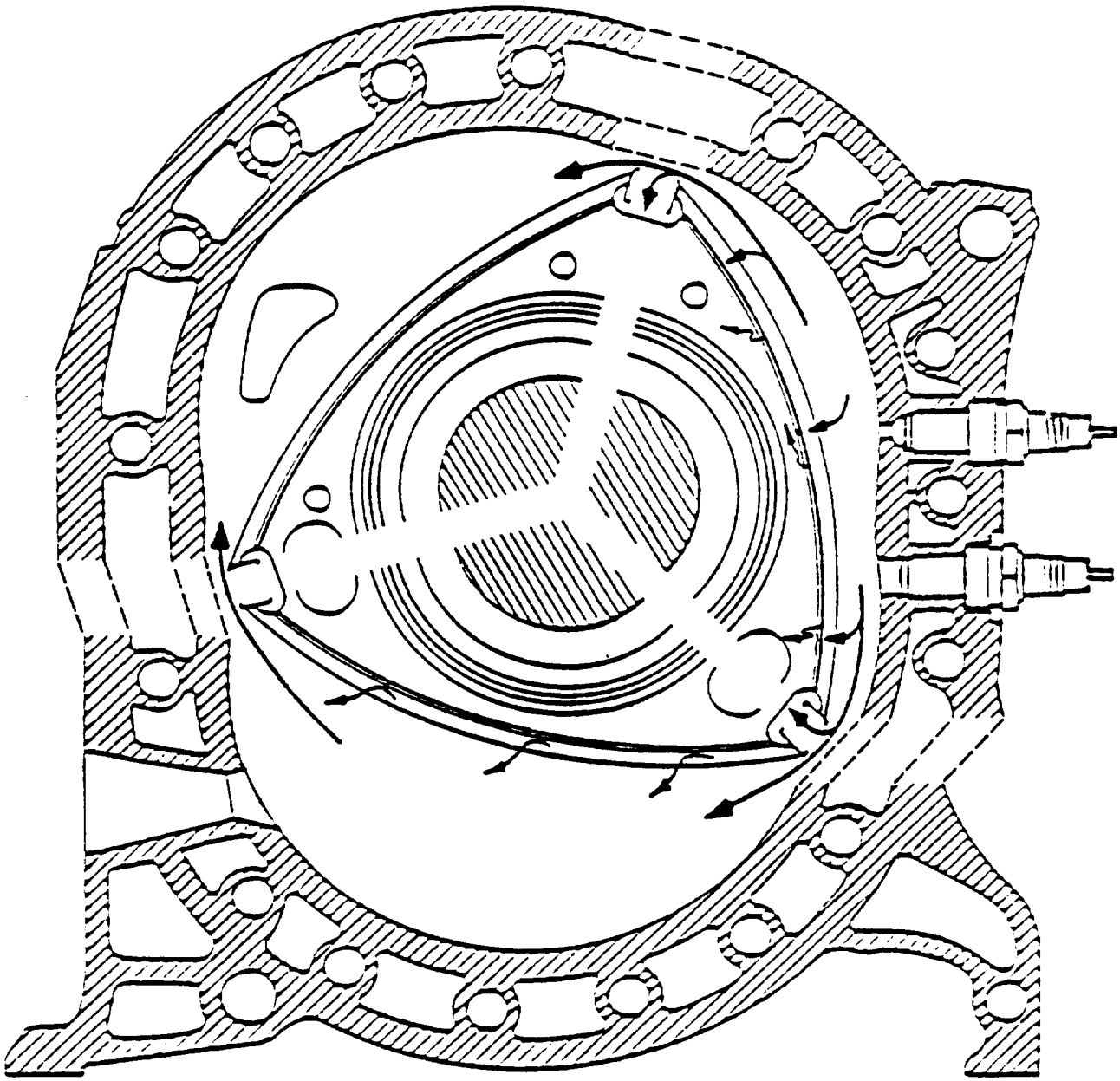

Figure 12. A pictorial schematic of crevice volumes and leakage gas flows.

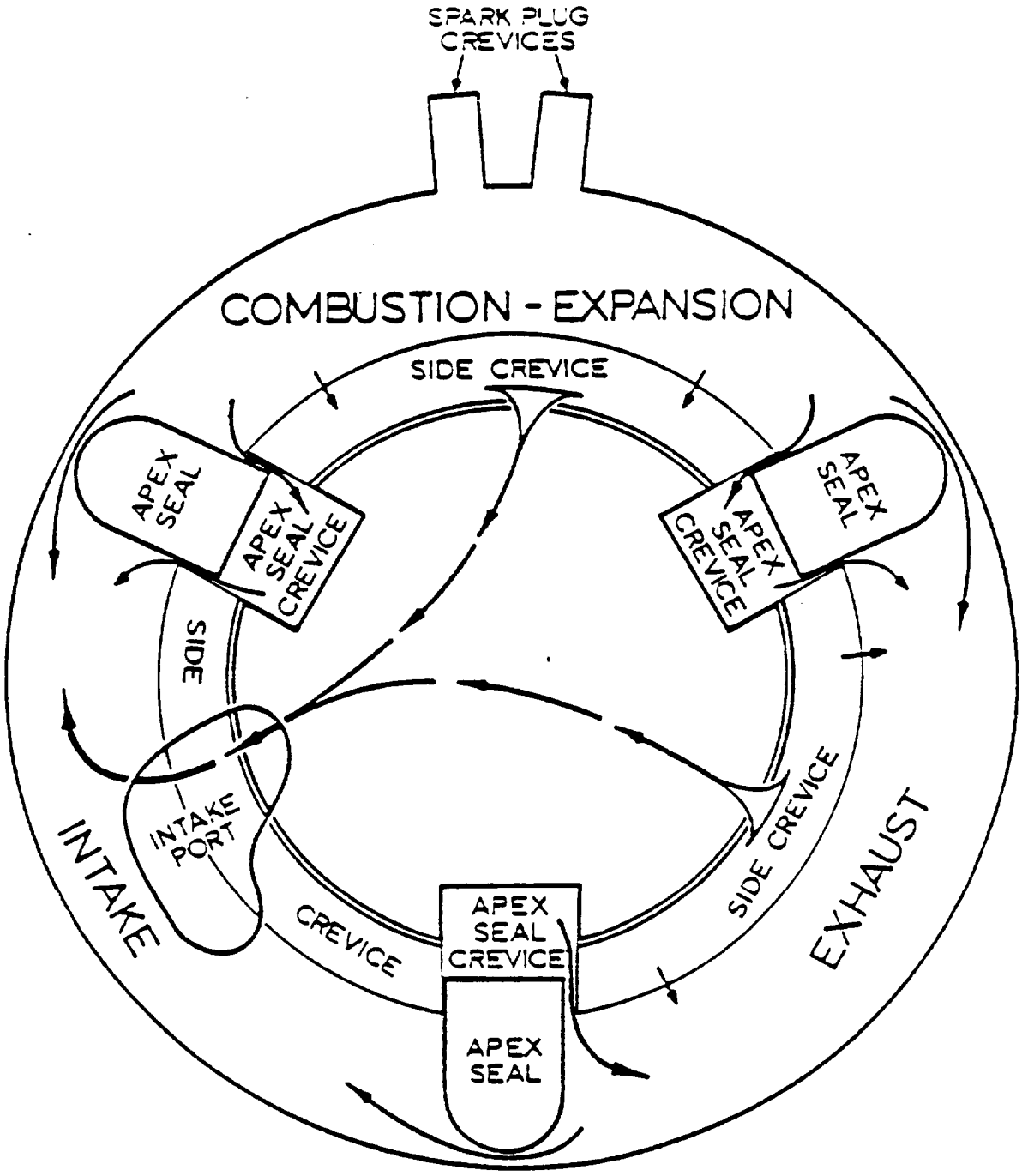

Figure 13. Schematic diagram of a simulation that explicitly models all leakage paths and crevice volumes.

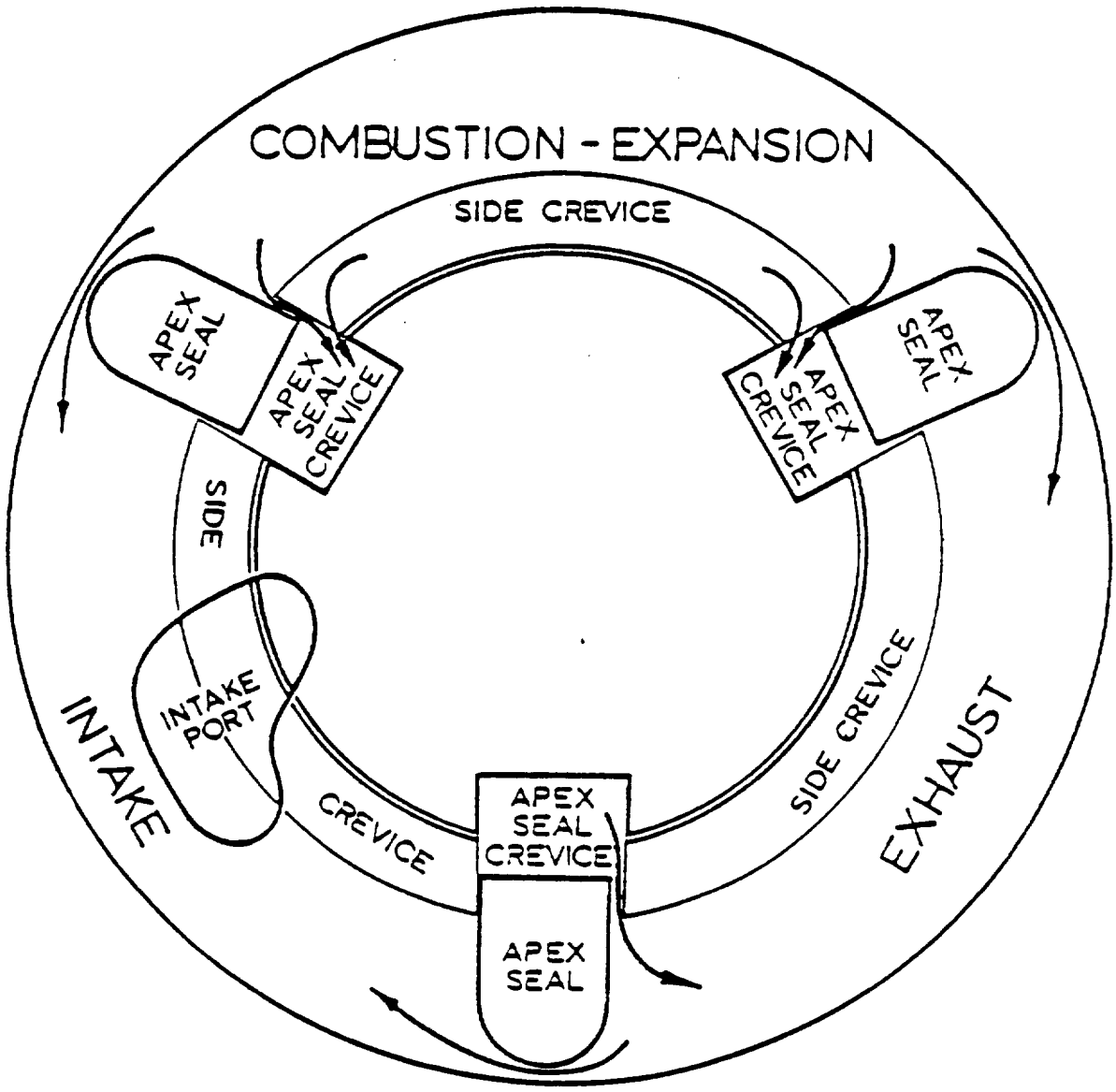

Figure 14. Schematic diagram of the crevice volume and leakage model as used in the program.

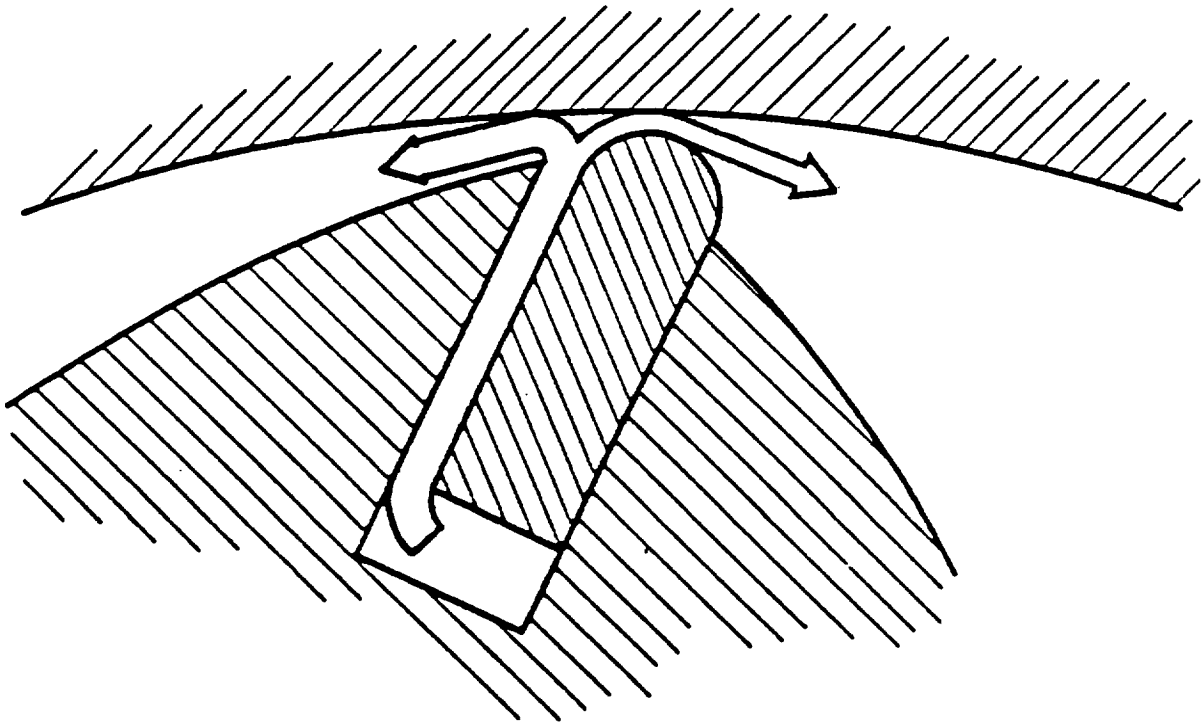

Figure 15. Diagram of crevice gas returning to chamber and being diverted into leakage flow.

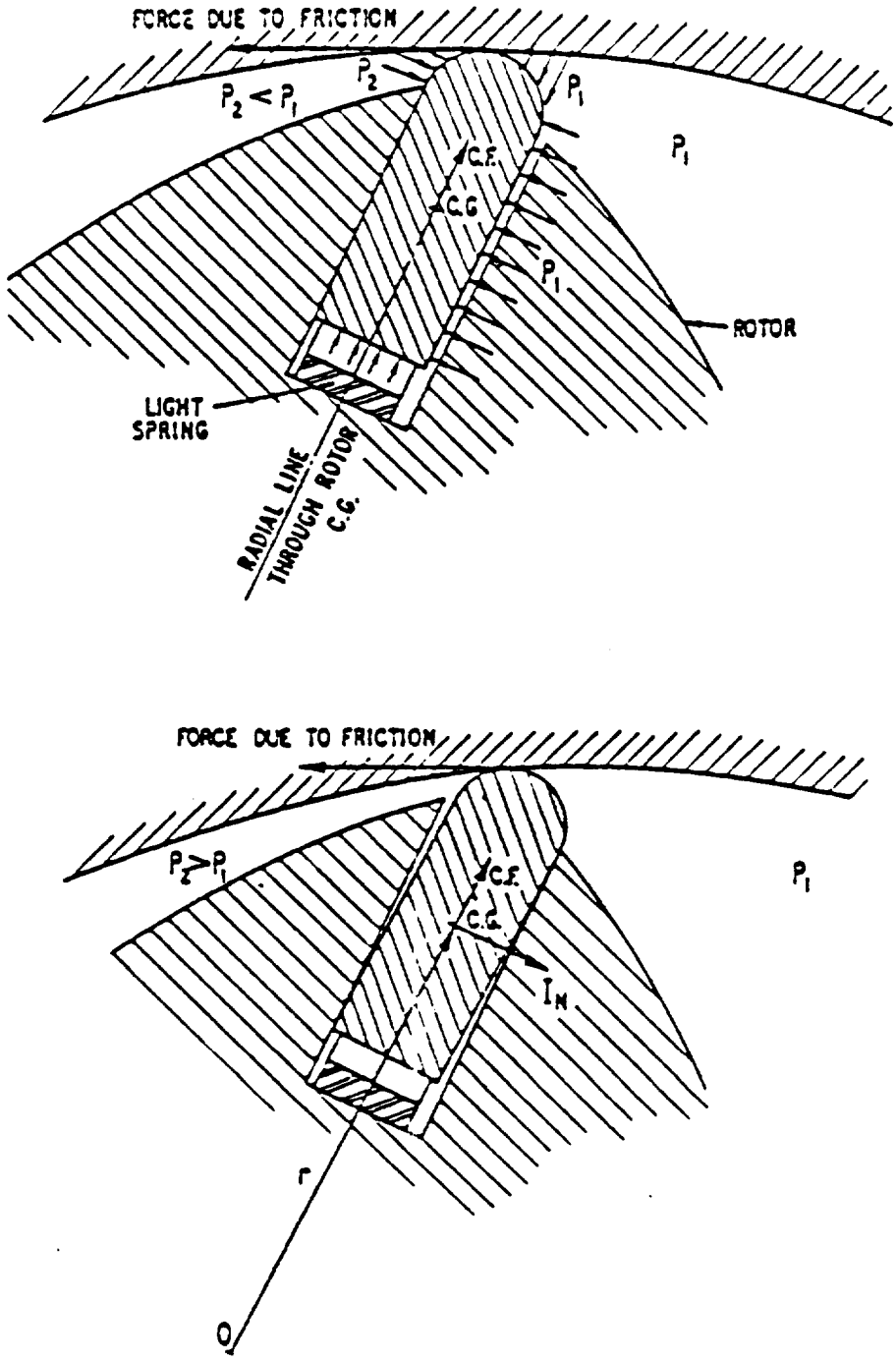

Figure 16. Motion of Apex seal as resultant pressure forces reverse direction.

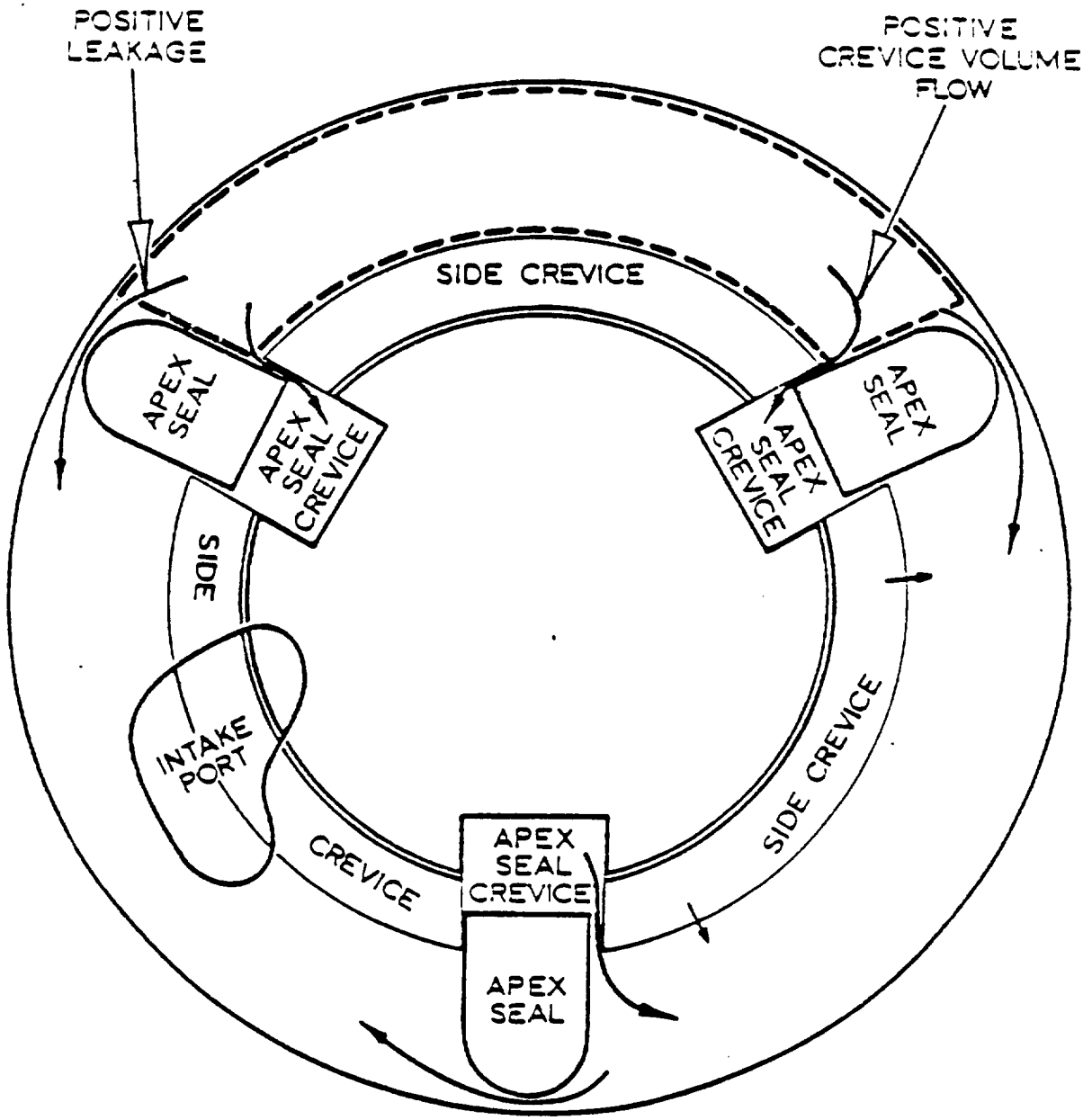

Figure 17. Schematic diagram of crevice volume and leakage model with a thermodynamic system imposed and positive mass flows shown.

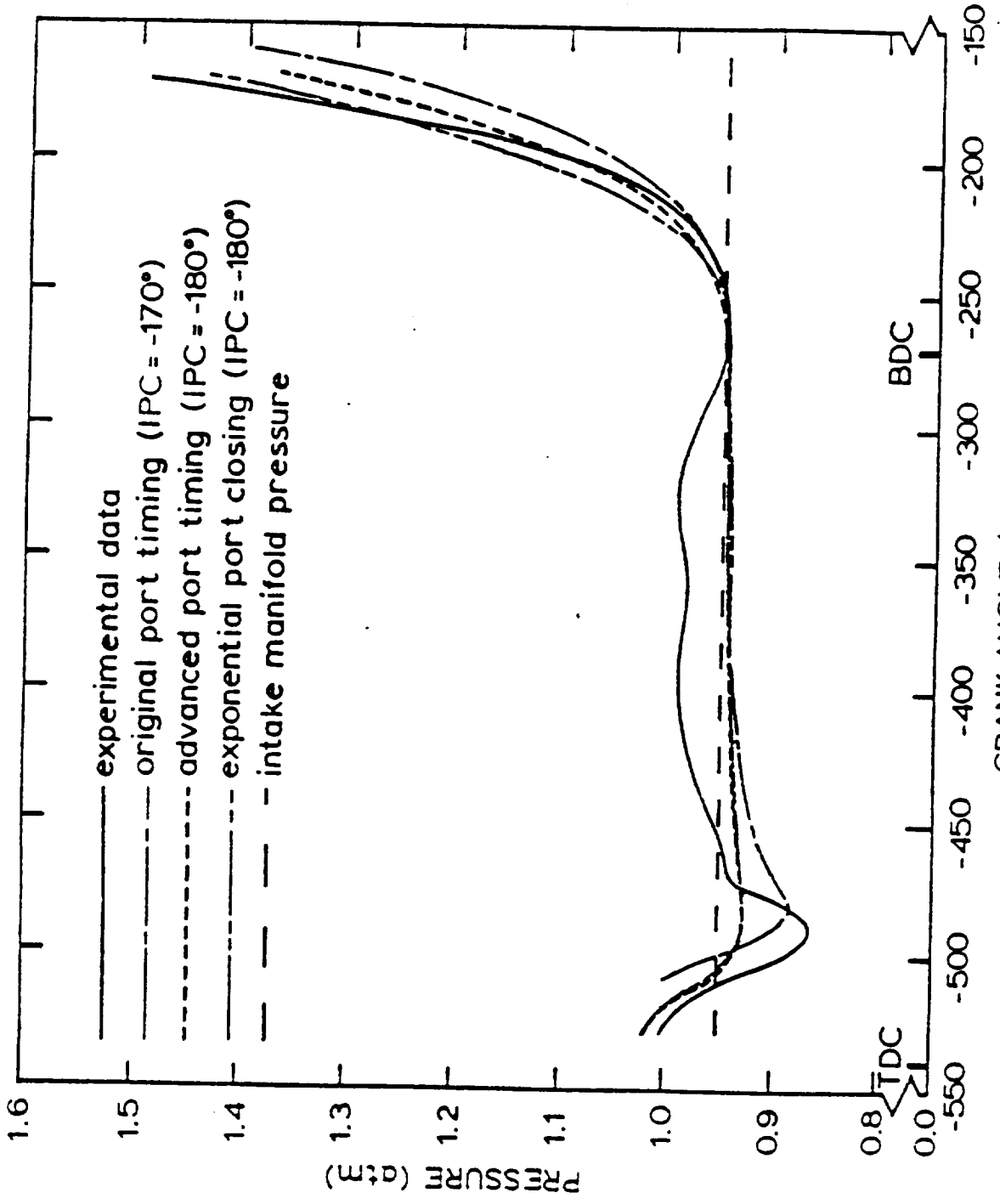

Figure 18. Comparison of intake chamber pressure for different intake port area profiles and experimental data.

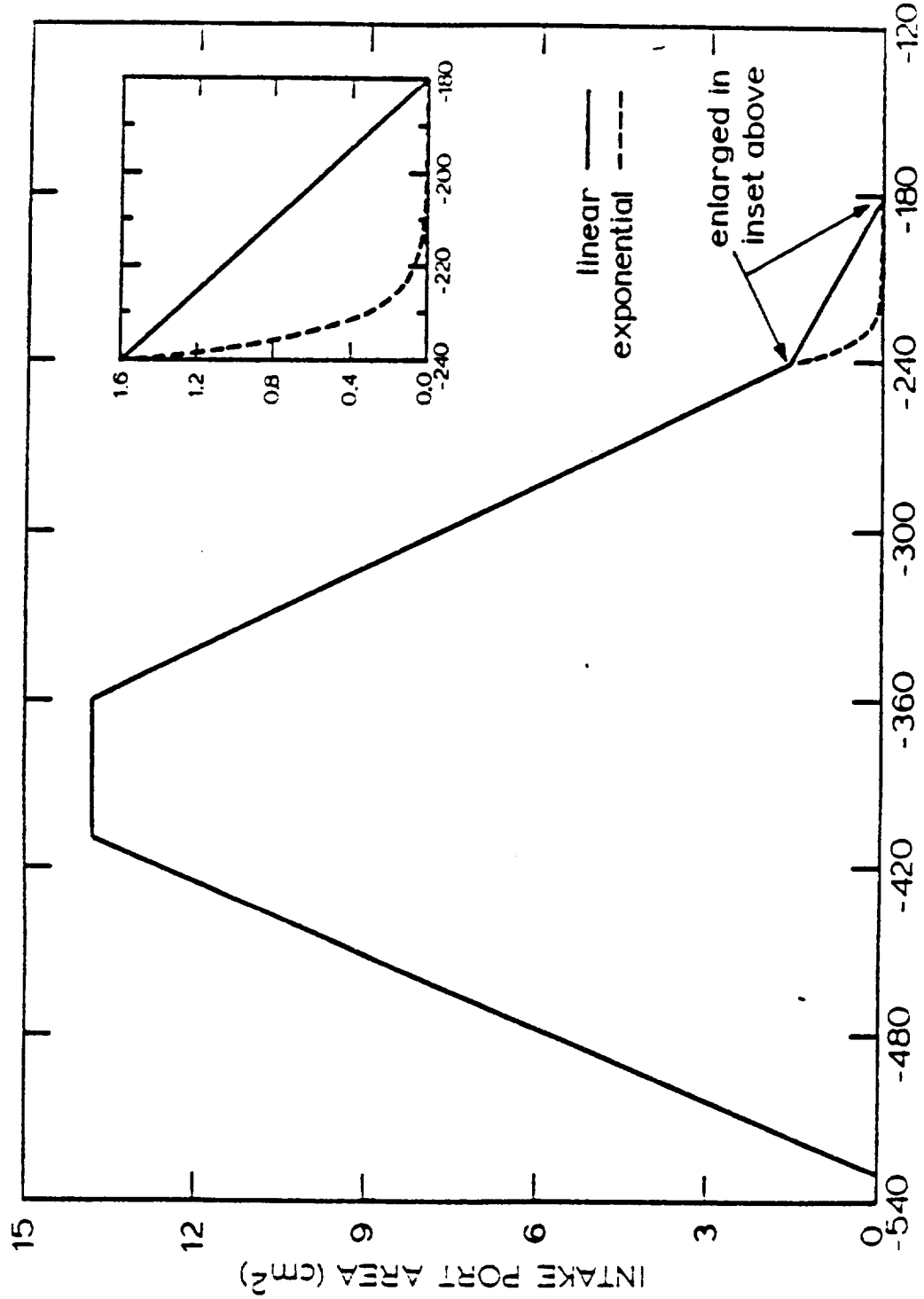

Figure 19. Comparison plot of intake port area profiles used during model calibration.

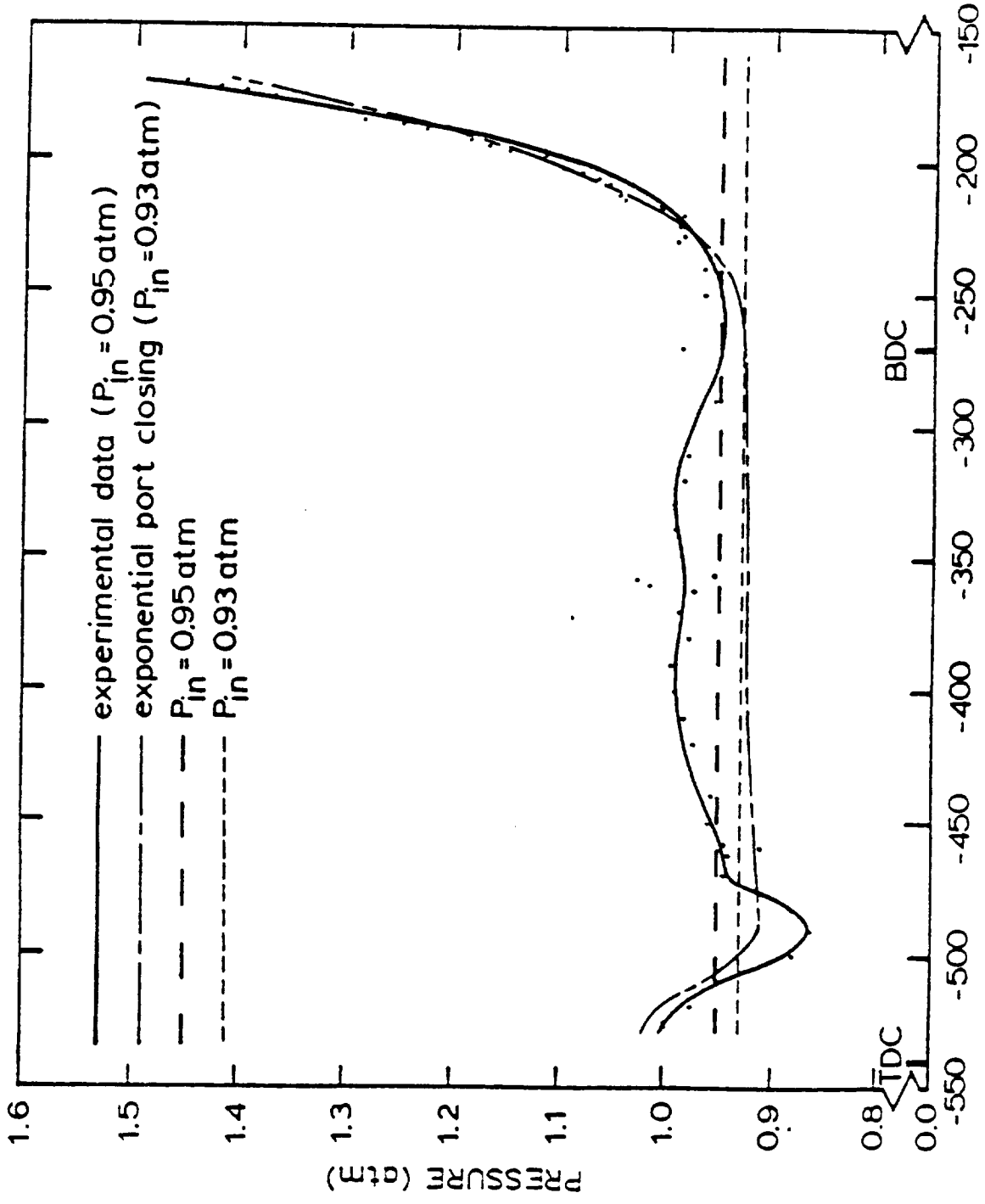

Figure 20. Comparison of intake chamber pressure between calibrated model and experimental data.

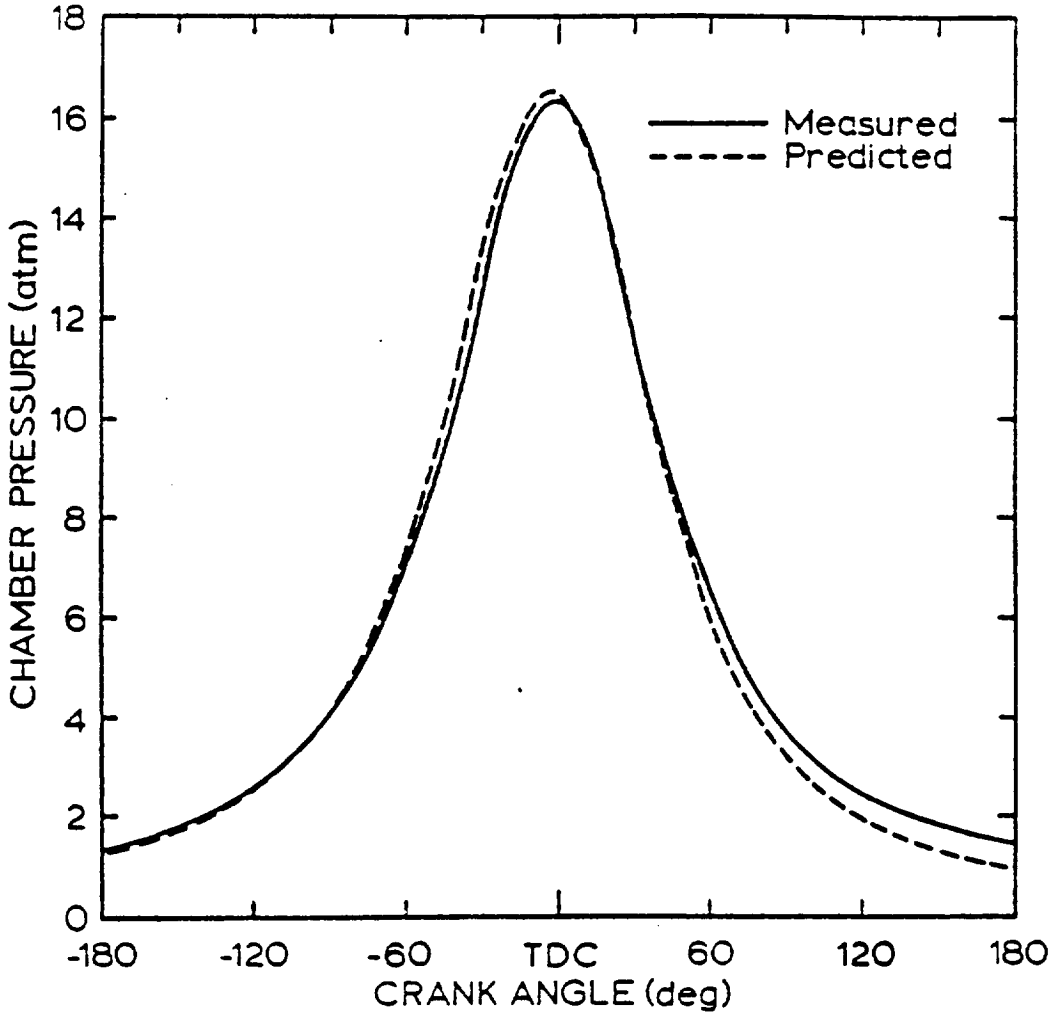

Figure 21. Comparison of measured and calibrated compression-expansion pressure trace for median engine speed and throttle setting.

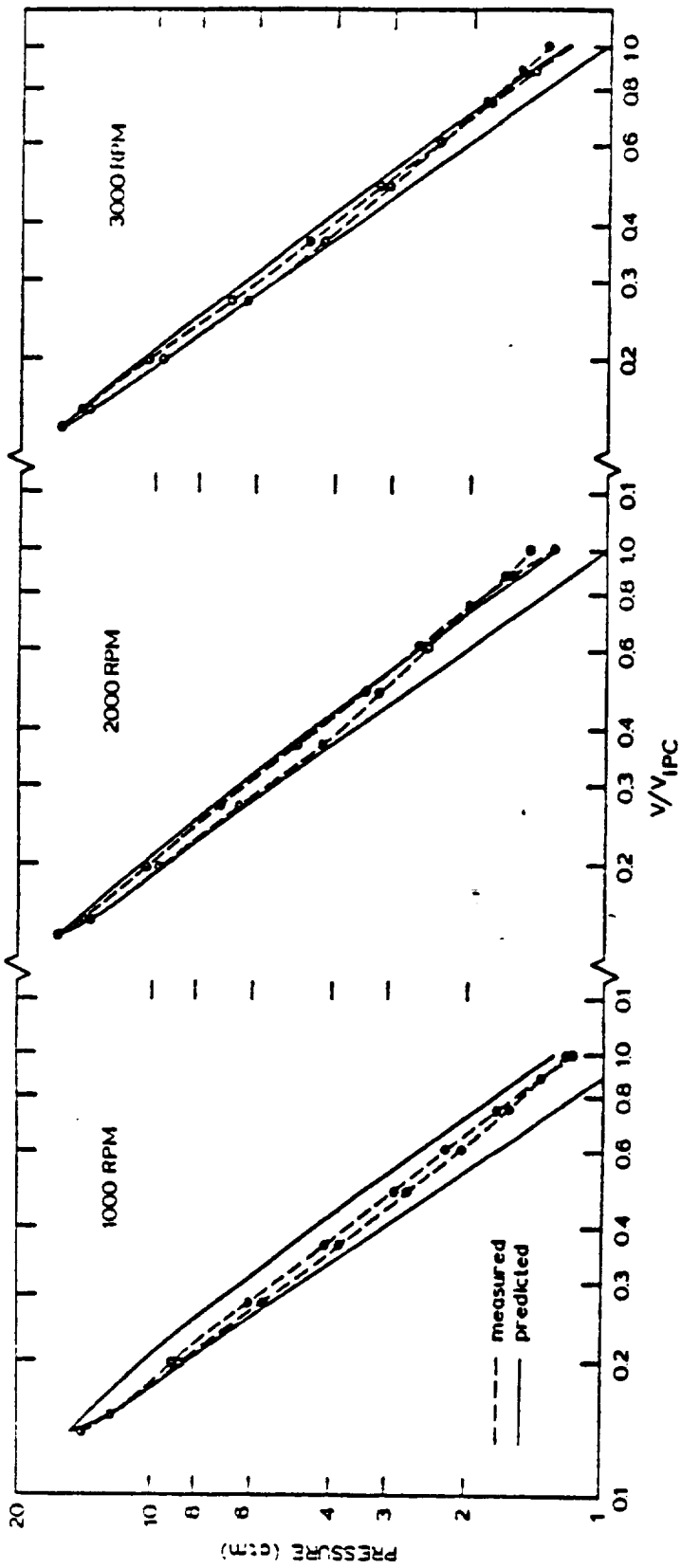

Figure 22. Log P versus normalized log V for motoring runs at three engine speeds: measured and predicted.

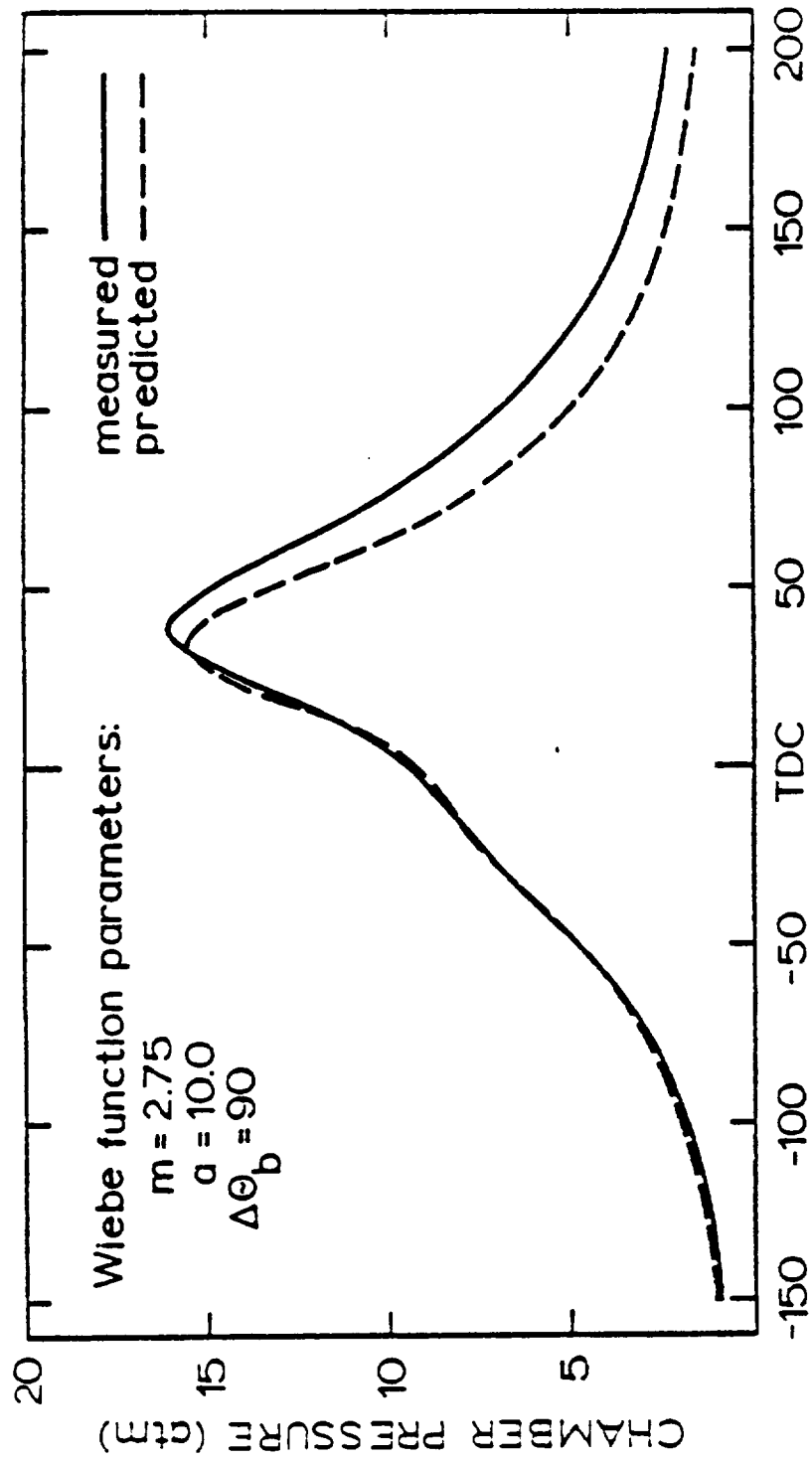

Figure 23. Comparison of predicted and measured pressure versus crank angle for low engine load and speed.

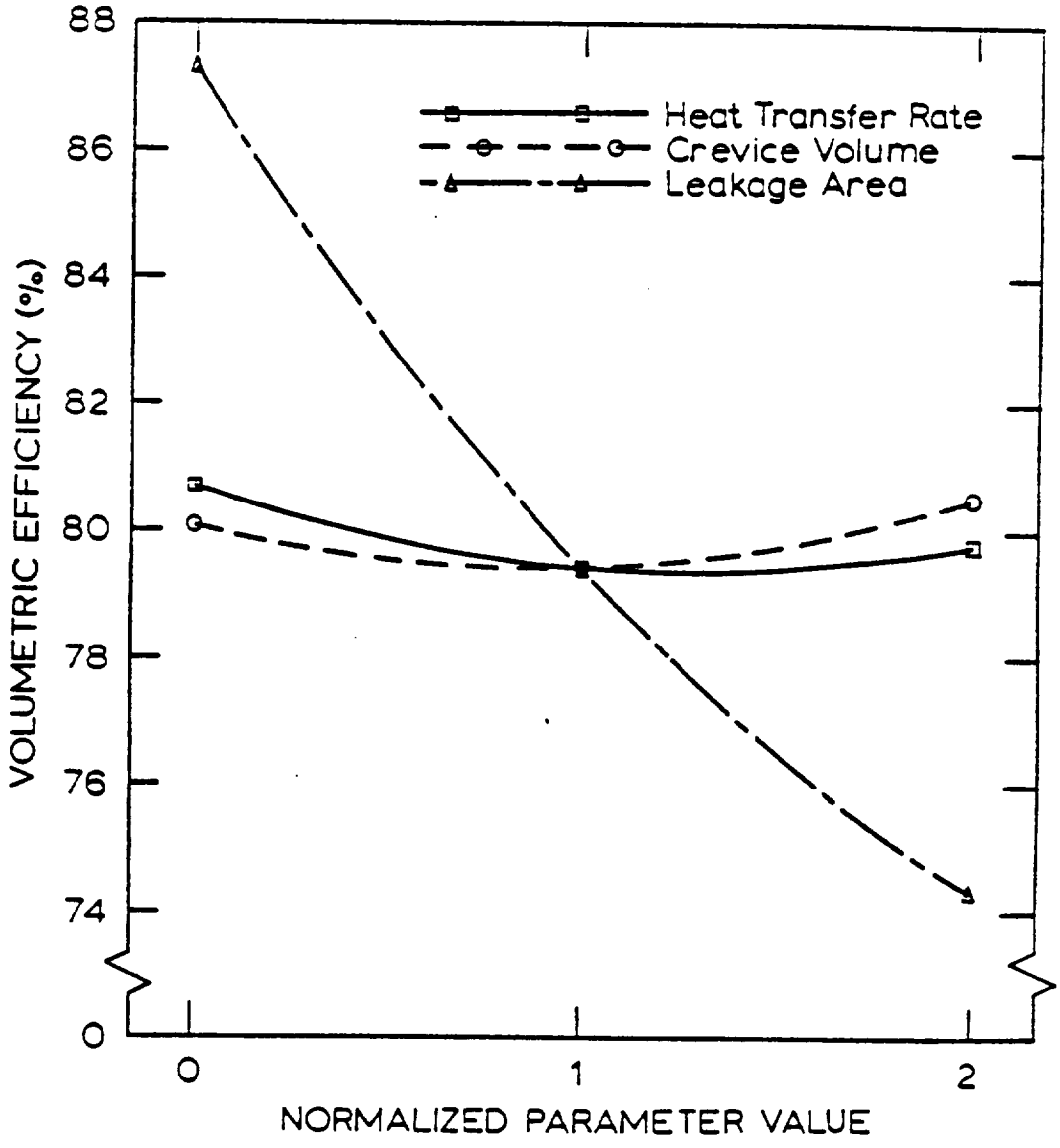

Figure 24. Effect of parametric variation on motoring volumetric efficiency.

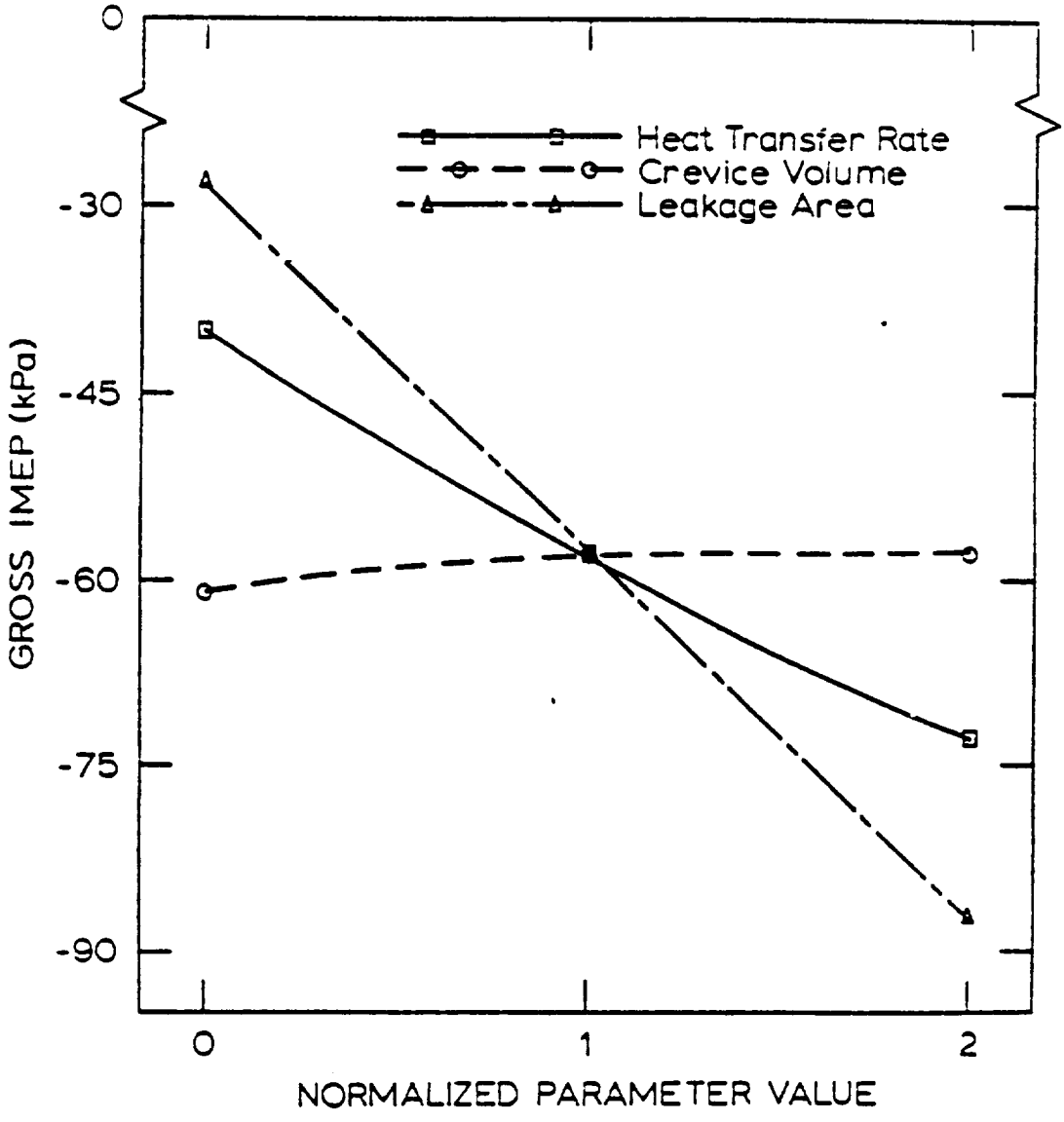

Figure 25. Effect of parametric variation on motoring gross IMEP.

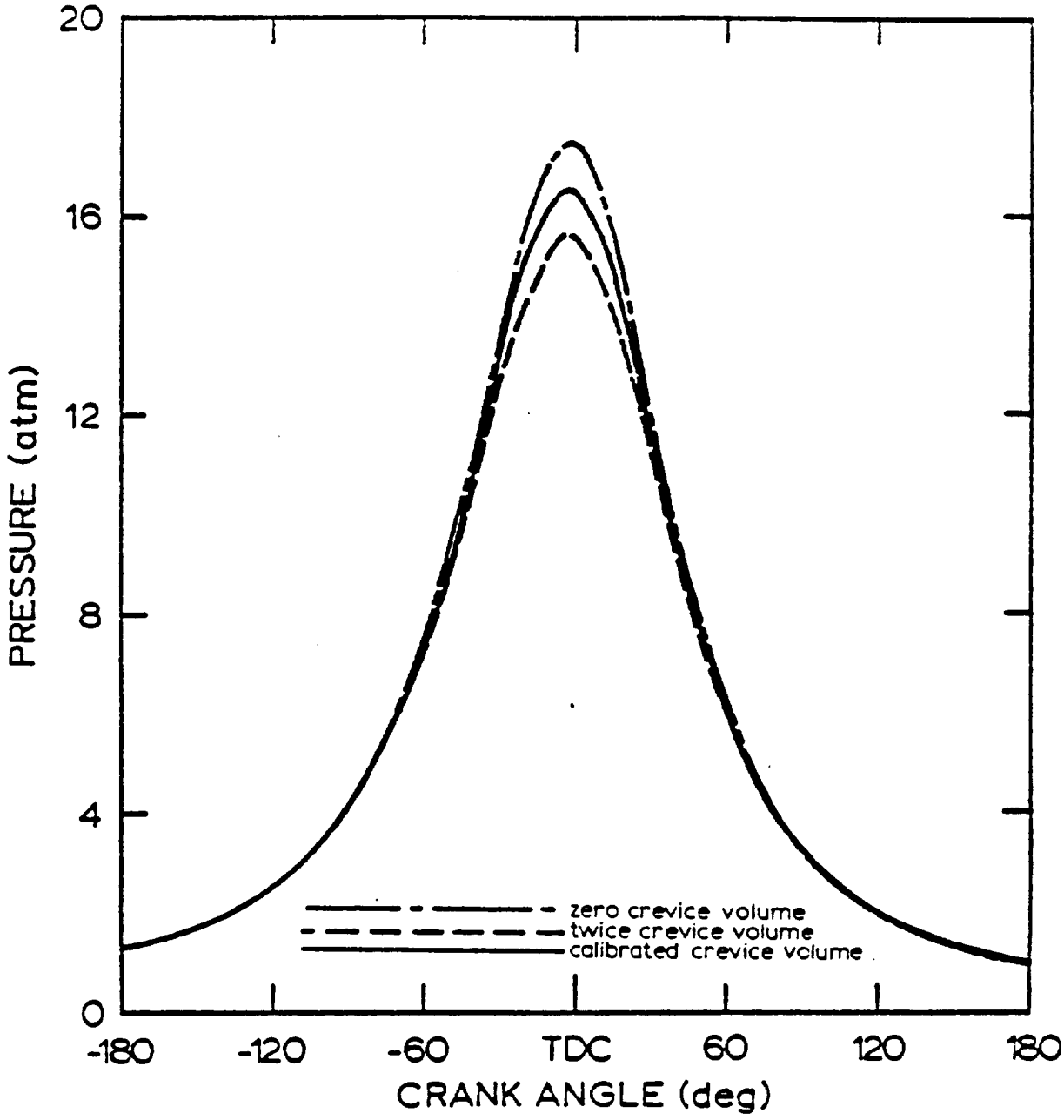

Figure 26. Effect of reducing crevice volumes on compression - expansion pressure trace (motoring).

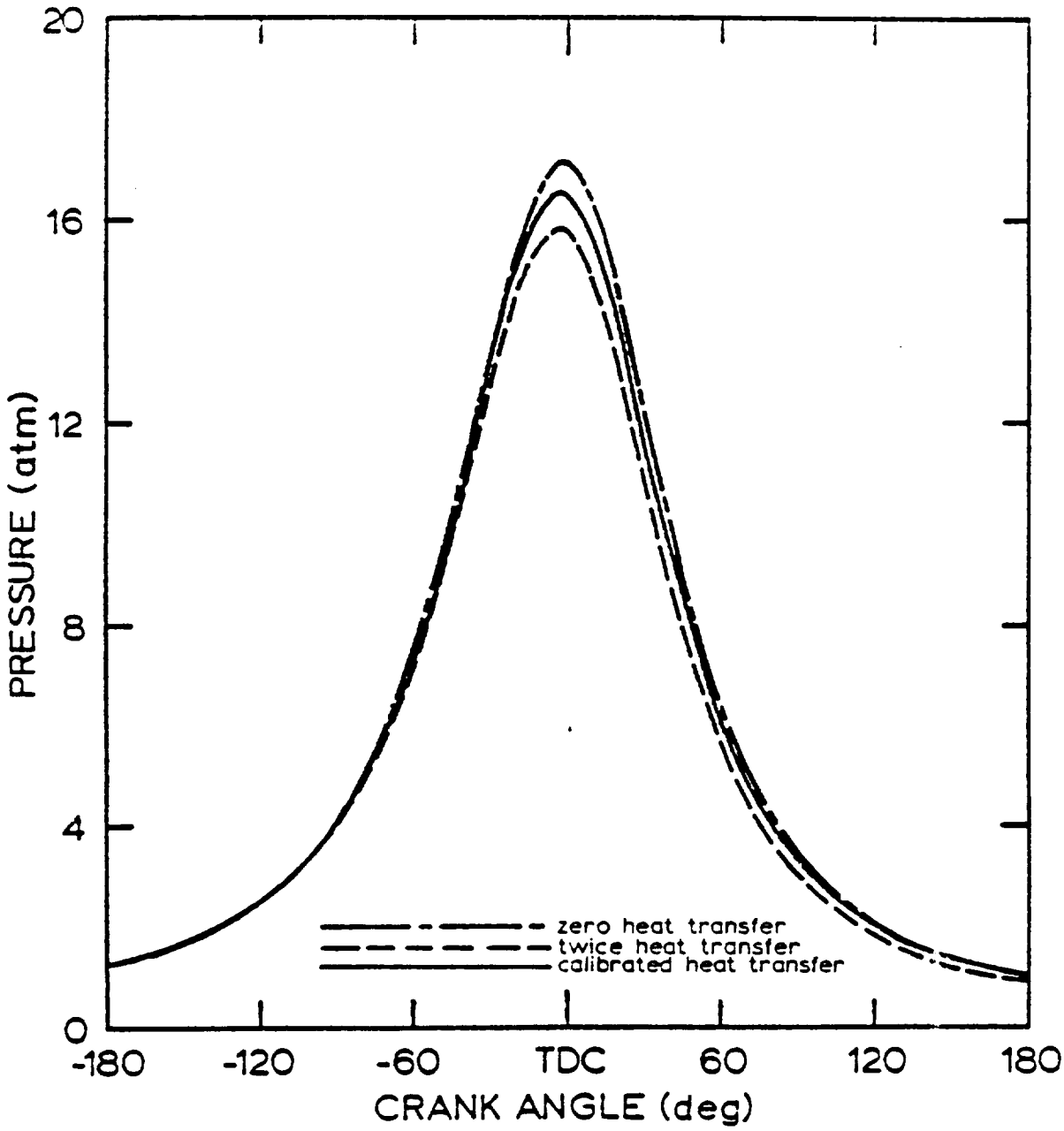

Figure 27. Effect of reducing leakage area on compression - expansion pressure trace (motoring).

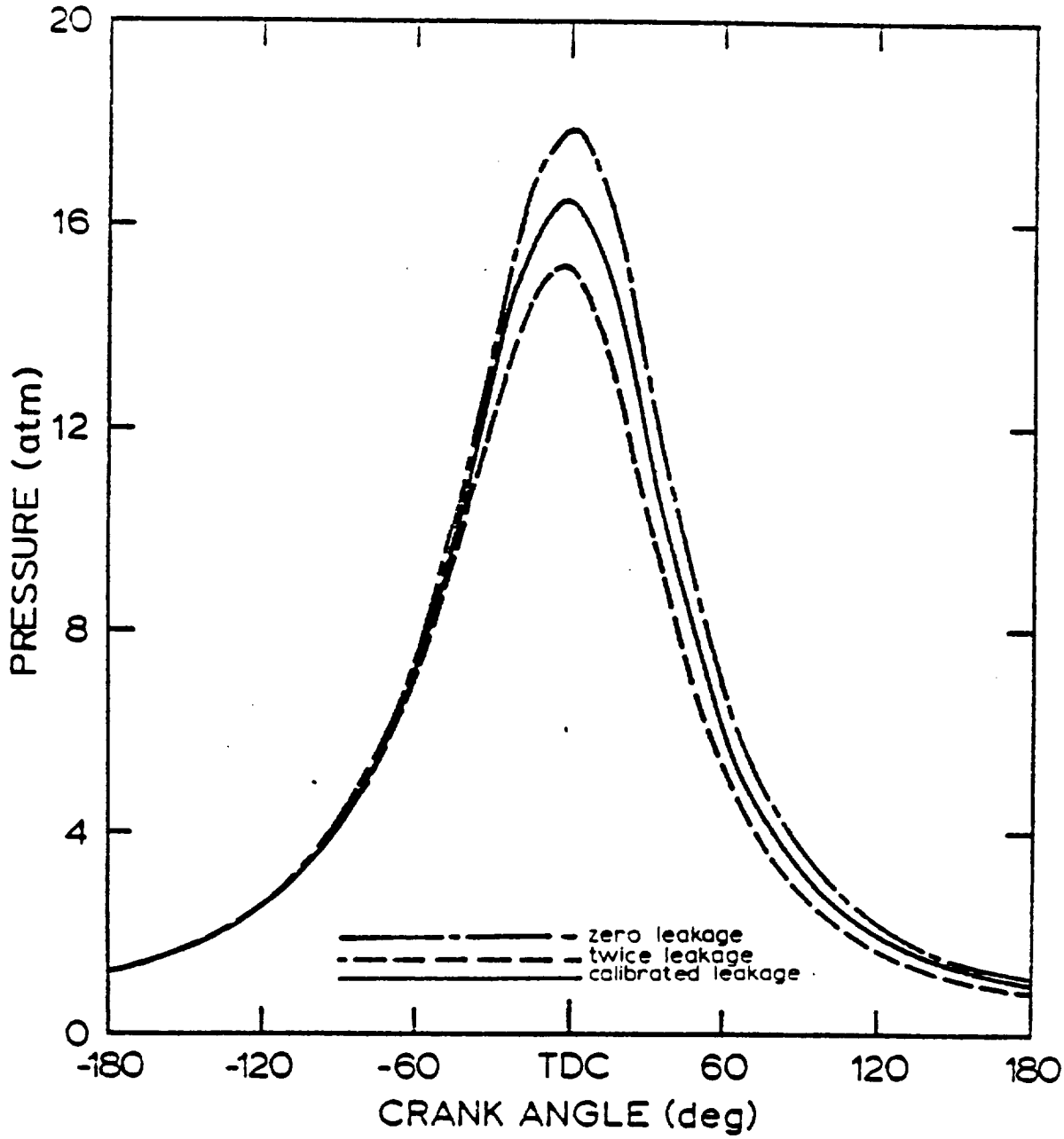

Figure 28. Effect of reducing leakage area on compression - expansion pressure trace (motoring).

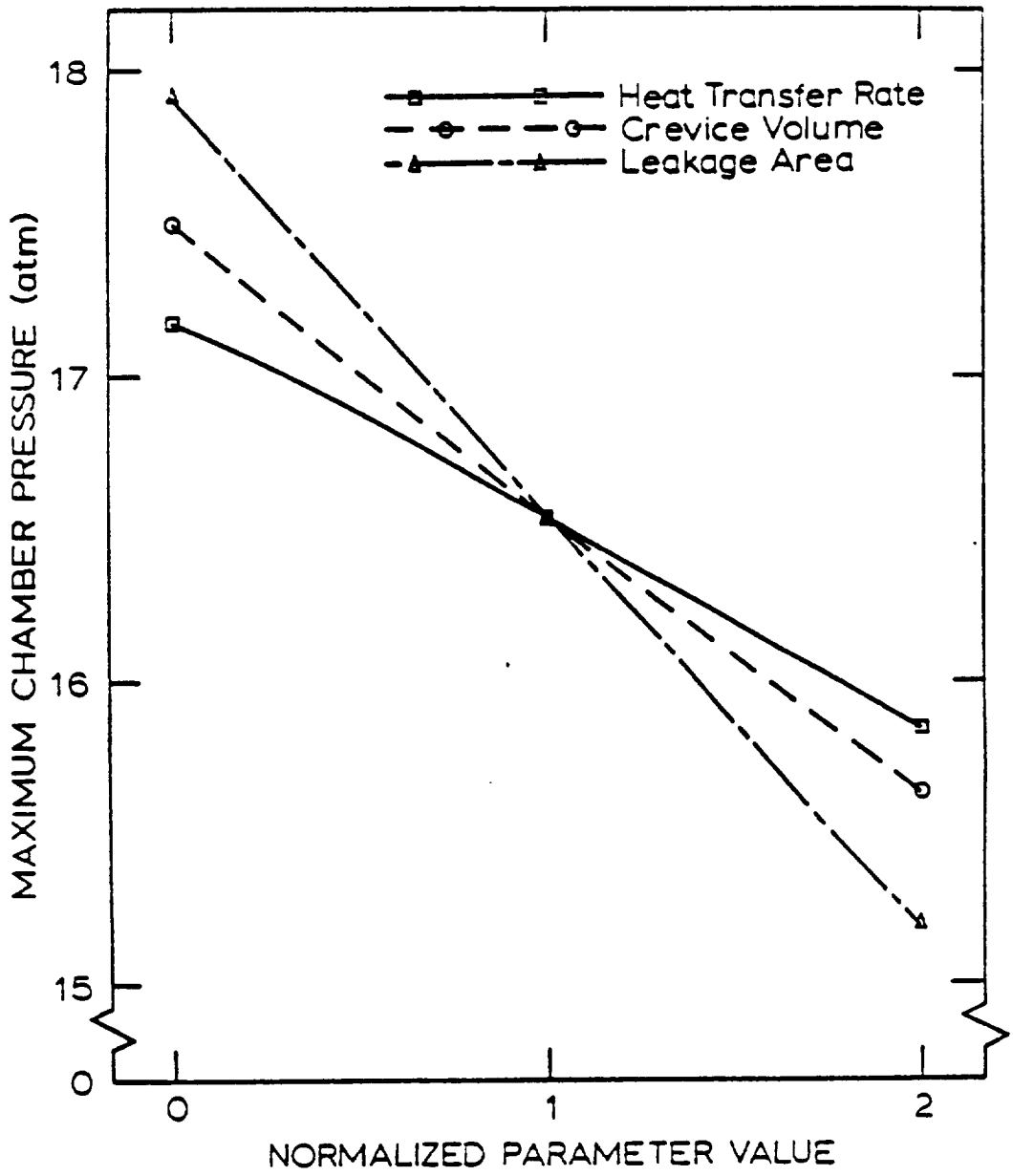

Figure 29. Effect of parametric variation on maximum motoring pressure.

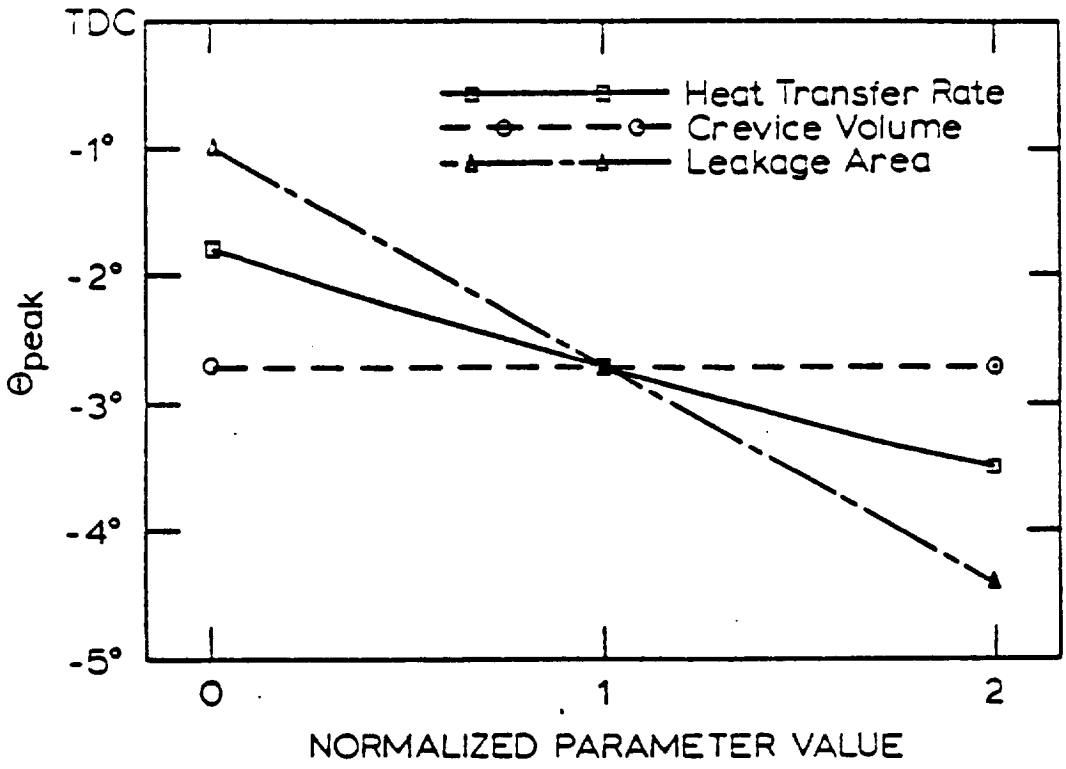

Figure 30. Effect of parametric variation on motoring θ_{peak}.

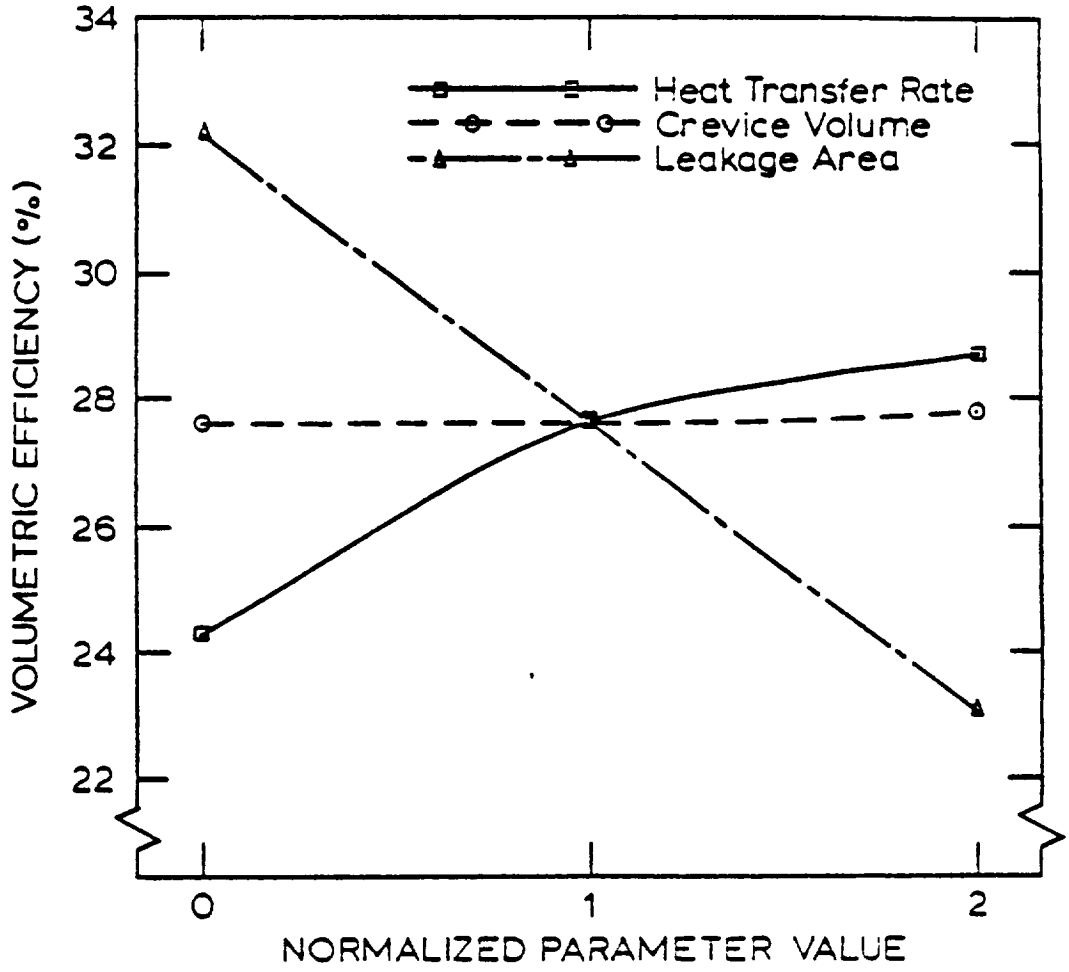

Figure 31. Effect of parametric variation on firing volumetric efficiency.

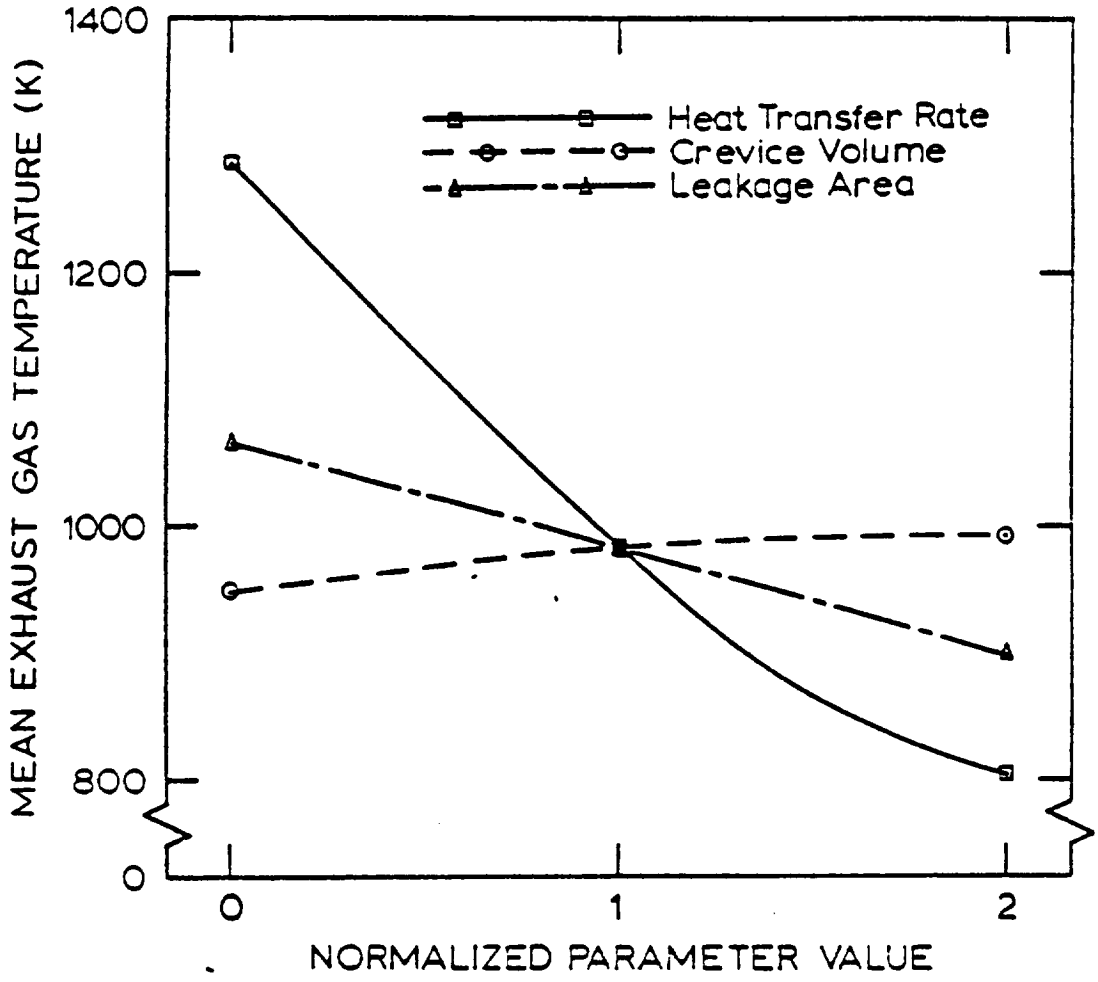

Figure 32. Effect of parametric variation on mean exhaust gas temperature at light load.

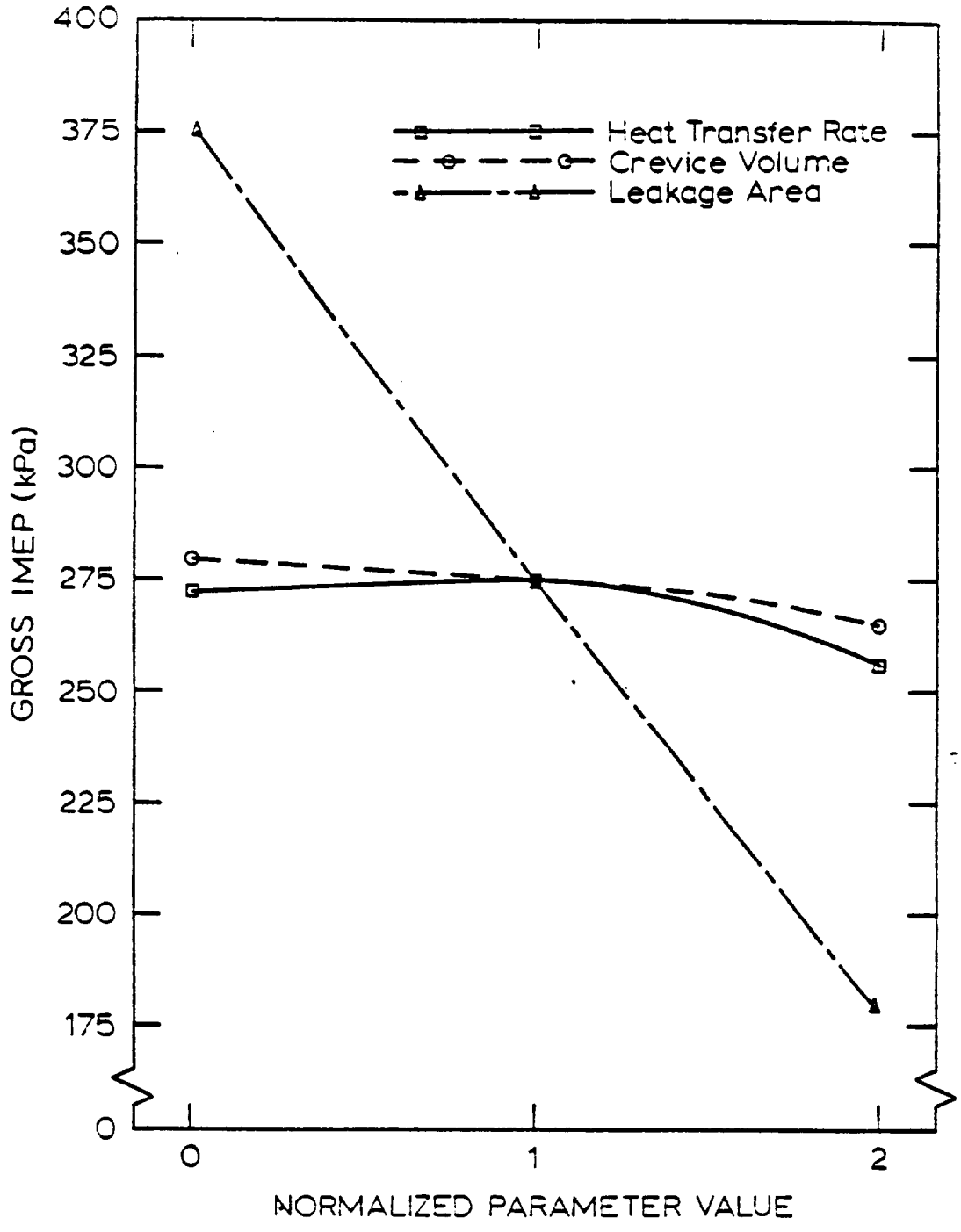

Figure 33. Effect of parametric variation on light load gross mean effective pressure.

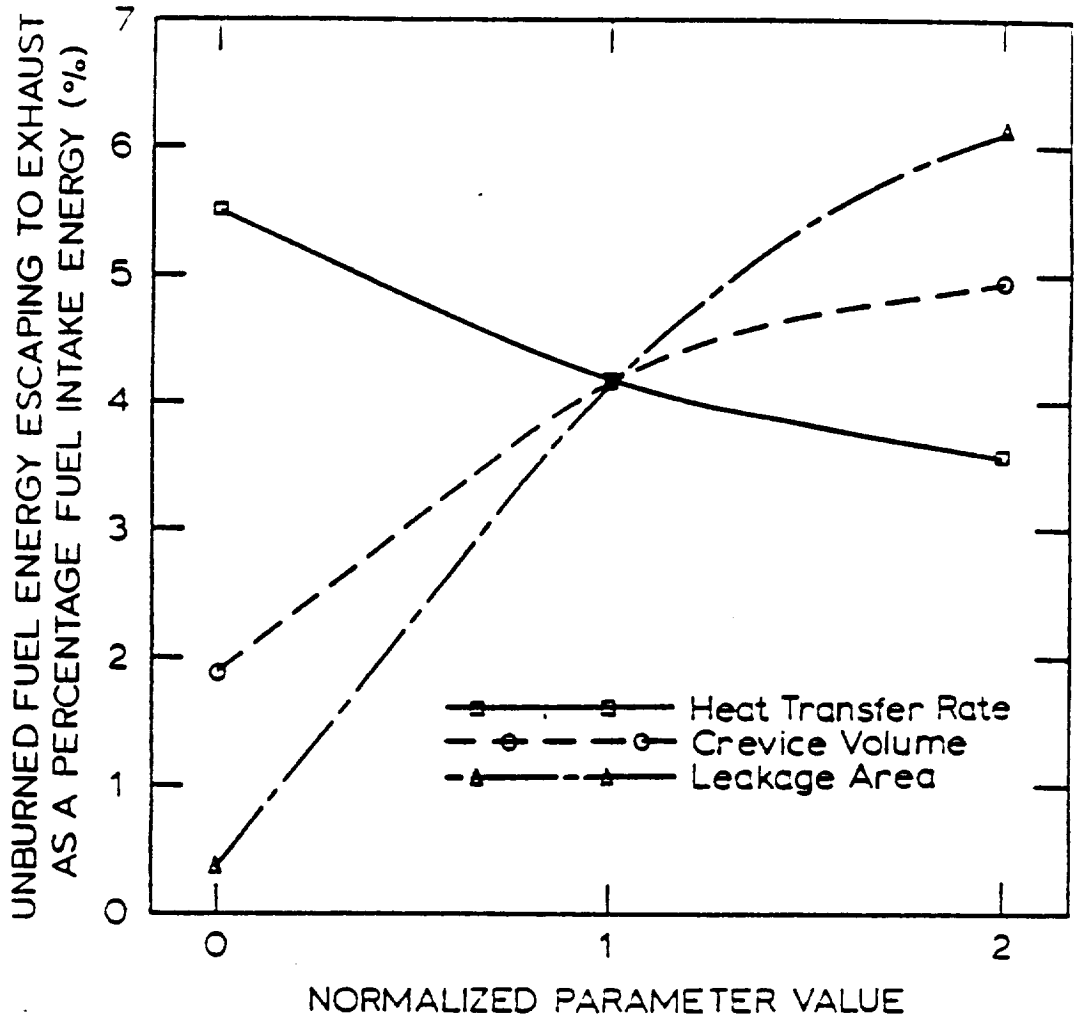

Figure 34. Effect of parametric variation on unburned fuel energy escaping to exhaust at light load.

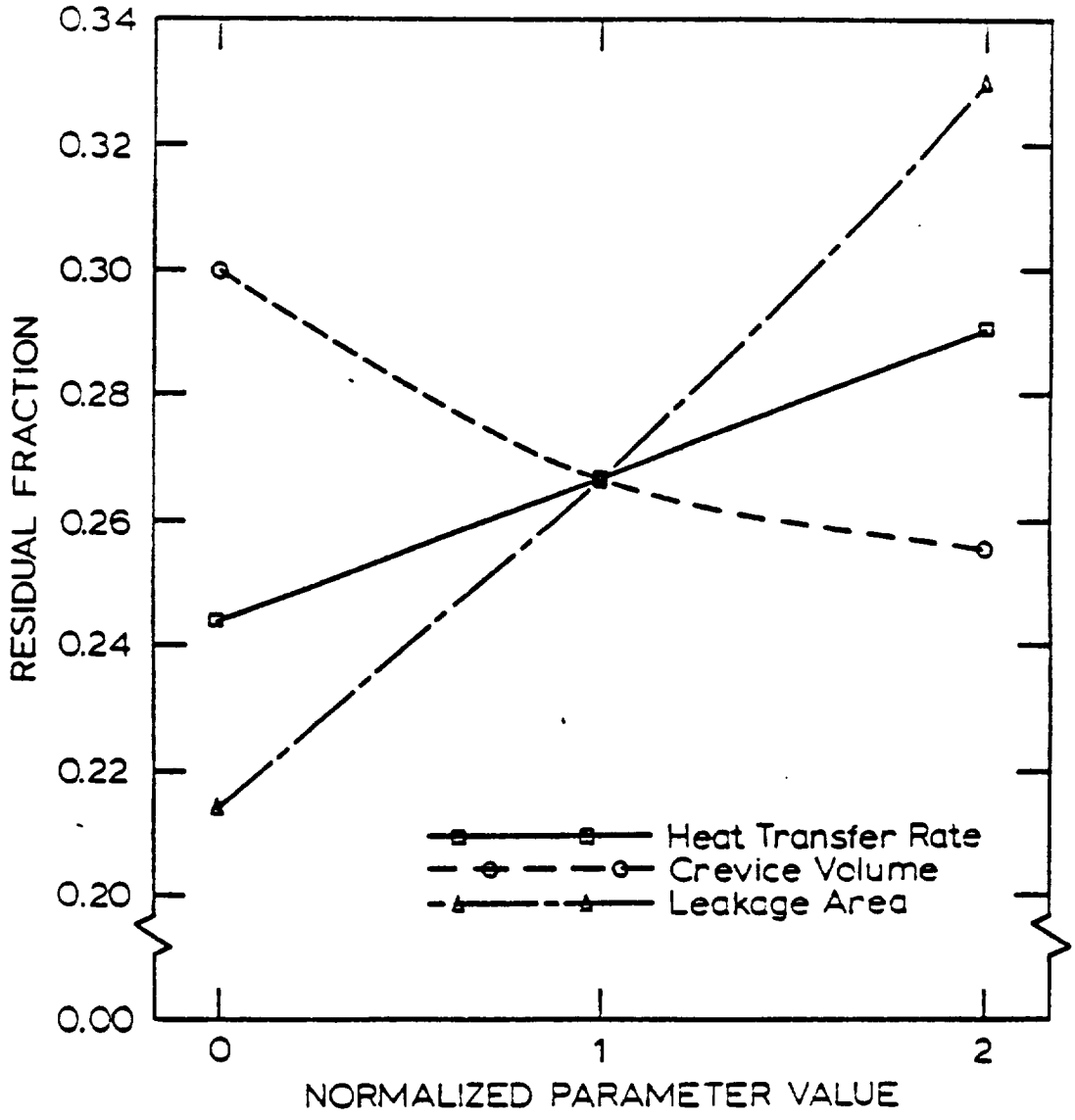

Figure 35. Effect of parametric variation on residual gas fraction at light load.